Agenzia nazionale per le nuove tecnologie,
l'energia e lo sviluppo economico sostenibile

MINISTERO DELLO SVILUPPO ECONOMICO

Compact Heat Exchangers/Steam Generators and Decay Heat Removal in Passive Safety Systems: Comparison of Thermal Hydraulic Features

M. Caramello, M. De Salve, B. Panella, G. Maronati, M.E. Ricotti

CIRTEN - CONSORZIO INTERUNIVERSITARIO PER LA RICERCA TECNOLOGICA NUCLEARE

Report RdS/PAR2013/096

Compact Heat Exchangers/Steam Generators and Decay Heat Removal in Passive Safety Systems: Comparison of Thermal Hydraulic Features

M. Caramello, M. De Salve, B. Panella - CIRTEN POLITO, G. Maronati, M.E. Ricotti - CIRTEN POLIMI

Settembre 2014

Report Ricerca di Sistema Elettrico

Accordo di Programma Ministero dello Sviluppo Economico - ENEA
Piano Annuale di Realizzazione 2013
Area: Produzione di energia elettrica e protezione dell'ambiente
Progetto: Sviluppo competenze scientifiche nel campo della sicurezza nucleare e collaborazione ai programmi internazionali per il nucleare di IV Generazione
Obiettivo: Sviluppo competenze scientifiche nel campo della sicurezza nucleare
Responsabile del Progetto: Felice De Rosa, ENEA

Il presente documento descrive le attività di ricerca svolte all'interno dell'Accordo di collaborazione "Sviluppo competenze scientifiche nel campo della sicurezza nucleare e collaborazione ai programmi internazionali per il nucleare di IV generazione"

Responsabile scientifico ENEA: Felice De Rosa

Responsabile scientifico CIRTEN: Giuseppe Forasassi

CIRTEN

Consorzio **I**nteruniversitario per la **R**icerca **TE**cnologica **N**ucleare

POLITECNICO DI MILANO

Department of Energy - Nuclear Reactors Group

POLITECNICO DI TORINO

Energy Department

Compact Heat Exchangers/Steam Generators and Decay Heat Removal in Passive Safety Systems: Comparison of Thermal Hydraulic Features

Autori

Marco Caramello (POLITO)

Mario De Salve (POLITO)

Bruno Panella (POLITO)

Giovanni Maronati (POLIMI)

Marco E. Ricotti (POLIMI)

CERSE-POLIMI-POLITO RL 1494/2014

Settembre 2014

Lavoro svolto in esecuzione dell'Attività LP1.C2.3

AdP MSE-ENEA sulla Ricerca di Sistema Elettrico - Piano Annuale di Realizzazione 2013

Progetto B.3.1 "Sviluppo competenze scientifiche nel campo della sicurezza nucleare e collaborazione ai programmi internazionali per il nucleare di IV generazione

Index

1 Abstract 8

2 Introduction 9

3 Heat Exchangers Description 14

3.1 Microchannel heat exchangers 14

3.1.1 Microchannels fabrication processes 16

3.2 Helical coil heat exchangers 17

3.2.1 Geometry 17

3.2.2 Fluid-dynamics 19

3.3 Air Heat Exchangers 21

3.4 In-Pool heat exchangers 22

4 I²S-LWR Project 28

5 RELAP5 simulation of passive DHRS 34

5.1 The intermediate heat exchanger 40

5.2 The final heat sink 40

5.3 Accident sequences 40

6 Simulations results: steady state conditions 42

6.1 Full power, steady state condition 43

6.2 Power load effect 47

7 Simulations results: accident conditions with pump inertia neglected 52

7.1 Case 1: Helical Coil Heat Exch. (A) and Air Cooled Heat Exch. (C) 53

7.2 Case 3: Helical Coil Heat Exch. (A) and Isolation Condenser (D) 70

8 Simulations results: accident conditions with pump inertia effect ____ 82
8.1 Case 3+4: Isolation Condenser (Pool) as final heat sink _____ 84
8.2 Case 1+2: Air Cooled Heat Exchanger as final heat sink _____ 98
9 Conclusions _____ 112
10 References _____ 113
11 Appendix: components of the system _____ 121
11.1 Primary system _____ 121
11.2 Intermediate loop _____ 137
11.3 Primary system: microchannel heat exchanger _____ 146
11.4 Final heat sink: Pool loop _____ 147
11.5 Final heat sink: Air heat exchanger _____ 151

List of figures

Figure 1. Schematic of microchannel heat exchangers. 15
Figure 2. Schematic of an helical coil tube. 17
Figure 3. Example of velocity profiles in a coiled pipe 18
Figure 4. Different flow patterns in coiled pipes 19
Figure 5. Chimney general layout and design parameters 22
Figure 6. General layout of a pool-type heat exchanger 23
Figure 7. BWR isolation condenser 23
Figure 8. ESBWR layout 25
Figure 9. ESBWR ICS layout 25
Figure 10. PCCS layout 26
Figure 11. passive safety systems for AP1000 27
Figure 12: schematic of the PRHRS in the AP1000 reactor 27
Figure 13. I^2S layout and radial cross-section of the RPV [26, 51] 29
Figure 14. I^2S insight 30
Figure 15. Schematic of the flashing drum [26, 59] 31
Figure 16. Helical coil DHRS coupled with air cooling [26, 60] 32
Figure 17. Microchannel heat exchanger 33
Figure 18. Case 1, Relap5 model: helical coil heat exchanger + air cooled heat exchanger (A+C) 36
Figure 19. Case 2, Relap5 model: microchannels heat exchanger + air cooled heat exchanger (B+C) 37
Figure 20. Case 3, Relap5 model: helical coil heat exchanger + isolation condenser (A+D) 37
Figure 21. Case 4, Relap5 model: microchannels heat exchanger + isolation condenser (B+D) 38
Figure 22. Primary pressure (Case: steady state) 45
Figure 23. Temperatures (Case: steady state) 46
Figure 24. Secondary pressure (Case: steady state) 46
Figure 25. Heat flux (Case: steady state) 47
Figure 26. General layout of the model for power load analysis 48
Figure 27. Primary temperatures (Case: steady state, power load variation) 48

Figure 28. Normalized global heat transfer coefficient (Case: steady state, power load variation) ..50
Figure 29. Mean logarithmic temperature (Case: steady state, power load variation) 51
Figure 30. Power load as a function of the inlet temperature (Case: steady state, power load variation) 51
Figure 31. Primary pressure at the beginning of the transient (Case 1).....54
Figure 32. Primary pressure in the first 2 hours (Case 1) 55
Figure 33. primary pressure (Case 1).....56
Figure 34. Core temperatures in the first 10 hours of the transient (Case 1).....57
Figure 35. Primary temperatures during the transient (Case 1) 57
Figure 36. Core flow rate in the first 10 hours (Case 1) 58
Figure 37. Core flow rate (Case 1).....59
Figure 38. intermediate loop pressure (Case 1) 60
Figure 39. Intermediate loop pressure at start-up (Case 1).....60
Figure 40. Intermediate loop temperatures at start-up (Case 1).....61
Figure 41. Intermediate loop temperatures (Case 1).....62
Figure 42. Intermediate loop flow rate at start-up (Case 1).....63
Figure 43. Intermediate loop flow rate (Case 1).....63
Figure 44. Air temperatures at start-up (Case 1).....64
Figure 45. Air temperatures (Case 1).....65
Figure 46. Air flow rate at start-up (Case 1).....66
Figure 47. Air flow rate (Case 1).....66
Figure 48: Thermal power at the beginning of the transient (Case 1) 68
Figure 49. Power removed in the first 30 hours (Case 1) 68
Figure 50. Power removed in the long term (Case 1) 69
Figure 51. Primary pressure at start-up (Case 3) 71
Figure 52. Primary pressure after 2 hours (Case 3) 71
Figure 53. Primary system's pressure (Case 3).....72
Figure 54. Primary system's temperatures – start-up (Case 3).....73
Figure 55. Primary system temperatures in the long term (Case 3).....73
Figure 56. Primary flow rate at start-up (Case 3) 74

Figure 57. Primary flow rate (Case 3)....75
Figure 58. Intermediate loop pressure at start-up (Case 3)....76
Figure 59. Intermediate loop pressure (Case 3)....76
Figure 60. Intermediate loop temperatures at start-up (Case 3)....77
Figure 61. Intermediate loop temperatures (Case 3)....78
Figure 62. Intermediate loop flow rate at start-up (Case 3)....79
Figure 63. Intermediate loop flow rate (Case 3)....79
Figure 64. Power removed at the system start-up (Case 3)....80
Figure 65. Power removed during the first hour (Case 3)....81
Figure 66. Power removed in the long term (Case 3)....81
Figure 67. Primary pump flow rate after SBO....83
Figure 68. Secondary pump flow rate after SBO [kg/s]....83
Figure 69. Primary pressure (Case 3+4)....84
Figure 70. Primary pressure at the beginning of the transient (Case 3+4)....85
Figure 71. Primary system's temperatures in the first hour (Case 3+4)....86
Figure 72. Primary system's temperatures during the first 10 hours (Case 3+4)....87
Figure 73. Primary system's temperature (Case 3+4)....88
Figure 74. Core flow rate (Case 3+4)....89
Figure 75. Core flow rate (Case 3+4)....90
Figure 76. Core flow rate at the beginning of the transient (Case 3+4)....90
Figure 77. Intermediate loop pressure (Case 3+4)....91
Figure 78. Intermediate loop pressure at the beginning of the transient (Case 3+4)....92
Figure 79. Intermediate loop pressure in the first 10 hours (Case 3+4)....92
Figure 80. Intermediate loop temperatures (Case 3+4)....93
Figure 81. Intermediate loop temperatures (Case 3+4)....94
Figure 82. Intermediate loop flow rates in the long terms (Case 3+4)....95
Figure 83. Intermediate loop flow rates in the first 10 hours (Case 3+4)....95
Figure 84. Intermediate loop flow rates at the beginning of the transient (Case 3+4)....96
Figure 85. Thermal power (Case 3+4)....97
Figure 86. Thermal power in the first 10 hours (Case 3+4)....97

Figure 87. Primary system's pressure (Case 1+2) 98
Figure 88. Primary system's pressure in the first 10 hours (Case 1+2) 99
Figure 89. Primary system's pressure in the first hour (Case 1+2) 99
Figure 90. Primary temperatures (Case 1+2) 100
Figure 91. Primary temperatures in the first 10 hours (Case 1+2) 101
Figure 92. Primary temperatures at the beginning of the transient (Case 1+2) 102
Figure 93. Core flow rate (Case 1+2) 103
Figure 94. Core flow rate at the beginning of the transient (Case 1+2) 103
Figure 95. Intermediate loop pressure (Case 1+2) 104
Figure 96. Intermediate loop pressure at the beginning of the transient (Case 1+2) 105
Figure 97. Intermediate loop temperatures (Case 1+2) 106
Figure 98. Intermediate loop temperatures at the beginning of the transient (Case 1+2) 106
Figure 99. Intermediate loop flow rate (Case 1+2) 107
Figure 100. Intermediate loop flow rate at the beginning of the transient (Case 1+2) 108
Figure 101. Air temperature (Case 1+2) 109
Figure 102. Air temperature at the beginning of the transient (Case 1+2) 109
Figure 103. Air flow rate at the beginning of the transient (Case 1+2) 110
Figure 104. Air flow rate (Case 1+2) 111

1 Abstract

The following report aims to compare and analyse the performance of innovative heat exchangers and passive safety systems (Decay Heat Removal Systems-DHRS), in different configurations, similarly to those proposed in several new generation reactor projects. Two in-vessel heat exchangers are described and adopted, namely the microchannel type and the helical coil type. Two ex-vessel heat exchangers are used to create a closed loop, natural circulation, passive DHRS: an air cooled type and an isolation condenser type, dipped into a water pool. The comparison of the in-vessel heat exchangers is made in steady state conditions and in an accident scenario, with the use of RELAP5 commercial software.
The new generation reactor adopted as a reference test bed for the DHRS implementation and analysis is the I^2S-LWR project from Georgia-Tech (an Integral PWR of large size).

In the steady state analysis, the two types of in-vessel heat exchangers designed to remove ¼ of the reactor power have been compared at full power and at reduced power considering a constant mean temperature of the primary system. The analysis allowed to highlight the features in terms of compactness, friction pressure losses and performances at different power levels.

In the analysis during accident conditions, a System Black-Out (SBO) followed by the reactor scram is used. In this case, the heat exchangers compared are used as a part of the DHRS, considering two possible solutions for the ex-vessel ultimate heat sink (the isolation condenser and the air cooled heat exchanger), resulting in 4 different DHRS configurations. The simulations results are compared in two chapters grouping them by the common ultimate heat sink, in order to isolate the effect on the transient of the heat exchanger.

2 Introduction

The objective of the major of components and fluids inside a nuclear station is to transfer thermal energy between the regions of the plants and between the plant and the external environment. The first heat transfer that takes place as nuclear energy is converted into heat is the one inside the core, where the refrigerant of the primary system removes energy from the fuel. The fuel itself may be of several geometries (small cylindrical pellets, spherical), while the refrigerant can be made of a single phase solution in case of light water, heavy water, liquid metals, molten salts and gas, or a two phase mixture in case of light water. The physical state of the refrigerant is the one obtained during nominal pressure and temperature conditions, but in case of water reactors a change of the physical state may happen during abnormal conditions.

The heat gained by the refrigerant of the core is normally transferred to a secondary system through intermediate heat exchangers or steam generators except in the case of boiling water or gas reactors, where the refrigerant has the potential to be sent directly to the turbine. These heat exchangers are used during nominal conditions and are characterized by different geometries and dimensions, surface areas and pressure losses, and for any different kind on plant in terms of power, thermodynamic cycle and refrigerant specific requirements (thermal-hydraulic, compactness, chemistry, economy) need to be fulfilled with different solutions. The most common steam generators and heat exchangers encountered in the existing nuclear fleet are made of straight pipes or U-tube pipes. Innovative geometries have been studied in the past and have been used in some commercial plants and several research reactors, as the helical coil, the bayonet and the spiral. The same components used for the heat removal during nominal conditions can be part of a safety system during accident conditions, though the working conditions are far from the nominal point they provide a large surface area in comparison to the heat produced in case of a protected transient. As another case, other heat exchangers different from the ones used in nominal conditions may be used to remove the power in accident scenarios: the design of specific components and of specific systems must be made taking into account a non-negligible variation of power passing from the first moments of the transient to the long term cooling, and for this reason several systems may be called

into action in the same plant depending on the time of the transient starting from the initiating event. Safety systems may have different goals depending on the time of the transient in which they are called: at a first stage, they may provide a cold storage of the coolant to reduce the specific internal energy of the primary system and avoid reaching excessive pressure or temperatures which may cause irreversible damages to the structures or to the core with possible hydrogen production and radioactive releases. In case of water reactors, the storage may be filled with borated water at a higher concentration than the one of the coolant to provide a negative reactivity insertion. These kinds of safety systems are not used for the heat removal from the primary system in a general sense, but they act to reduce the specific internal energy. Safety systems with the goal to remove power from the primary system, or more in general to the nuclear island, are the ones able to establish a continuous flow of heat through solid components or with the help of a flowing fluid, being it in a loop or not. Even these systems are not generic but specific for the type of plant.

As electric power is produced in the turbine, the fluid that underwent the expansion (the primary coolant or a secondary fluid) must release the remaining power to the external environment, and this duty is usually fulfilled with condensers in case of steam or other heat exchangers. The design of these heat exchangers is no more dependent only on the kind of plant, but also on the conditions of the external environment. Topology, topography, hydrology and meteorology of the site are examples of information needed for the construction of a thermal interface between the plant and the environment. The presence of water in the neighbourhood of the plant like the sea, rivers or lakes have the potential to be an excellent way to provide an external heat sink, so that in some cases of commercial plants artificial water basins are built to provide an external reservoir. In the absence of such natural sources, the heat sink may be provided by wet or dry evaporative towers, which make use of natural or assisted circulation of air. Even safety systems need an ultimate heat sink for the heat during incidental conditions, and if for any reason the nominal interfaces with the environment are not available other components must permit the heat removal from the plant. These systems are characterized by a lower power duty with respect to the ones used in nominal condition, although they may be forced to work in severe conditions, as in the case of a station black out. In this case, heat exchangers connected to natural circulation loops immersed in dedicated water storages, or smaller towers which make use of the natural circulation of air may provide an effective

cooling of the system for a certain period of time in the first case, or a long-lasting cooling in the second case.

The aim of the following report is to analyse the applications of passive systems for the decay heat removal in advanced nuclear reactors and critically discuss different design choices and components in the light of the most promising and innovative configurations. In the framework of passive safety systems for nuclear applications the International Atomic Energy Agency in 1991 [1] set the first guidelines for the definition of passive systems. The degree of passiveness of a system can be assessed considering its characteristics with respect to the 4 categories listed in table 1.

Table 1: Passive systems categories

Category	Requirements
A	• No signal inputs of "intelligence", no external power sources or forces, • no moving mechanical parts, • no moving working fluid.
B	• No signal inputs of "intelligence", no external power sources or forces, • no moving mechanical parts,
C	• no signal inputs of "intelligence", no external power sources or forces • moving mechanical parts, whether or not moving working fluids are also present.
D	Borderline category: passive execution/active initiation • Energy must only be obtained from stored sources such as batteries or compressed or elevated fluids, excluding continuously generated power such as normal AC power from continuously rotating or reciprocating machinery • Active components are limited to controls, instrumentation and valves, but valves used to initiate safety system operation must be single-action relying on stored energy • manual initiation is excluded.

Among the four categories listed in Table 1 most of the decay heat removal systems (DHRS) belong to category B or C since they make use of natural circulation for the fluid flow. The DHRS is the system that has the purpose to remove the decay heat in nominal or accident conditions from the primary system to the environment.

The complex set of thermal-hydraulic phenomena that occur in a gravity environment when geometrically or materially distinct heat sinks and heat sources are connected by a fluid can be identified as natural circulation [2, 3].

The studies of natural circulation in the past have been made both with experimental and numerical tools. From the point of view of the experimental tests on natural circulation, many facilities around the world have been built in the past to analyse transient phenomena, such as CAPCN, ITL, LSTF, PUMA and MASLWR. IAEA reports gathered a comprehensive list of information about the facilities [3], and several articles in public literature reports the results of the experiments performed [5-10]. From the point of view of the numerical analysis, thanks to the great effort in numerous experiments several code have been validated for the analysis of natural circulation, such as ATHLET, RELAP5, CATHARE2 and FLUENT [11].

To compare different configurations and components for the stability and efficiency of natural circulation systems, compact heat exchangers and steam generators must be contextualised in generic or specific layouts of safety systems because the behaviour of natural circulation is strongly dependent on both thermal and geometric specifications such as operating conditions and height differences, therefore a complete analysis can't be made without specific constraints. To overcome the previous issue, the I^2S integral reactor international project has been chosen as a reference geometry for the numerical analysis.

The tool chosen for the analysis is RELAP5-3D, version 4.0.3. The code is based on a nonhomogeneous and non-equilibrium model for the two-phase system that is solved by a fast, partially implicit numerical scheme to permit economical calculation of system transients [4]. The Relap5 code will be used to create a representative model of the system in terms of piping, components, heat sources and sinks.

The report is organized as following. The Chapter 3 covers the description of the heat exchangers considered for the DHRS. As a primary heat exchanger in contact with the primary system, a

compact plate heat exchanger with micro channels and a helical coil heat exchanger are proposed as possible solution, while the comparison for the external heat sink is made between an air heat exchanger and a pool heat exchanger. Chapter 4 presents the I^2S-LWR project with a focus on its heat removal systems. Chapter 5 describes the Relap5 models used for the analysis, the boundary and initial conditions used and the accidental sequence. Chapter 6 reports the results of a comparative analysis between helical coil and microchannel heat exchangers. Chapters 7 and 8 reports the numerical simulations done for the accident sequence reported in Chapter 5 for the different configurations, as well as the results obtained. Finally, Chapter 9 contains a critical discussion of the results and a comparison among the possible solutions to highlight their benefits and drawbacks, as well as a description of the future works that needs to be done to deepen the knowledge on natural circulation safety systems.

3 Heat Exchangers Description

3.1 Microchannel heat exchangers

One of the most important challenges of current technology is the removal of high thermal fluxes with the aim of very compact components. One way to address such issue is to enhance the convective heat transfer coefficient or increase the surface to volume ratio of the components. Among the different solutions there are the compact heat exchangers, which make use of microchannels. The application of microchannels is a fairly new field, which finds applications in biological and life science, biomedical and genetic engineering [12, 13] and also for the cooling of small electronic components [14]. Up to now the application of these heat exchangers has been done almost entirely for the removal of low thermal powers in a relatively small scale, but the high performance of these components is also interesting for larger modular devices which face higher values of power to be removed. In this context, the possibility arises to use compact microchannel heat exchangers for the decay heat removal in integral nuclear reactors, where critical constraints exist for the location of the primary components in the reactor pressure vessel.

The fluid dynamics in microchannels is strongly dependent on the flow characteristic, the geometry of the channel and the condition of the surface [15]. Channels with hydraulic diameters lower than 1 mm have a great geometrical impact in the enhancement of heat transfer, but, on the other hand, the frictional pressure loss per unit length results higher than the ones of standard-size heat exchangers. For this reason, the path of the fluid is kept as small as possible, and the developing flow region may be a non-negligible length fraction. To account the developing region for the frictional pressure loss it is common to use an apparent friction factor f_{app}, which is found to be dependent, both on the position from the inlet (degree of development), on the Reynolds number and on the geometry of the cross section [16,17]. For the frictional pressure loss in fully developed laminar flow, the friction factor and the Reynolds number are usually correlated with the Poiseuille number (Po) as in equation 1.

$$f = \frac{Po}{Re} \qquad (1)$$

As for the developing region, the friction pressure loss in fully developed flow is dependent on the Reynolds number and on the geometry of the cross section [18-20]. The laminar to turbulent transition in microchannels has also been studied recently [21]. It has been found that the transition happens with Reynolds numbers in the range of 2000-2300 and does not depend on the channel dimension.

As far as the heat transfer is concerned, for the laminar flow the Nusselt number is predicted as a function of the geometry of the cross section and on the boundary condition used (constant wall temperature, constant heat flux) [22].

As mentioned previously, the developing flow region plays an important role for the fluid dynamics in microchannel, and this is also true for the heat transfer. Different correlations are available in literature where the Nusselt number dependent to the distance from inlet the Reynolds number and the Prandtl number [18,19,23]. For fully developed turbulent flow, Adams et al. [24] suggested to correlate the Nusselt number to the one obtained by the Gnielinski correlation [25] corrected by a geometrical factor that takes into account the heat transfer enhancement provided by the microchannel.

For the heat exchangers taken into account in this study, a series of corrugated plates are stacked together and squared cross section channels are formed for the fluids. Figure 1 shows a schematic of the heat exchanger module currently under study for the steam production, as well as the flow path of the fluids [26].

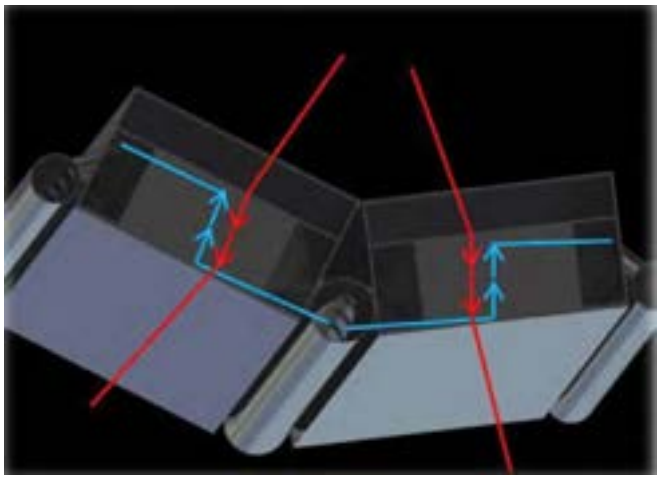

Figure 1. Schematic of microchannel heat exchangers.

3.1.1 Microchannels fabrication processes

Microchannel heat exchangers can be manufactured through miniaturized traditional technologies and "modern" innovative technologies. Miniaturized traditional techniques are rooted in conventional machine shop and manufacturing practices but adapted to achieve microscale features [27]. Some of these techniques, such as lithography, laser exposure, electroplating and molding, have been widely adopted and are encountered in multiple fabrication methodologies. The "modern" technologies are more difficult to characterize but are generally based on advances that occurred in the latter half of the twentieth century, such as lasers and micron-level photolithography. In some respects, miniaturized traditional techniques are the most straightforward approach to creating micro-features.

Standard machining techniques, such as sawing and micro-electro discharge machining can readily produce channels at dimensions down to a few hundred microns. Other Miniaturized traditional techniques, such as ultrasonic and waterjet machining are demonstrated to be very effective, especially on hard brittle materials. Commercial electroforming, molding, and stereolithographic fabrication have been brought into the micro-regime through the incorporation of lithographic and laser-based patterning.

As opposed to traditional technologies, "modern" technologies are able to accommodate channels down to few microns, with low material removal rates and low throughput. However, these techniques are often used for specialized high-value, low-repetition operations like micro-feature repair and via formation. These techniques have been reviewed by many authors [28, 29]. Laser machining has become an increasingly powerful tool that can handle a wide variety of difficult materials. Focused ion beam machining offers many similar benefits and can operate in the submicron regime.

3.2 Helical coil heat exchangers

3.2.1 Geometry

Heat exchangers composed of helical coiled pipes are currently used in process industries and power plants for their great capability to remove high thermal fluxes with a high degree of compactness even if with non-negligible pressure drops. The geometry of an helical pipe is defined by an internal and external diameter (d_i, d_e), an helical diameter D_h, the pitch p_h and a number of turns N as in figure 2 where N=2. All the equations of the paragraph are reported in Table 2 at the bottom.

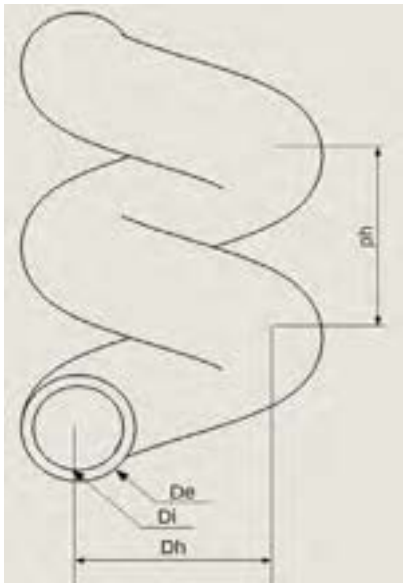

Figure 2. Schematic of an helical coil tube.

The length of the coil is obtained from equation 1. A heat exchanger or steam generator is equipped with several helical coils set in parallel with different helical radii and pitches. Different families of coils can be gathered together by defining two dimensionless quantities, namely the curvature ratio δ as in equation 2 and the torsion ratio τ as in equation 3 [30].

The curvature ratio and the torsion ratio are not used just for the geometry characterization but also for the fluid dynamics because it is affected by these quantities. The peculiarity of coiled pipes is the presence of centrifugal forces in the Navier-Stokes equations. The unbalance between

centrifugal, inertial and gravity forces lead to the formation of secondary motions lying on the pipe's cross section which create an alteration of the velocity and temperature fields with respect to the ones of a straight pipe. The motion of the fluid particles along the streamlines is not parallel to the helix centreline, and the particles experiences a series of accelerations and decelerations while moving in different regions of the velocity field.

The velocity maximum is shifted from the centre of the cross section to the external peripheral region. The temperature field has the same characteristics of the velocity field: considering a cold fluid flowing in an helical pipe heated from the external side, the coldest region on the cross section will be shifted from the centre to the peripheral region. The weight of these phenomena is related to the values of the curvature ratio. For high values of the curvature ratio the centrifugal forces dominate over gravity and inertia and so the asymmetry is pronounced, while if the curvature ratio tends to zero the flow field inside the helical pipe tends to the one of a straight horizontal pipe. Figure 3 shows the typical velocity field of a fully developed flow in a coiled pipe [33].

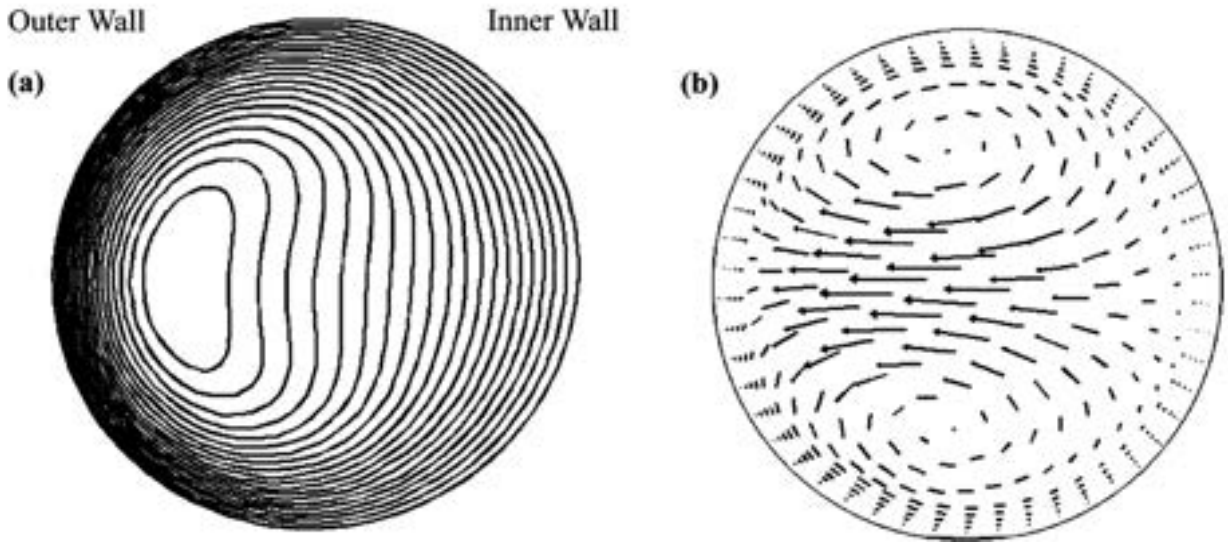

Figure 3. Example of velocity profiles in a coiled pipe

Another important feature of the coiled pipes is the tendency to laminarize the flow. Not only the laminar to turbulent transition happens at higher Reynolds number with respect to a straight pipe, also the transition is smoother. These effects increase as the curvature ratio increases. Cioncolini et

al. [31] studied experimentally the laminar to turbulent transition in coiled pipe highlighting the causes of the enhancement of the laminar region.

3.2.2 Fluid-dynamics

As far as heat transfer and pressure drops are concerned, many reviews are available in literature, covering the researches done from the first studies to the last years' [32-38]. The heat transfer in coiled pipes is strongly asymmetric because of the centrifugal forces: the heat transfer coefficient and the wall temperatures are not constant on the cross-section. The highest values of heat transfer coefficient are recorder on the external side of the curvature, while the lowest ones are in the inner part. For an estimation of the average heat transfer coefficient in single-phase flow the most validated correlations are the one by Mori and Nakayama [40] which are reported in equations 4 and 5. Equation 4 is valid for liquids while equation 5 is for superheated steam and gas.

During two-phase flow the centrifugal forces have a separation effect on the phases depending on their densities: the heavier phase is shifted towards the external side of the curvature. The parting capacity is used in industrial processes for liquid extraction or slurry separation. The curvature ratio also affects the flow pattern of the phases, as it can be seen from figure 4 [33].

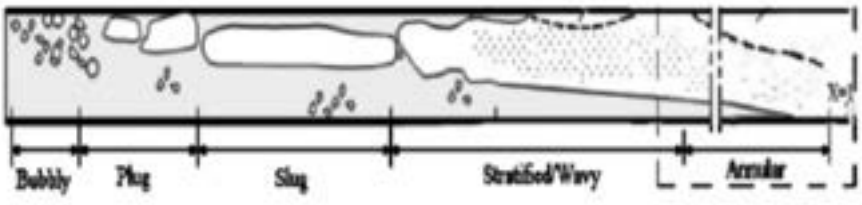

Figure 4. Different flow patterns in coiled pipes

The heat transfer coefficient estimation is usually based on modified versions of the Chen [40] correlations for subcooled and saturated flow boiling such as the one from Owhadi [41] where the centrifugal forces are taken into account by adding the curvature ratio in the equations.

The frictional pressure losses are evaluated using equation 6.

One of the most validated correlations for the friction factor calculation in coiled pipe is the one by Ito [42] in system 7.

In system 8 Re_{crit} is the laminar to turbulent Reynolds transition number. Several correlations for the calculations of this parameter are available in [31].

The estimation of frictional pressure drop in two phase flow is usually done with the aim of two-phase multipliers. Santini et al. [43] analysed experimentally the two-phase pressure drops inside helical coiled pipe and compared the experimental results with several correlations available in literature, underlining the increased pressure loss with respect to a straight pipe.

Table 2: equations for Helical Coil Heat Exchangers

$$l_h = 2\pi N\sqrt{\left(\frac{D_h}{2}\right)^2+\left(\frac{p_h}{2\pi}\right)^2} \quad (1)$$
$$\delta = \frac{d_i}{D_h} \quad (2)$$
$$\tau = \frac{p_h}{\pi D_h} \quad (3)$$
$$Nu = \frac{1}{41}\left(\frac{Pr}{Pr^{0.6}-0.062}\right)Re^{\frac{5}{6}}\left(\frac{d_i}{D_{hx}}\right)^{\frac{1}{12}}\left(1+\frac{0.061}{\left\{Re\left(\frac{d_i}{D_{hx}}\right)^{2.5}\right\}^{\frac{1}{6}}}\right) \quad (4)$$
$$Nu = \frac{1}{26.2}\left(\frac{Pr}{Pr^{0.6}-0.074}\right)Re^{\frac{4}{5}}\left(\frac{d_i}{D_{hx}}\right)^{\frac{1}{10}}\left(1+\frac{0.098}{\left\{Re\left(\frac{d_i}{D_{hx}}\right)^{2}\right\}^{\frac{1}{5}}}\right) \quad (5)$$
$$\Delta P = \frac{1}{2}(4f)\frac{L}{d_i}\frac{G^2}{\rho} \quad (6)$$
$$f = \begin{cases} \dfrac{344\left(\frac{D}{d}\right)^{-0.5}}{\left\{1.56+\log_{10}\left[Re\left(\frac{D}{d}\right)^{-0.5}\right]\right\}^{5.73}} & Re < Re_{crit} \\ 0.076\,Re^{-0.25} + 0.00725\left(\frac{D_h}{d_i}\right)^{-0.5} & Re \geq Re_{crit} \end{cases} \quad (7)$$

3.3 Air Heat Exchangers

Another key component of the system has the aim to provide an heat sink in order to remove the decay heat from the secondary loop and transfer it to an external environment, being it the ambient or a third system. The component designed for this purpose must accomplish the task by means of several constraints:

- It must be a passive system without the need of intelligent signal for activation,
- It must guarantee the heat removal for a minimum amount of time (grace time).

Considering the lessons learned from the recent Fukushima accident the meaning of grace time has become more important since the condition of an isolated system for a long period of time without the possibility of human intervention is now important to be carefully investigated. As an extreme scenario, the perfect heat sink from the safety point of view must be able to remove indefinitely the power of the system without any human intervention.

The first system proposed for the task and described hereafter in this paragraph has the potential capability to successfully guarantee this last condition. It is constituted by a chimney containing a tube bundle where the secondary fluid circulates. The bundle is composed of parallel vertical or slightly inclined pipes, externally cooled by air at ambient pressure and temperature which flows in natural circulation thanks to the head provided by the height of the chimney. Figure 5 shows the general layout of a commercial chimney and the key parameters to be determined [44].

As a general rule, the dimension of the chimney can be assessed considering the following design parameters [44].

$$\frac{2\,r_b}{h} = 0.75 \div 0.85 \qquad (1)$$

$$\frac{r_T}{r_B} = 0.55 \div 0.65 \qquad (2)$$

$$\frac{h_c}{2r_B} = 0.1 \div 0.2 \qquad (3)$$

$$\tan(\beta_1) \geq \frac{r_B - r_T}{h_T - h_C} \qquad (4)$$

For secondary fluid flowing inside the tube bundle the heat transfer conditions that may arise are a single phase natural convection of a two-phase condensation.

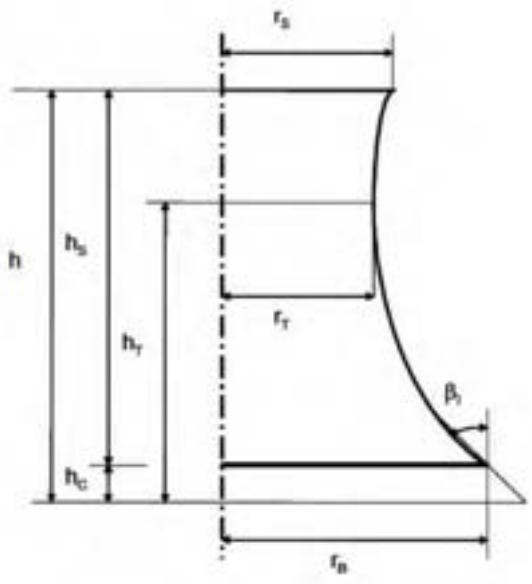

Figure 5. Chimney general layout and design parameters

3.4 In-Pool heat exchangers

Another possible solution for the final heat sink is constituted by a heat exchanger immersed in a water pool. With this configuration, the fluid from the secondary loop transfers heat to a mass of water stored in a dedicated pool initially set at ambient pressure and temperature. Figure 6 shows a general layout of the system. The water inside the pool evaporates because of the heat transfer and the level of water reduces during time. As a general rule, the height of the pool is designed to keep the level of water above the top of the heat exchanger when the power to be removed from the primary system is high. For long term cooling the decay heat decreases and the water level drops under the top of the heat exchanger: during these conditions the free convection of the surrounding air is sufficient to remove the decay heat. The amount of water required as well as the height of the pool are calculated on the basis of the latent and sensible heat needed for the complete evaporation of water starting from ambient pressure and temperature. Considering that the pool must be installed at a higher altitude with respect to the reactor core to establish natural circulation, the

design of the pool height is made as a compromise between the need to guarantee a water head on the heat exchanger for a certain period of time and ensure the system integrity during the design basis earthquake.

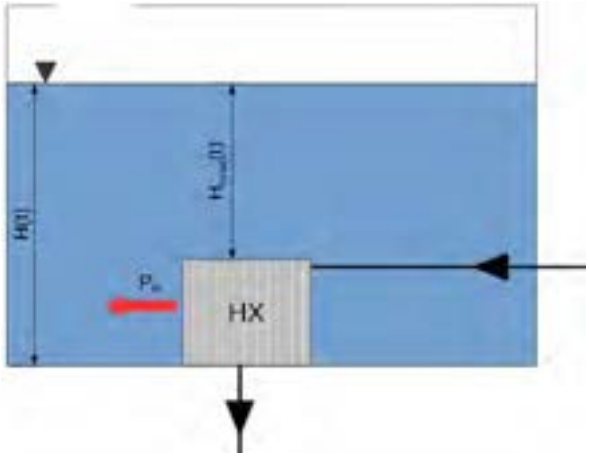

Figure 6. General layout of a pool-type heat exchanger

The first applications of this system have been done in the first boiling water reactors like the Dresden 1 in 1995 in the USA. The system is called isolation condenser (IC). Figure 7 [45] shows the layout of the heat exchanger and the connections with the primary system. When the system starts its operations the steam is sent from the upper part of the RPV to the immersed tube bundle where it condensate. The liquid is then redirected to the RPV establishing an assisted circulation loop with the recirculation pumps.

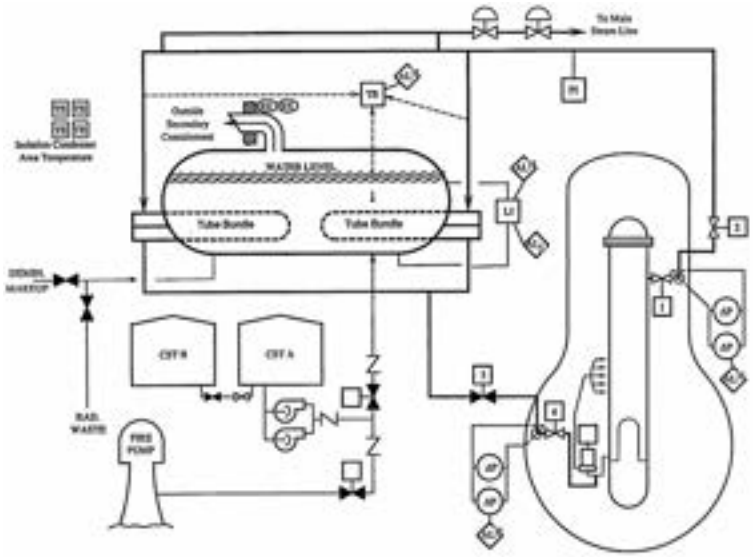

Figure 7. BWR isolation condenser

In the last years the concept of isolation condenser has turned back into favour in numerous reactor projects. One of them is the ESBWR (Economic Simplified Boiling Water Reactor). Figure 8 shows a layout of the reactor [46].

The ESBWR is a III+ generation boiling water reactor. It is characterized by a simple and safe design where the coolant is driven by natural circulation both in nominal and incidental conditions [47]. A pool-type system is used both for the pressure increase suppression or residual heat removal when the normal DHRS is unavailable (ICS) and also for the cooling system of the containment during LOCA. This second system is called passive containment cooling system (PCCS) [48]. The ICS is constituted by 4 independent trains set above the containment. Figure 9 shows a train of the ICS [46]. The pool is connected to the environment by means of the venting system. each pool is used respectively by a train of ICS and a train of PCCS. The ICS receive steam from the RPV from which it is injected in two immersed heat exchangers formed by tube bundles connected with headers at the top and at the bottom. The condensate is then redirected with a direct connection to the RPV on the top of the downcomer. The steam-side connection is normally open while the condensate line is closed. This allows the system to be full of subcooled water at the system pressure and reduce the start-up operations. Once the system is completely connected to the RPV a natural circulation is established at least for 72 hours.

Figure 10 represents the layout of one of the six PCCS trains [46]. The system is similar to the ICS except for the steam inlet of the heat exchangers which is connected to the containment's environment. The aim of the system is to condensate the steam in the containment after a LOCA scenario and redirect the mixture of condensate and noncondensable gases to the gravity driven cooling system pool and the suppression pool respectively. The system has no valves and does not need activation.

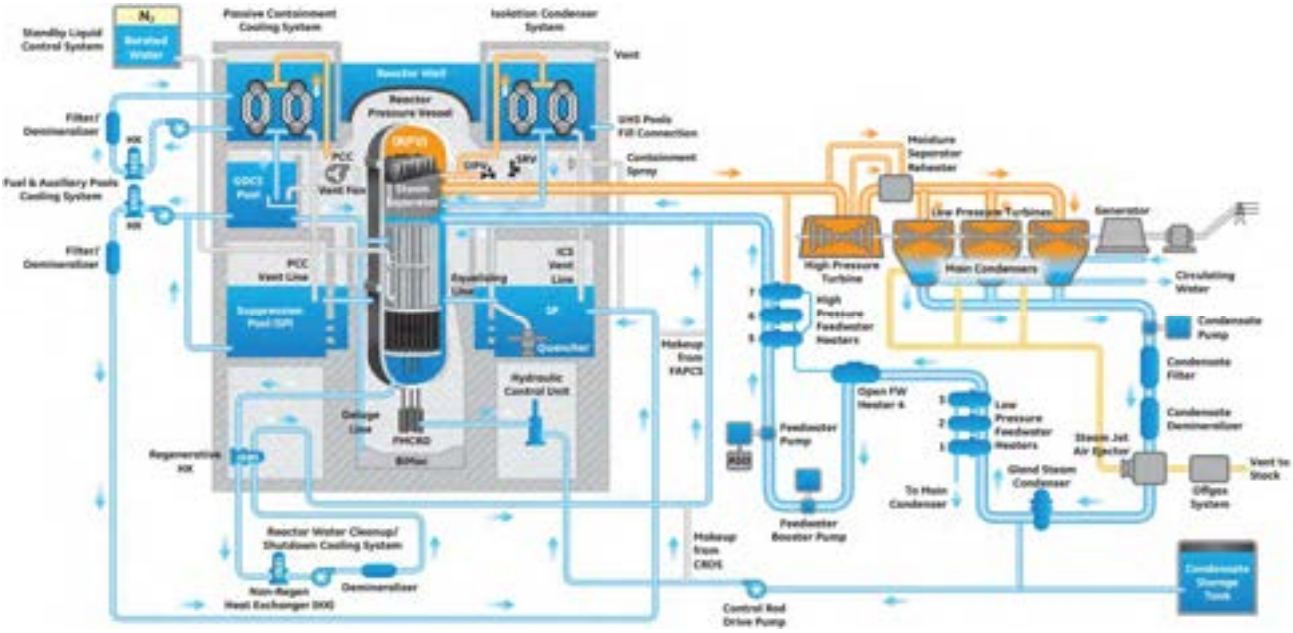

Figure 8. ESBWR layout

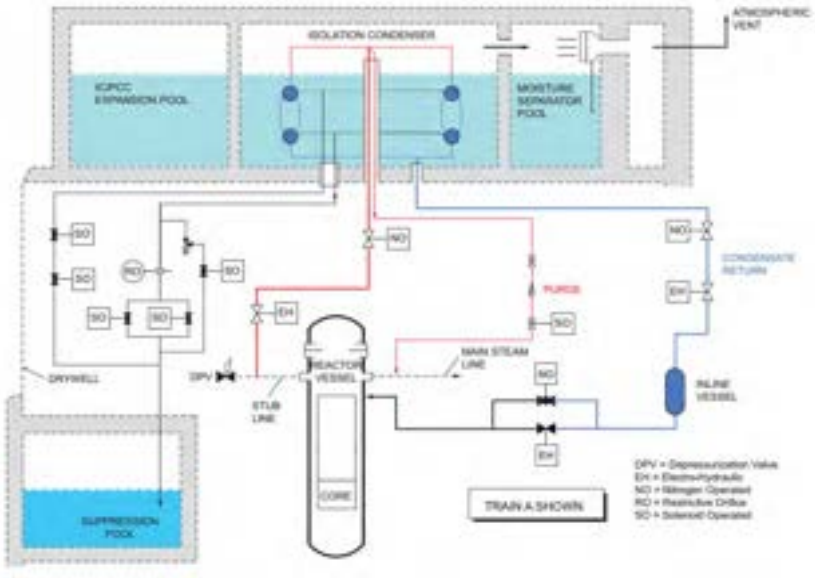

Figure 9. ESBWR ICS layout

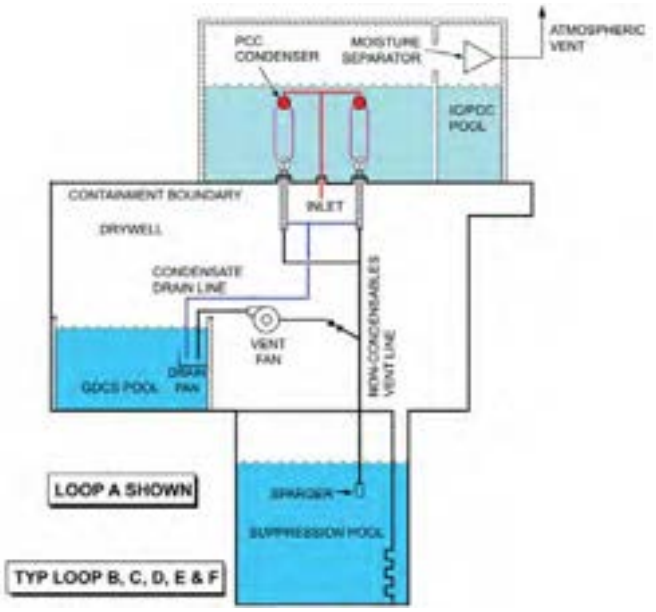

Figure 10. PCCS layout

Another recent project which uses pool-type heat exchangers is the AP1000 [49]. AP1000 is a III+ generation two loop PWR born from the previous knowledge of the Westinghouse company in the AP600 project: it is designed with proven technologies for a near term licensing and makes great use of safety passive systems. Figure 11 shows the safety systems employed for the reactor [48].

The passive residual heat removal system is equipped with a C shaped heat exchanger which protects the plant against transients that upset the normal steam generator feedwater and steam systems. The heat exchanger is immersed in the In-Containment Refuelling Water Storage Tank (IRWST). When the system is called in operations valves are open and water from the hot leg is sent to the heat exchanger in the pool where it is cooled by the stored refuelling water. After that, the coolant is sent to the one of the steam generator cold-leg channel heads. This system can also operate while the primary pumps are working [48]. Figure 12 shows a layout of the PRHR system [50].

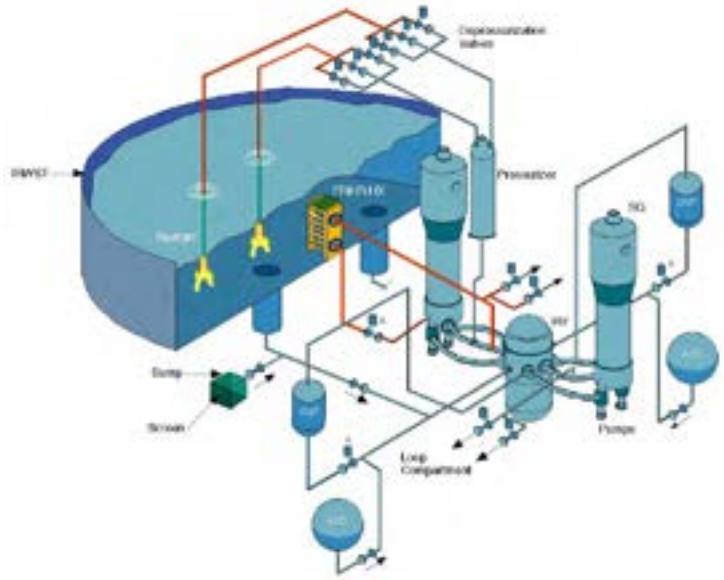

Figure 11. passive safety systems for AP1000

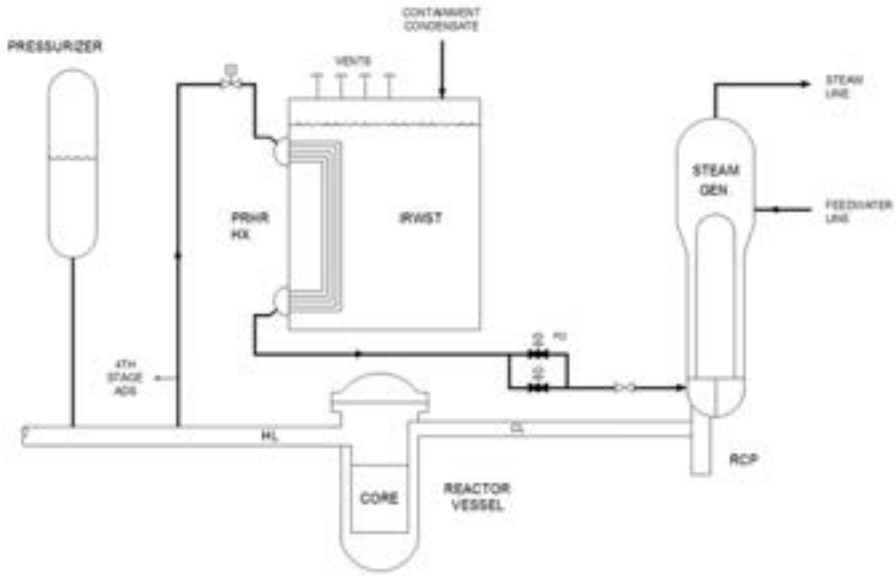

Figure 12: schematic of the PRHRS in the AP1000 reactor

4 I²S-LWR Project

The I²S-LWR project [51] is the result of an international collaboration consisting of numerous research centres, universities and actors of the nuclear industry. The list of the principal actors is shown in Table 3.

Table 3: research group for I²S project

	Team Members	Co-PIs/Co-Is
Lead	Georgia Tech (GT)	B. Petrovic (PI) F. Rahnema (Co-PI) C. Deo, S. Garimella, P. Singh, G. Sjoden (Co-Is)
Acade-mia	University of Idaho (U-Id)	I. Charit (Co-PI)
	University of Michigan (U-Mich)	A. Manera (Co-PI) T. Downar, J. Lee (Co-Is)
	Morehouse College (MC)	L. Muldrow (Co-PI)
	University of Tennessee (UTK)	B. Upadhyaya, W. Hines (Co-PIs)
	Virginia Tech (VT)	A. Haghighat (Co-PI), Y. Liu (Co-I)
Industry	Westinghouse Electric Company (WEC)	P. Ferroni (Co-PI) F. Franceschini, M. Memmott (Co-Is)
	Southern Nuclear (SNOC)	R. Cocherell (Co-PI)
Nat'l Lab	Idaho National Laboratory (INL)	A. Ougouag (Co-PI), G. Griffith (Co-I)
Int'l	Politecnico di Milano, Milan, Italy (PoliMi)	M. Ricotti (Co-PI)
	University of Cambridge, Cambridge, UK (U-Cambridge)	G. Parks (Co-PI)
Consultant		H. Garkisch

The combination of the economics provided by large electrical power, Inherent safety features and passive safety systems are the basis of the I²S-LWR (Integral Inherently Safe Light Water Reactor) concept based from the previous knowledge gained during the IRIS project [52-54].

Figure 13 shows the layout of I²S reactor. Most of the principal components are still under investigation at the moment and for each of them different solutions are currently under study; for

this report, the description of the reactor will focus on the safety system components proposed for the DHRS, and the rest of the system will be explained in terms of possible solutions.

The reactor is an integral PWR: pressurizer, control rod mechanism, primary heat exchangers and safety systems are integrated within the reactor pressure vessel (RPV), and the RPV is surrounded by a pressurized steel containment vessel (CV). Figure 14 shows the insight of the reactor with a particular of the control rods mechanism, the core barrel and the DHRS in the configuration with the helical coil heat exchanger. The main penetrations on the RPV are at a higher height than the core top.

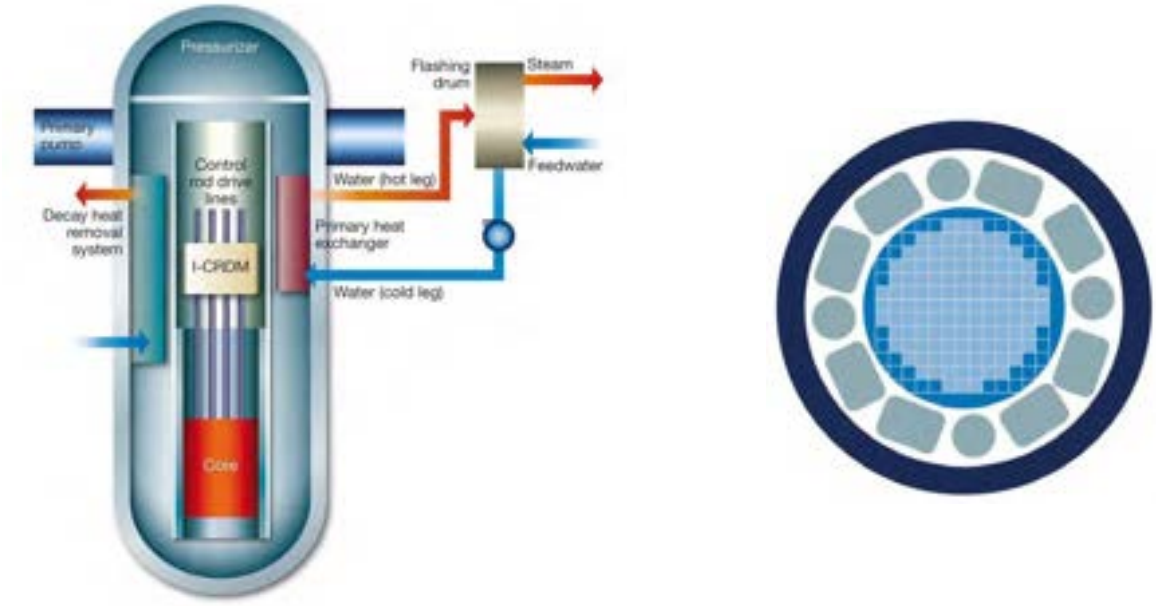

Figure 13. I²S layout and radial cross-section of the RPV [26, 51]

The reactor core is designed to obtain higher values of power density than typical pressurized water reactors (PWRs) in the order of 130 MW_{th}/m^3. To achieve this condition, innovative fuel pins in composition and geometry are considered to maintain a satisfactory thermal margin in terms of distance from the melting temperature. The primary choice consists of U_3Si_2 cylindrical pellets and high corrosion resistance stainless steel cladding. The secondary choice is to use UN petal-shaped rods and SiC as cladding.

The 8 primary heat exchangers are made of stacks of plates among which microchannels are formed where the fluids flow in single-phase conditions. From the preliminary analysis two-phase flow on the secondary side is not suggested because of instabilities that may arise inside the small channels of the heat exchanger. Also, two-phase flow may induce unacceptable pressure losses due to friction and probable channel blockage due to deposition of corrosion products. The steam is then produced in 4 flashing drums outside the RPV [59]. Figure 15 shows a schematic of the flashing drum. The fluid entering the volume experiences an abrupt pressure reduction reaching the pressure where its temperature is the saturation temperature and steam is produced. The steam is mechanically separated from the liquid phase with a separator on the top of the drum and is then sent to the high pressure stage of the turbine.

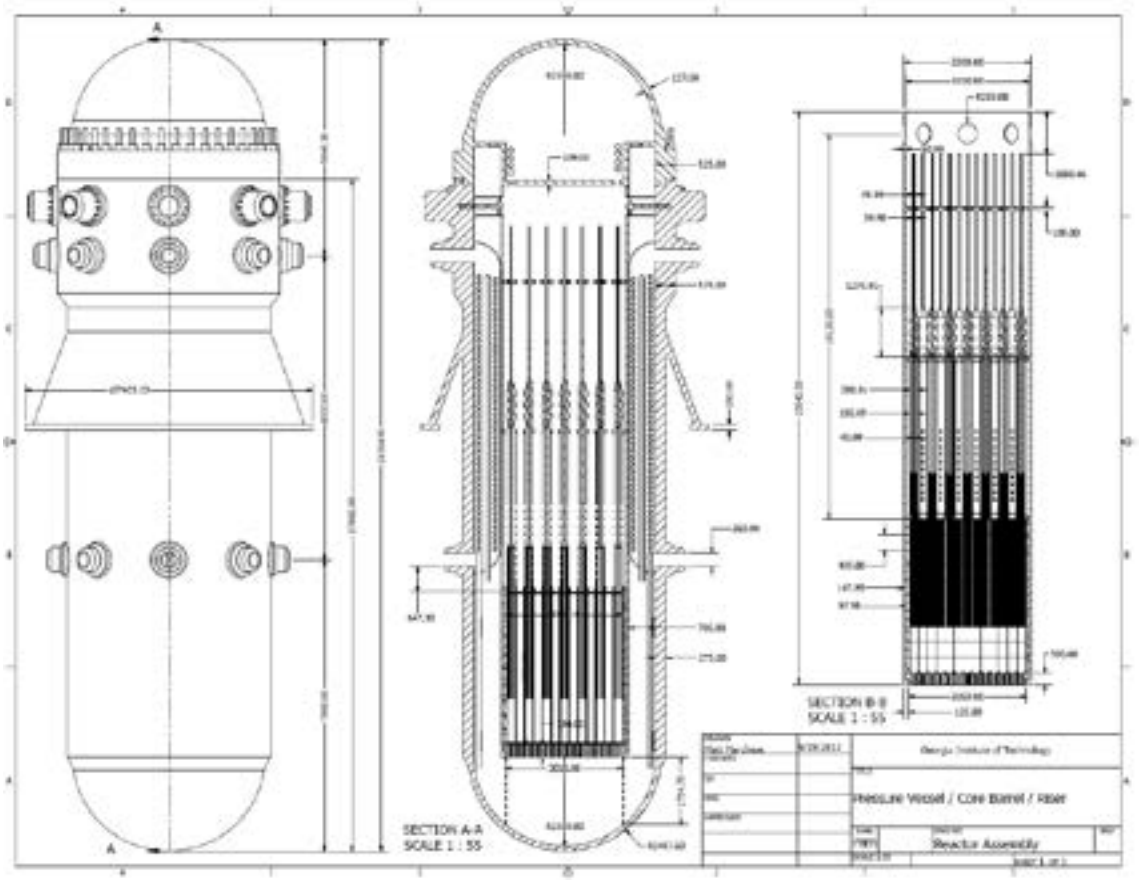

Figure 14. I²S insight

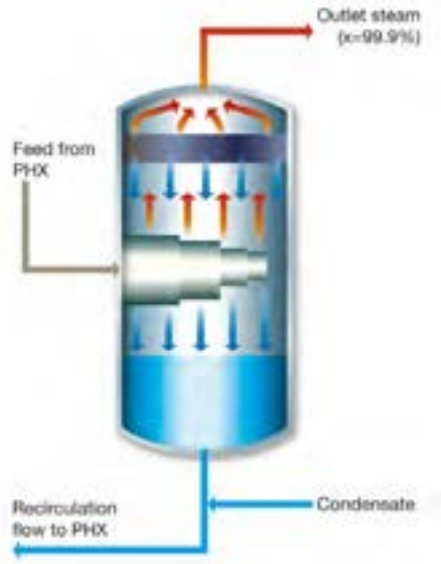

Figure 15. Schematic of the flashing drum [26, 59]

Microchannel heat exchangers give the opportunity to reach high values of power density and therefore they provide a good solution for integral reactors, although many phenomena are still to be numerically and experimentally investigated to understand their behaviour during anomalous and incidental conditions, as it will be partially done in this report.

From the base of safety philosophy of the GEN-III+ reactors the I^2S project have the aim to further increase the safety of LWRs with an inherent safety approach by eliminating accident initiators as much as achievable, limiting the loss of inventory during loss of coolant accident (LOCA) scenarios and increasing the components' degree of passiveness above category C.

The DHRS [60] is equipped with four independent loops designed for a category B passivity thanks to the absence of valves. Each loop consists of a compact heat exchanger (microchannel or helical coil). In case of the helical coil heat exchanger, the tube side is connected to the primary system and the shell side is connected to the secondary loop. The fluid for the secondary loop is currently under study, and the most promising solutions are the ones with molten salts or nanofluids rather than water because of the heat transfer enhancement [56, 57]. The ultimate sink of the system is under investigation and the possible solutions are an air-cooled heat exchanger and a pool-type heat exchanger.

Figure 16 shows the layout of the in-vessel heat exchanger in case of the helical coil configuration coupled with the air-cooling sink.

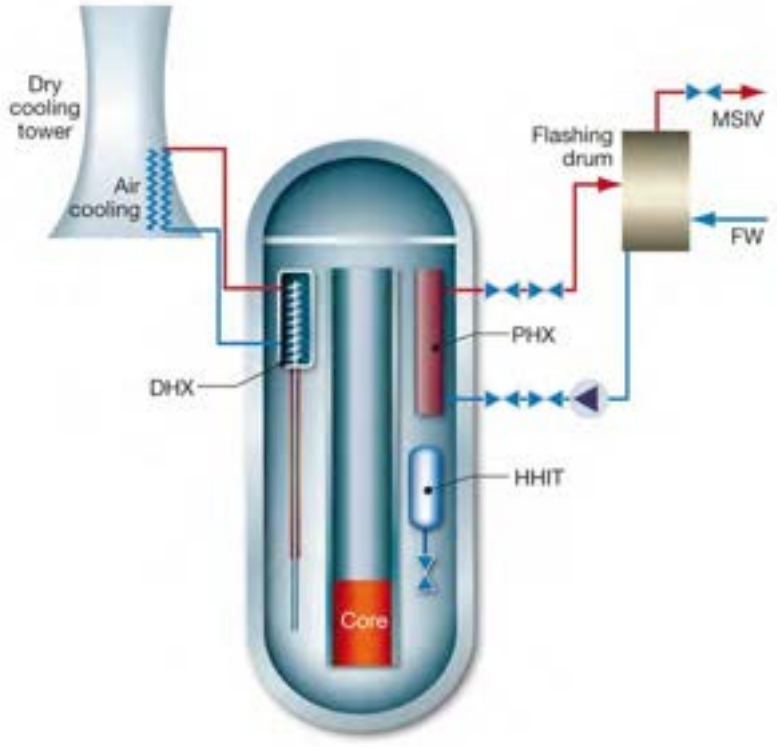

Figure 16. Helical coil DHRS coupled with air cooling [26, 60]

In the configuration proposed in figure 4 the primary fluid enters the annular region around the discharge tube. The inlet position is located in the downcomer region at the same height of the top of the core. Then, the hot primary fluid goes up to the heat exchanger and is subsequently sent in the helical tube where the heat is transferred to the shell side. Once the fluid completed the passage in the helical tube it descends into the discharge conduit and is sent back into the lower region of the downcomer to re-enter the core.

The second possibility for the DHRS is to use the same type of heat exchanger used for the steam production. These are compact microchannel heat exchangers. Figure 17 shows an example of an heat exchanger, the plates and the microchannels.

With this configuration, the DHRS are placed at the top of the downcomer region. The hot primary fluid goes from the riser into the heat exchanger and then it descends in the downcomer.

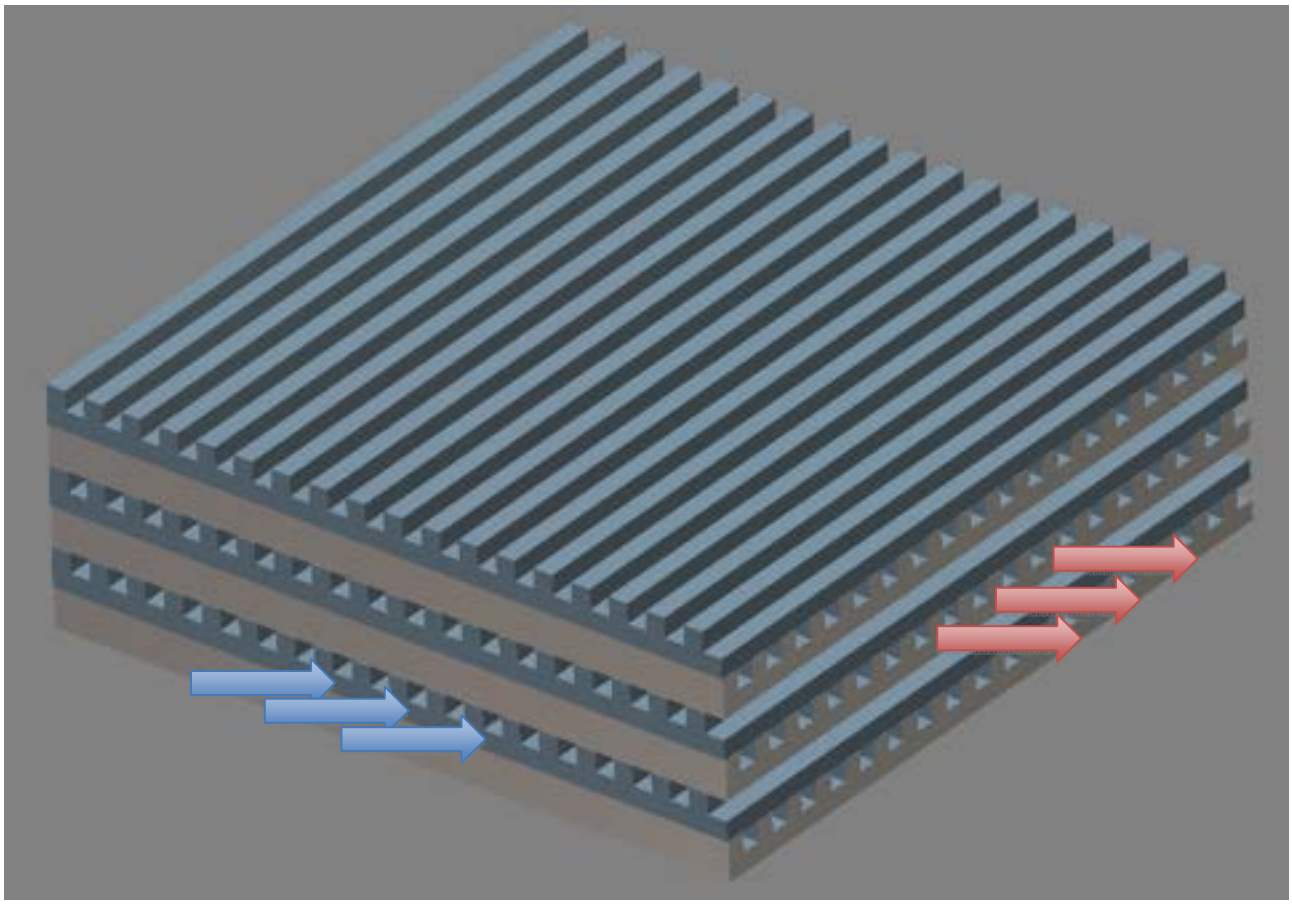

Figure 17. Microchannel heat exchanger

5 RELAP5 simulation of passive DHRS

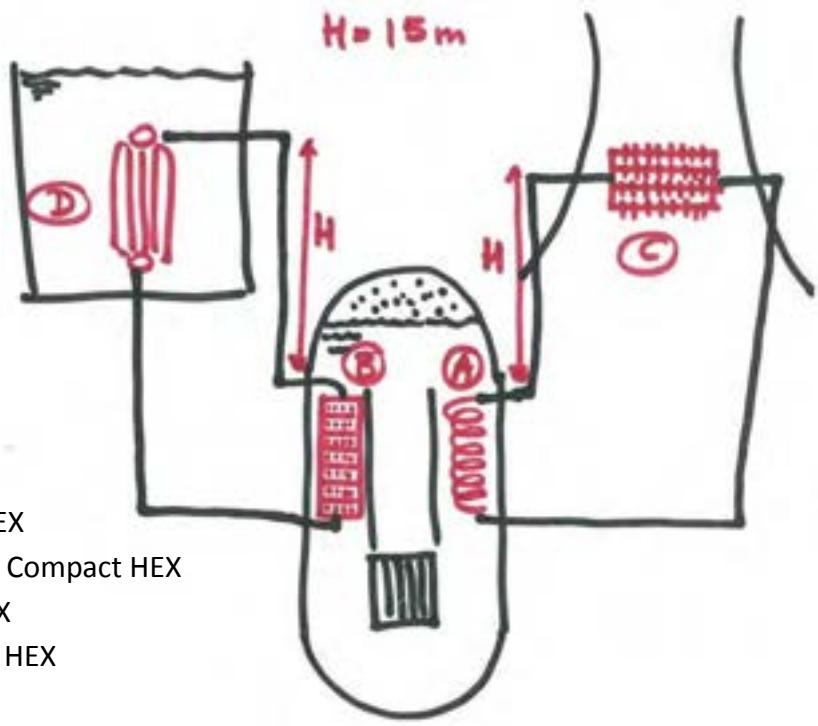

A= Helical Coil HEX
B= Microchannel Compact HEX
C= Air cooled HEX
D= Water cooled HEX

In this chapter, the four different DHRS configurations and related RELAP5 inputs are reported.
All the analyses were performed using a semi-implicit advancement scheme with time step control. The analysis has been carried out considering four different configurations of the DHRS in terms of in-vessel and external heat exchangers, but the architecture of the system and some parameters are the same in order to make the results comparable. The chapter is organized in the following way: in the first part, a general description of the loops and of the common components is presented. In the second part, the heat exchangers of the DHRS are described and the different solutions are compared in terms of modelling. In the appendix, a description of the cards used for the modelling of the single components is reported.
The model is divided into 4 subsystems representing 1/4 of the total system (since 4 trains of DHRS are envisaged for the reactor):

- The primary loop (reactor)
- The secondary loop (steam generator)
- The intermediate loop (DHRS)
- The final heat sink

The four different configurations of the passive safety system are here summarized:

DHRS configuration	In-vessel HX	External HX
Case 1 (A+C)	Helical Coil Heat Exchanger (A)	Air Cooled Heat Exchanger (C)
Case 2 (B+C)	Microchannel Heat Exchanger (B)	Air Cooled Heat Exchanger (C)
Case 3 (A+D)	Helical Coil Heat Exchanger (A)	Isolation Condenser (Pool) (D)
Case 4 (B+D)	Microchannel Heat Exchanger (B)	Isolation Condenser (Pool) (D)

A general view of the whole system modelled with RELAP5 code is depicted in the Figures from 18 to 21, corresponding to the four different configurations for the DHRS. The figures are not in scale.

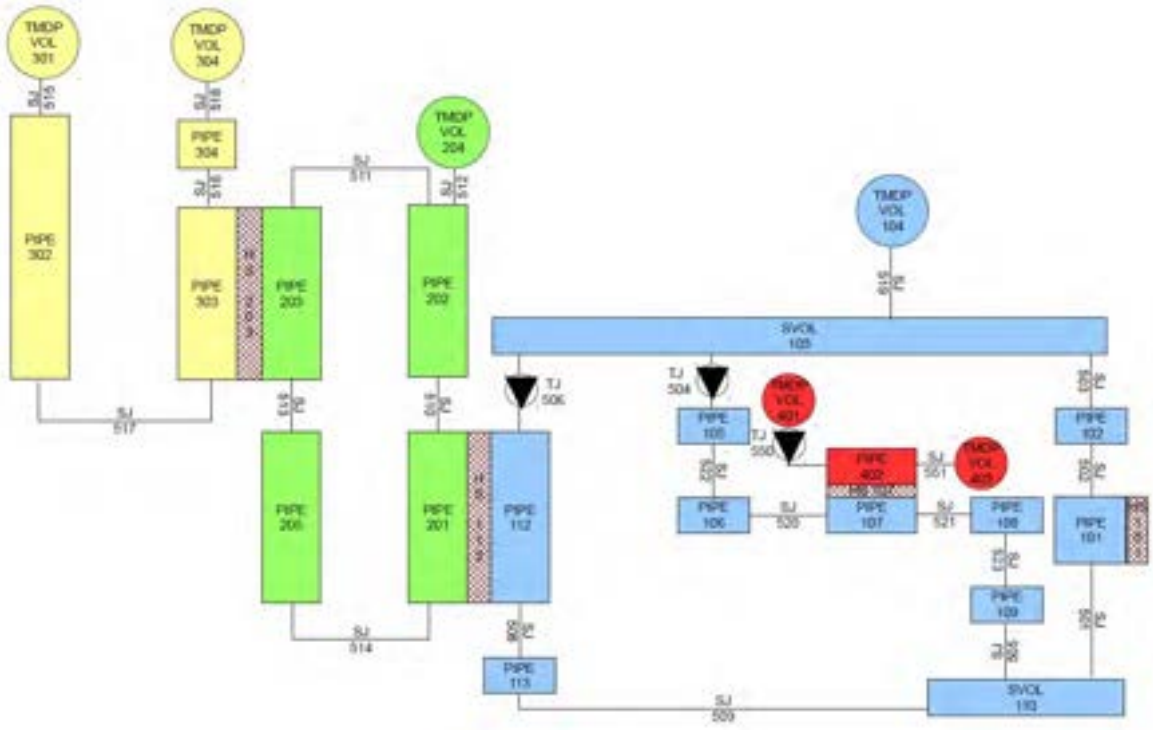

Figure 18. Case 1, Relap5 model: helical coil heat exchanger + air cooled heat exchanger (A+C)

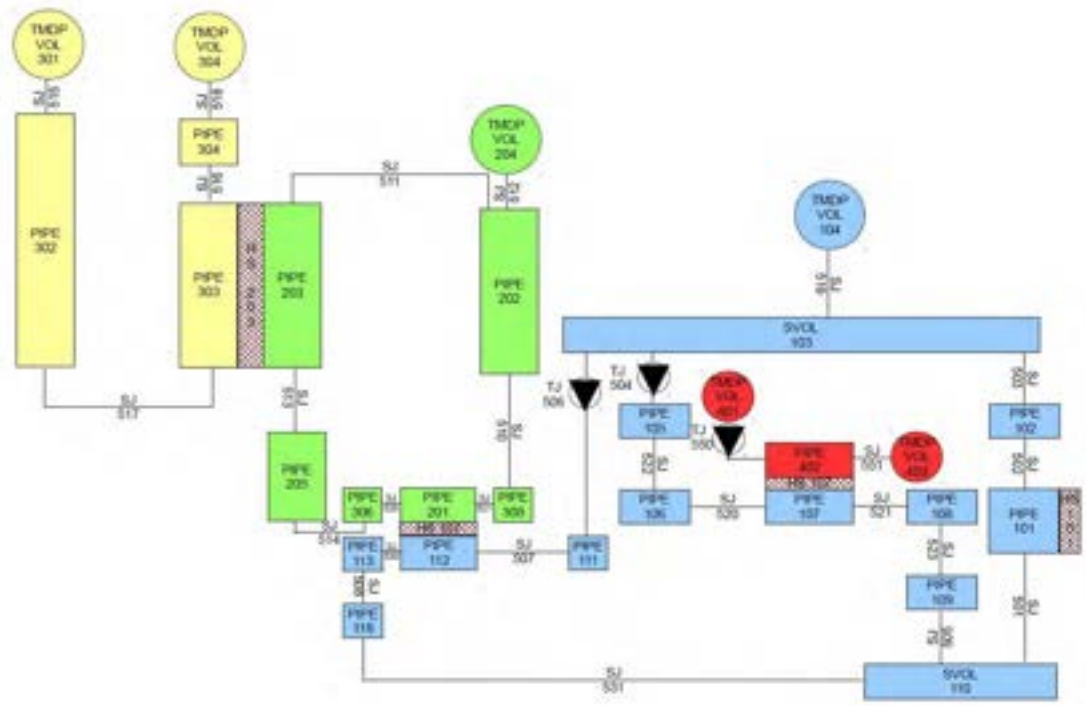

Figure 19. Case 2, Relap5 model: microchannels heat exchanger + air cooled heat exchanger (B+C)

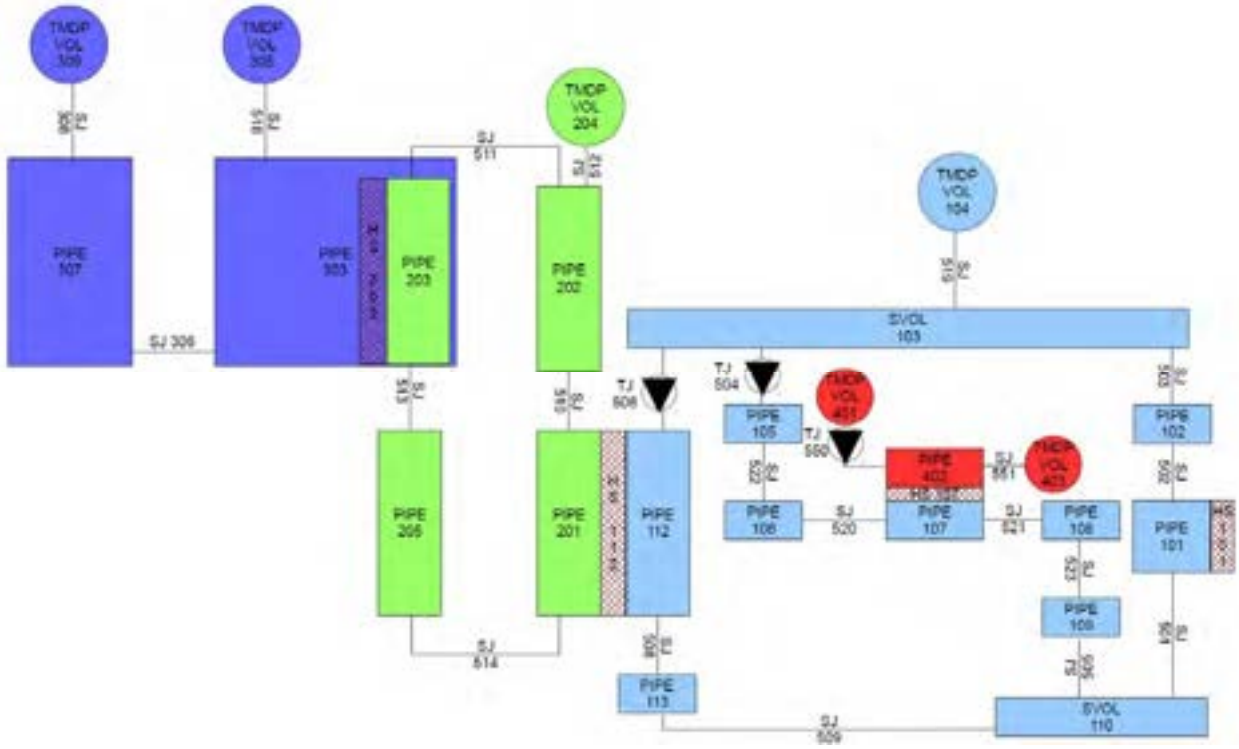

Figure 20. Case 3, Relap5 model: helical coil heat exchanger + isolation condenser (A+D)

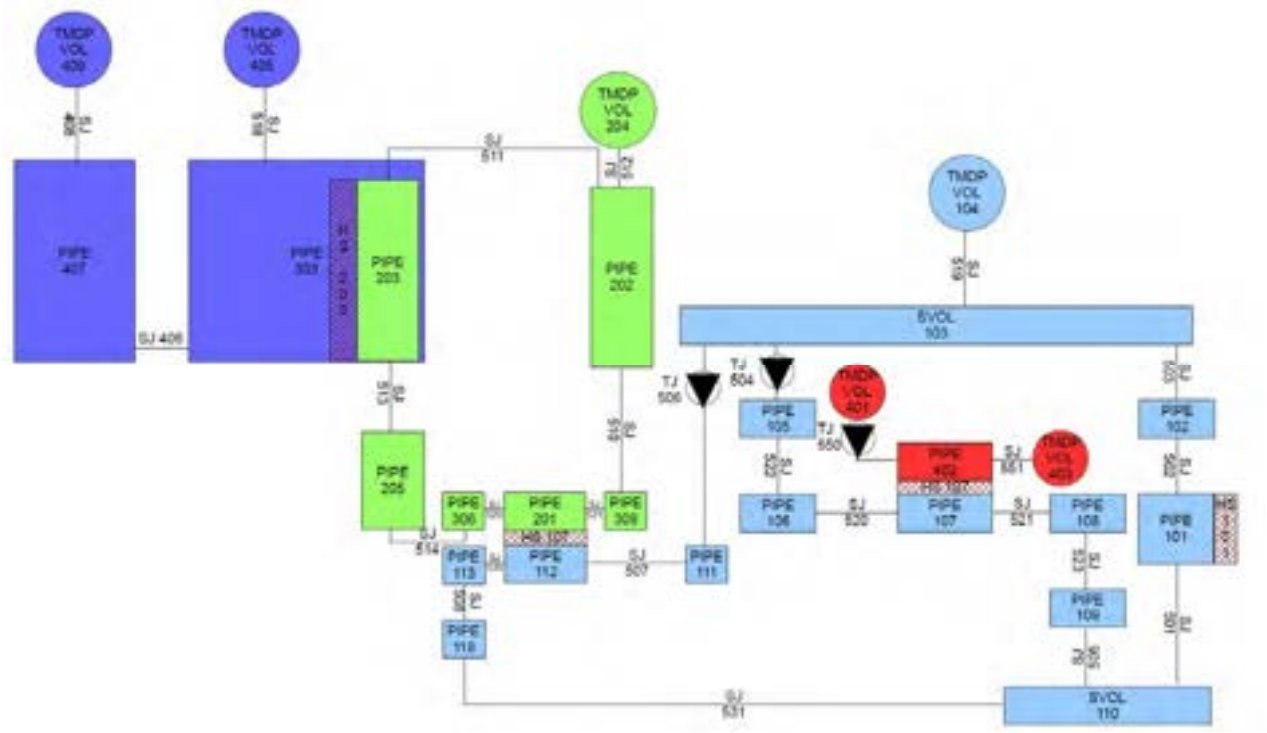

Figure 21. Case 4, Relap5 model: microchannels heat exchanger + isolation condenser (B+D)

The primary system is the one drawn with blue volumes. The core (Pipe 101) is modelled as a single channel made of 10 volumes with more or less 1 m diameter and 3.65 m height, considering a negligible bypass flow rate. The heat structure linked to the core (101) is modelled with an internal heat source, characteristic of the nominal power during full power conditions and of the decay heat after the scram signal. Heat structure 101 is designed in order to simulate the fuel pin, with a cylindrical volume made of UO2, an helium gap and a stainless steel clad. The power during nominal condition is distributed with the characteristic chopped cosine. Adiabatic boundary condition is set on the left side of the heat structure while a convective boundary condition is set on the right side. From the core, the fluid passes into a 10 m riser (Pipe 102) and reaches the upper plenum of the vessel, which works as the pressurizer of the system as for other SMRs. The pressurizer is linked to three safety relief valves with increasing pressure set points starting from 157 bar. From the upper plenum the fluid moves into the annular region beside the riser. In this region, microchannel heat exchangers having 1 m^2 area and 20 cm length are installed (Pipe 107) to remove the heat during full power conditions and transfer energy to the secondary system of the steam production line. Before the heat exchangers for the full power condition primary pumps

(Time dependent junction 504) are installed to ensure the correct flow rate distribution. The other components installed in the annular region are the DHR heat exchangers (Pipe 112), which in this case have an helical coil or microchannel geometry depending on the simulation. During nominal conditions a passive valve (Time dependent junction 506) is set at the inlet of the components to avoid heat losses and isolate the DHR system. By the time the scram signal is sent to the safety system these valves are opened and the flow is permitted, linking the primary system with the intermediate loop. The valve in the model is represented by a time dependent junction with a null flow rate during nominal conditions. When the scram signal is sent and the DHR is called the time dependent junction is substituted with a single junction with a null flow rate initial condition. The annular region ends in the lower plenum of the vessel (Single volume 110), where the refrigerant is sent back to the core to restart the turn.

The secondary loop for the steam production is simplified to the interaction region with the primary system. The model considers a flow rate inlet with a time dependent junction (550) modelling the feedwater pump, the heat transfer region inside the microchannel heat exchangers (Pipe 402) and a pressure outlet boundary condition (time dependent volume 403). During the nominal conditions the flow rate imposed is the nominal flow rate.

The intermediate loop is modelled as a simplified connection loop from the primary system to the final heat sink. The intermediate loop is initially detached from the primary system, and it's initial conditions are of an ambient pressure and temperature. The secondary loop is connected with the primary system with the helical coil/microchannel heat exchanger tank (Pipe 201), which in the case of the helical coil heat exchanger has an area of 0.1315 m^2 and a total length of 8 meters. From the outlet of the heat exchanger, the flow is sent to the final heat sink heat exchanger through a connection pipe (202) which has a diameter of 50 cm and a length of 15 meters. Linked to the connection pipe, a time dependent volume (204) gives the pressure boundary condition for the system. At the time the scram signal is sent, the time dependent volume is substituted with a pressurizer component linked to 3 safety relief valves. The fluid in the intermediate loop is thermally linked to the final heat sink with pipe 203, which is the equivalent condensed pipe of the air heat sink heat exchanger or the isolation condenser depending on the simulation. As the fluid is

cooled in the final heat sink, the flow is redirected to the intermediate heat exchanger to remove once again the decay heat.

The final heat sink is the only system whose components are completely different depending on the solution (air heat sink or isolation condenser) and the description will be given hereafter.

5.1 The intermediate heat exchanger

The intermediate heat exchanger configurations are a helical coil heat exchanger or a microchannel heat exchanger. The two configurations are comparable since they have been designed considering an equal outer surface area on the primary system side. The helical coil heat exchanger has been modelled following the instruction of the Idaho national laboratory [58], which suggest to use an equivalent inclined pipe whose length and height is the same as the real coil. The heat exchanger is made of 304 helical coils set in parallel with a length of 38 meters. The refrigerant passes inside the helical pipes while the intermediate loop water passes on the shell side in a closed tank inside the RPV. The microchannel heat exchanger is a scaled-down component whose geometry is the same as for the microchannel heat exchangers used for the steam production line. It has 510 000 parallel microchannels with square cross section of 1 mm. The detailed dimensions of the components are reported in the appendix.

5.2 The final heat sink

The final heat sink configurations are an isolation condenser system and an air heat exchanger. Since the two system have an high difference in heat transfer (one is made with water while the other with air) the common point for the system is the difference in height between the intermediate heat exchanger and the final heat sink, which has been fixed at 15 meters. The surface area ratio between the two solution is around 2.55.

5.3 Accident sequences

The accidental sequences simulated are two. The first accident sequence is simulated in two cases using the helical coil heat exchanger configuration. In a first case the ultimate heat sink is constituted by the air heat exchanger while in the second case the isolation condenser has been

used. The accidental sequence in this case is made in the following way. Considering the initial conditions of 100% power for the reactor and of ambient pressure and temperature for the intermediate loop and for the final heat sink, at t=0 the scram signal is sent and in parallel the pumps are blocked. In that moment, the valve set at the inlet of the DHR is opened and the amount of fluid initially contained in thermal equilibrium with the intermediate loop is sent to the bottom of the downcomer. As the valve is opened, natural circulation is established in the three loops: the intermediate loop is heated and the power starts to be removed.

The second accident sequence is made considering 4 cases. The DHR heat exchanger is an helical coil heat exchanger or a microchannel heat exchanger and the ultimate heat sink is an air heat exchanger or an isolation condenser. The four simulations are created by the mutual combinations of the two couples of heat exchangers. What is considered in this case is the mechanical inertial of the pump for the first 100 seconds of the transient. In that period of time, a decreasing flow rate is imposed in the primary system and the nominal secondary system is able to remove thermal power. After 100 seconds the pumps are substituted by single junctions and the flow rate is completely dependent on natural circulation. The other hypothesis of the accidental sequence are the same of the previous one.

6 Simulations results: steady state conditions

For the comparison of the heat exchangers during a steady state condition where two fluids defined by their flow rates, inlet and outlet temperatures and outlet pressures exchange a finite amount of power, the reference conditions taken are the ones of the I^2S reactor. The conditions of the fluids and of the power exchanged are depicted in Table 4. The thermal power and flow rates considered are the ones of ¼ of the reactor. The design of the heat exchanger has been made considering the steady state, full power conditions. The objective of the comparison is to evaluate their characteristic features considering the design conditions and their variations for different power loads

Table 4. Characteristics of the fluids

Parameter	Value	Unit measure
Primary water inlet temperature	325.75	°C
Primary water outlet temperature	223	°C
Secondary water inlet temperature	293.72	°C
Secondary water outlet temperature	284.85	°C
Primary flow rate	4105.3	Kg/s
Secondary flow rate	2213	Kg/s
Thermal power	756447.4	kW
Primary pressure	155	bar
Secondary pressure	69.2	bar

In order to perform a comparison on the two configurations two type of heat exchangers are designed in terms of geometry and surface area and their characteristics are here shown and compared. The geometric characteristics of the microchannel heat exchanger, the helical coil heat

exchanger as well as the heat sink heat exchangers (air cooled and water cooled) are shown in Table 5 [51].

Table 5. Heat Exchangers main data

A Helical Coil HX		B Compact HX Microchannel		C Air cooled HX		D Water cooled HX Isolation Condenser	
Number of tubes	304	(Microchannels)		Tower Height [m]	25	(Straight pipes)	
Length [m]	38.32	Primary Channels	510 000	Heat Exchanger Height [m]	5.1	Number of tubes	53 182
Internal diam. [mm]	10.74	Secondary Channels	510 000	Diameter [m]	4.19	Internal diam. [mm]	7.93
External diameter [mm]	13	Channel length [mm]	192.4	External Tubes Diameter [m]	0.0053	External diameter [mm]	9.6
Inclination [deg]	12.07	Channel width [mm]	1	Internal Tubes Diameter [m]	0.0044	Heat transfer area [m2]	2 656
Total height [m]	8	Channel height [mm]	1	Number of tubes	56 408	Length [m]	2
Heat Exch. Area [m2]	**393**	Channel pitch [mm]	2	pitch/D	1.60	Pool area [m2]	202
Tank diameter [m]	0.7	Heat Exchanger Height [m]	7.5	Inclination of the tubes [deg]	-32.70	Water storage [t]	1 006
Number of rows	3	**Heat Exch. Area [m2]**	**393**	Heat Exchange Area [m^2]	8 865.8	Pool height [m]	5

The presentation of the results is organized in the following way. First, the results from the full power steady state condition will be presented and a comparison is made considering surface areas, pressure losses and volumes. Then, a parametric analysis on the behaviour of the power removed as a function of the primary system temperatures will be made.

6.1 Full power, steady state condition

Table 6 shows some characteristic features of the two heat exchangers taken into account. To transfer the same amount of power between the fluids a helical coil heat exchanger requires twice the surface area needed by a microchannel heat exchanger.

Table 6. Results from the steady state simulation

	Helical coil HX	Microchannel HX	Ratio
S [m2]	1444.4	692.64	2.09
ΔP II [kPa]	47.53	20	2.38
ΔP I [kPa]	6.468	53.55	0.12
V I [m3]	9.299	0.173	53.70
V II [m3]	4.69	0.173	27.11
V metal [m3]	2.18	1.39	1.58
V tot [m3]	16.18	1.732	9.34
Compactness [m2/m3]	89.28	400	0.22

The increase in heat transfer is paid at the price of non-negligible pressure drops on the primary system because of two characteristic features

- Microchannel heat exchangers have an horizontal configuration which nullifies the pressure gain by the elevation change provided by a vertical configuration,
- Microchannel heat exchangers create narrow channels for the primary flow rate which are not present in a shell and tube configuration such as the one of the helical coil HX.

From the point of view of the volumes of the components microchannel heat exchangers offer an extreme compact solution with respect to the helical coils, and one order of magnitude is present between the compactness ratios. The major difference between the volumes is provided by the space available for the fluids inside the component, while the volume for the metal parts is comparable.

The next figures shows the behaviour of temperatures, pressures and heat flux exchanged inside the heat exchangers. All the behaviours are set as a function of the percent surface area crossed.

From figure 22 it is possible to observe the pressure gain by the helical coil configuration and the pressure reduction of the microchannel geometry inside the primary system. From the point of view of the secondary system figure 24 shows the pressure behaviour. The microchannel configuration is particularly affected by the presence of subcooled boiling in the last part of the channels. From the point of view of the helical coil heat exchanger the presence of two phase flow has a low effect on

the pressure profile. The heat flux is different in amplitude between the two solutions (figure 25) and the microchannel heat exchanger is able to transfer higher values of thermal power per unit area.

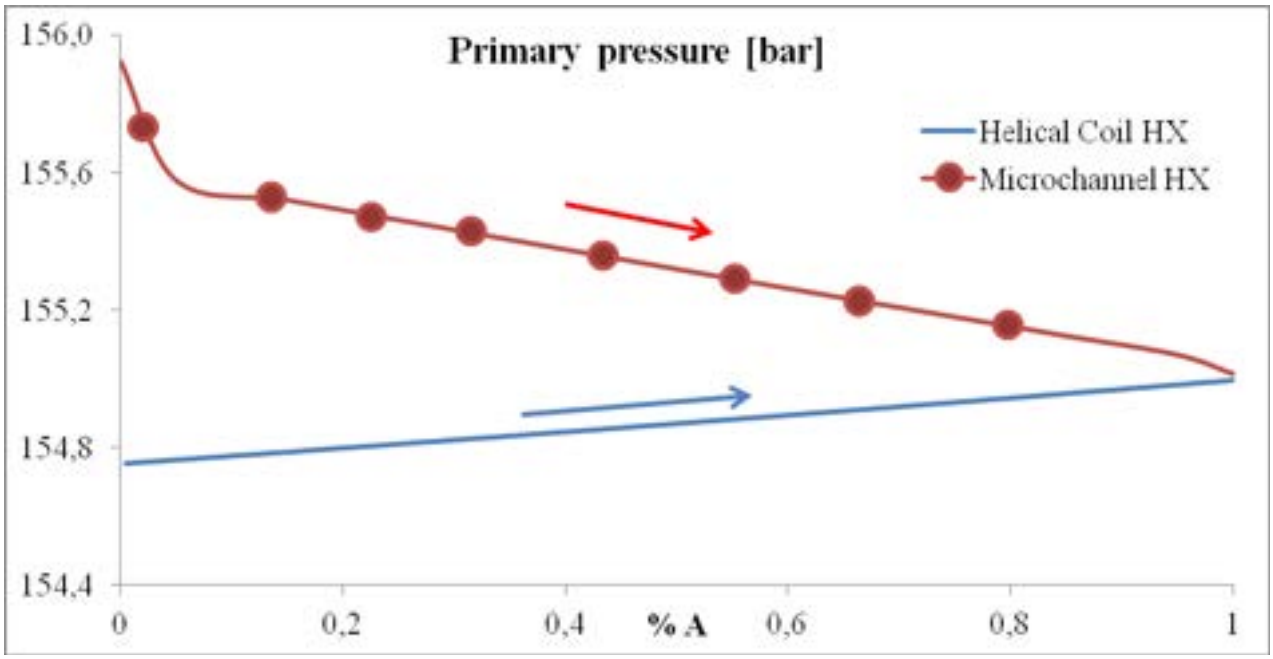

Figure 22. Primary pressure (Case: steady state)

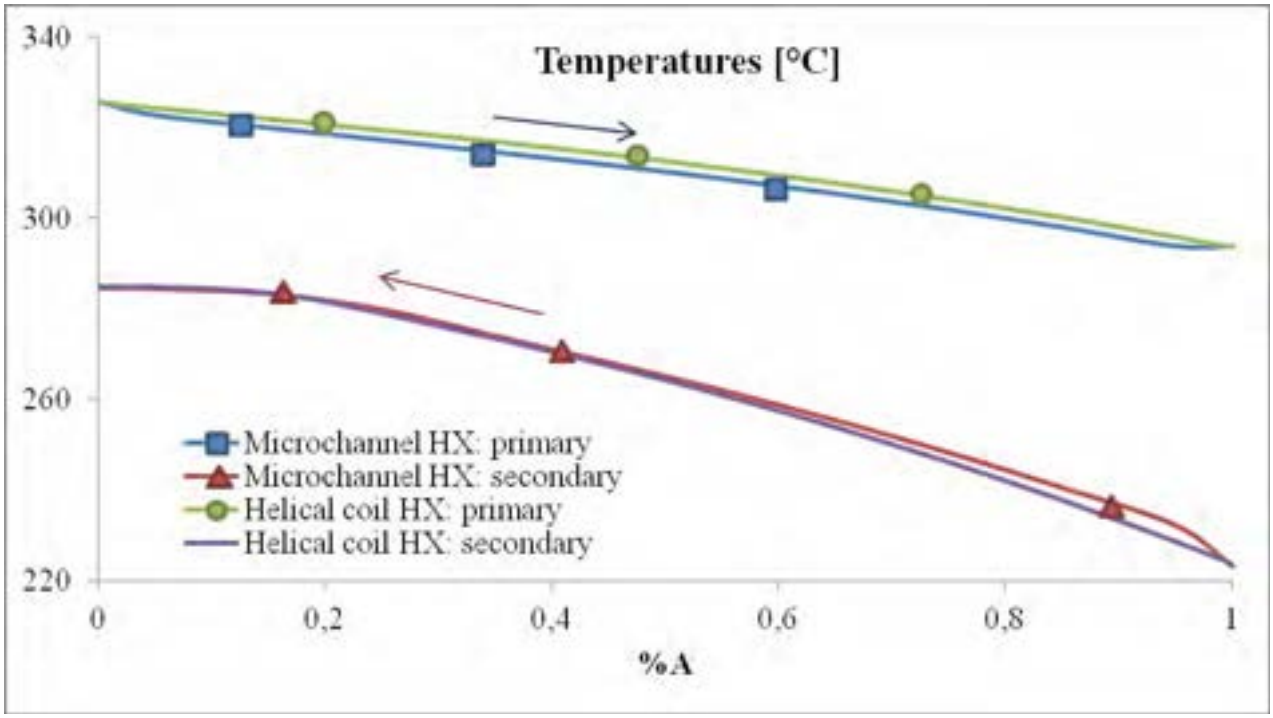

Figure 23. Temperatures (Case: steady state)

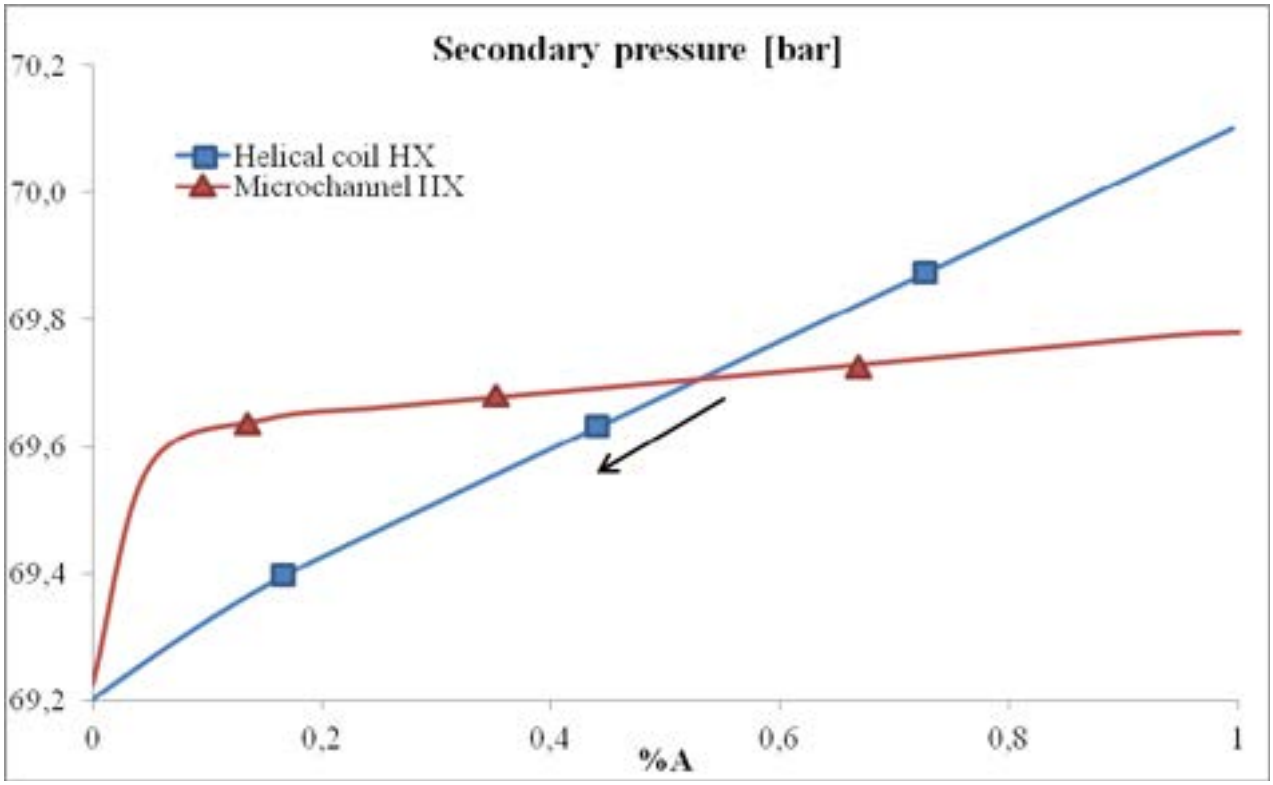

Figure 24. Secondary pressure (Case: steady state)

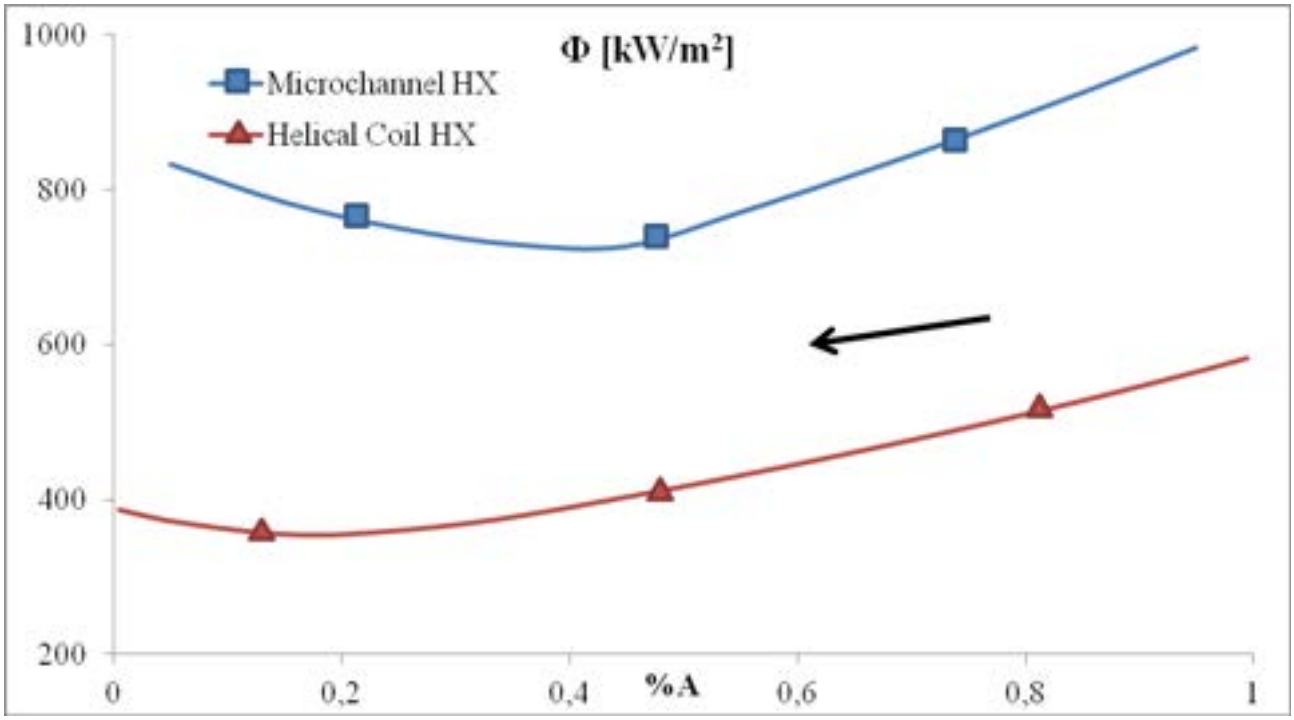

Figure 25. Heat flux (Case: steady state)

6.2 Power load effect

In order to perform a parametrical analysis on the behaviour of the heat exchanger as a function of the power fraction with respect to the nominal values, an analysis on the behaviour of primary temperatures as a function of the power conditions of the reactor has been made. The geometrical configuration of the heat exchangers are those described for the full power configuration. The condition set to the primary temperatures is to consider a constant value of the average primary temperature as in equation 1.

$$\overline{T}_l = \frac{T_{l,in} + T_{l,out}}{2} = constant \quad (1)$$

Figure 26 shows the general layout of the model.

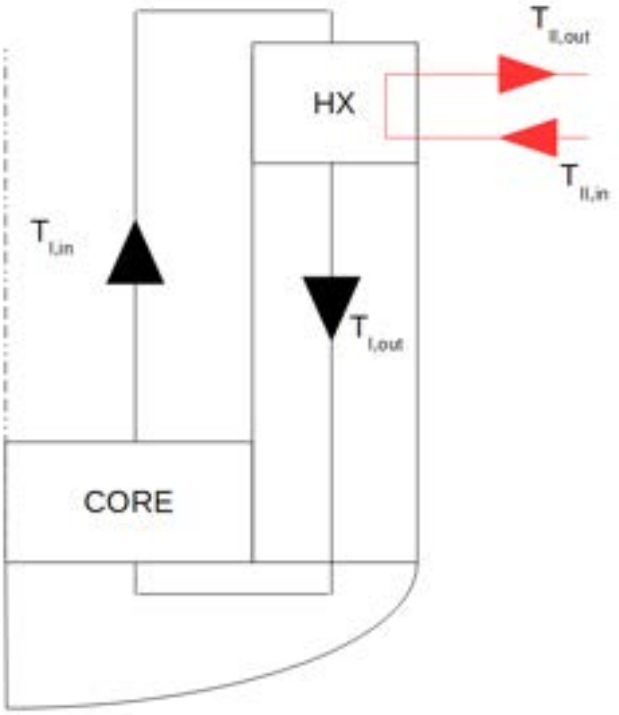

Figure 26. General layout of the model for power load analysis

The primary temperature behaviour as a function of the power load fraction is shown in figure 27. Inlet and outlet temperatures tends for the average temperature as the power load is reduced.

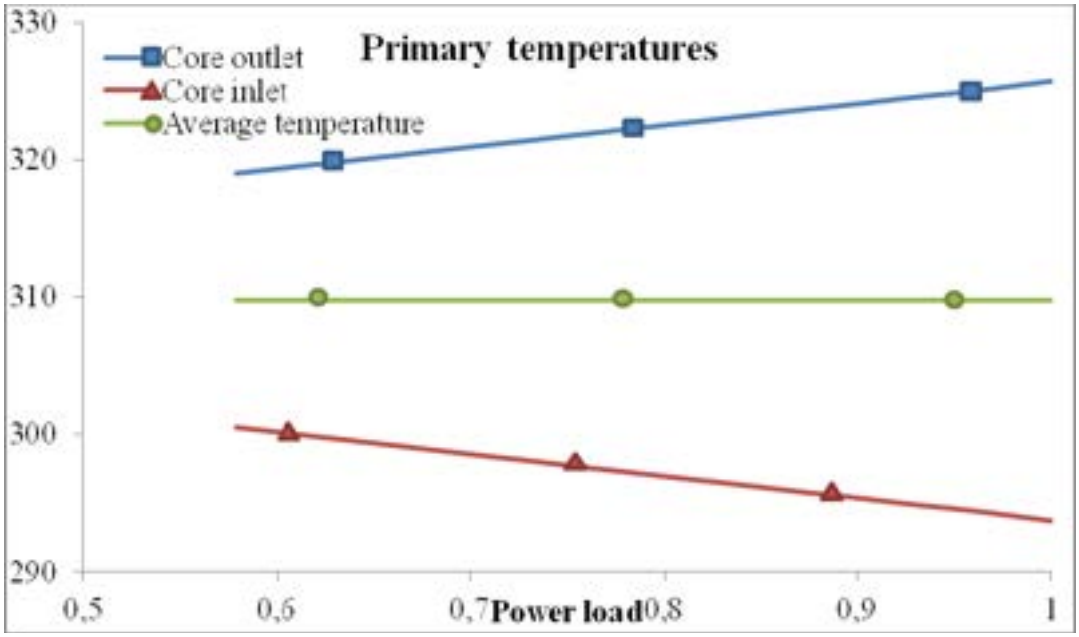

Figure 27. Primary temperatures (Case: steady state, power load variation)

Another condition of the analysis is to consider a constant value of the flow rates both in the primary and secondary side.

$$W_I = constant \quad (2)$$

$$W_{II} = constant \quad (3)$$

For each power level taken into account, the inlet and outlet temperatures on the secondary side have been obtained, and the average global heat transfer coefficient have been calculated on the basis of equation 4.

$$U = \frac{\Phi}{A\ \Delta T_{ml}} \quad (4)$$

Figure 28 shows the behaviour of the average heat transfer coefficient normalized with respect to the value obtained at full power as a function of the power load. As it can be seen in figure 28, the global heat transfer coefficient obtained with the helical coil configuration shows a linear behaviour in the high power load region. The microchannel configuration has a more complex behaviour and has a greater dependence on the conditions of the fluids rather than the helical coil configuration. The global heat transfer coefficient has a lower degradation in the high power load region in the case of the helical coil geometry, while in the low power region the global heat transfer enhancement due to the increase of boiling region in the secondary side has a greater impact for the microchannel configuration. Further studies are required to assess the effect of thermal resistances on the global heat transfer coefficient behaviour. Figure 29 reports the behaviour of the mean logarithmic temperature for counter-current flow as a function of the power load, while the power load as a function of the primary system inlet temperature is depicted in figure 30.

The results show that the microchannel heat exchanger has a less predictable behaviour in lower power load regions, and further studies are required to assess the effects of single parameters on its power removal efficiency. From the point of view of the helical coil configuration the component shows a more stable behaviour in the high power level region with a lower effect on its performance on the conditions of the fluids.

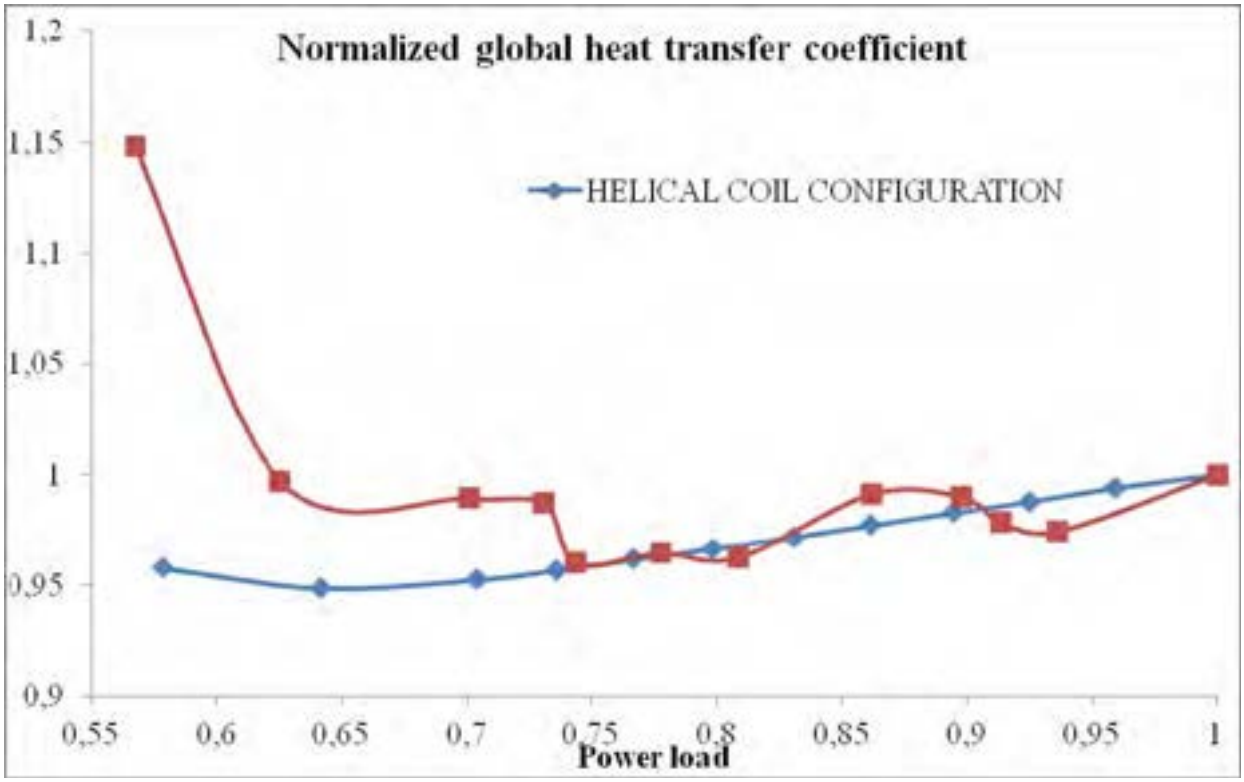

Figure 28. Normalized global heat transfer coefficient (Case: steady state, power load variation)

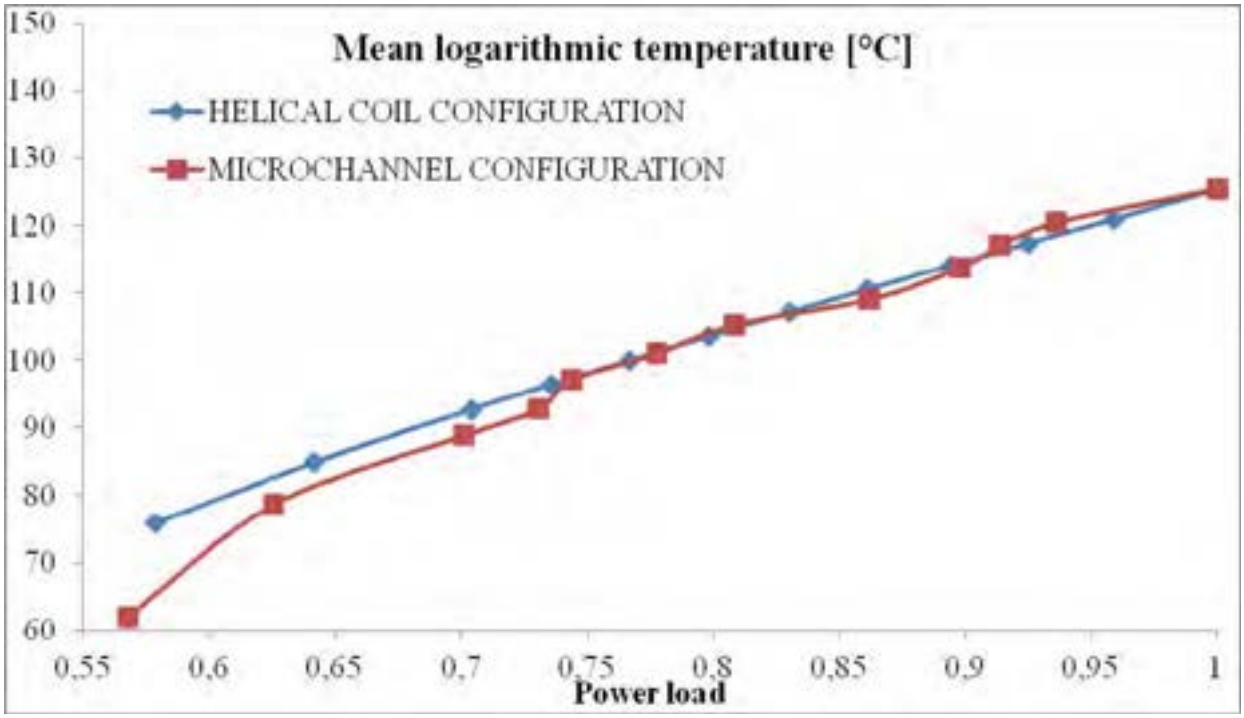

Figure 29. Mean logarithmic temperature (Case: steady state, power load variation)

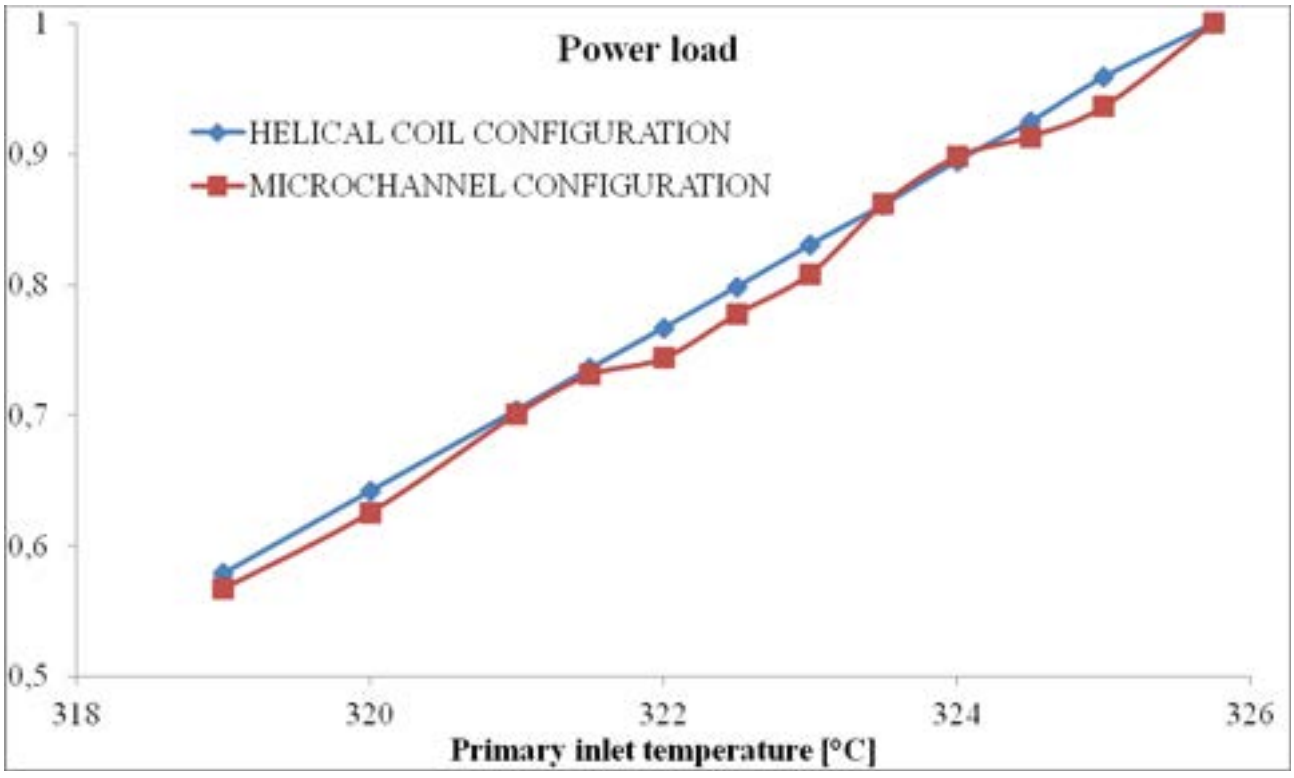

Figure 30. Power load as a function of the inlet temperature (Case: steady state, power load variation)

7 Simulations results: accident conditions with pump inertia neglected

Two simulations were performed to analyse the system response of a system black out and instantaneous pump shut down with consequent isolation of the primary system from the steam production line. The two simulations are recalled in Table 7. By the time the accidental sequence starts (t=0) the pumps are stopped and substituted with single junctions, the core power is set from the hot full power conditions to the 7% of power and subsequently it will follow the standard decay heat curve for UO_2 fuel. At the beginning of the transient, the DHR system is set in thermal contact by the actuation of a valve inside the RPV. The detailed description of the models and of the hypothesis of the accidental transient are reported in Chapter 5.

Table 7. Simulations performed

DHRS configuration	In-vessel HX (DHR heat exchanger)	External HX (Ultimate heat sink)
Case 1 (A+C)	Helical Coil Heat Exchanger (A)	Air Cooled Heat Exchanger (C)
Case 3 (A+D)	Helical Coil Heat Exchanger (A)	Isolation Condenser (Pool) (D)

In the following chapter, the results obtained from the two simulations will be presented separately in order to describe the system response and create a base for the comparison.

7.1 Case 1: Helical Coil Heat Exch. (A) and Air Cooled Heat Exch. (C)

In this first simulation the DHR heat exchanger is constituted by the helical coil heat exchanger, while the final heat sink is constituted by the air heat exchanger.

Primary pressure

The primary pressure behaviour is shown in figures 22, 23 and 24 Figure 22 shows the primary pressure at the beginning of the transient. As the primary system is isolated from the steam production loop the DHR system is not able to remove the amount of power needed in the very first moments of the transient, so the pressure of the system increases until it reaches the value of 160 bar where the safety relief valves on the top of the vessel are forced to open and a mass fraction of the primary inventory is released in the primary containment. The mass fraction lost with respect to the total mass inventory is in the order of the 4%. As the intermediate loop starts to remove thermal power the pressure of the primary system starts decreasing.

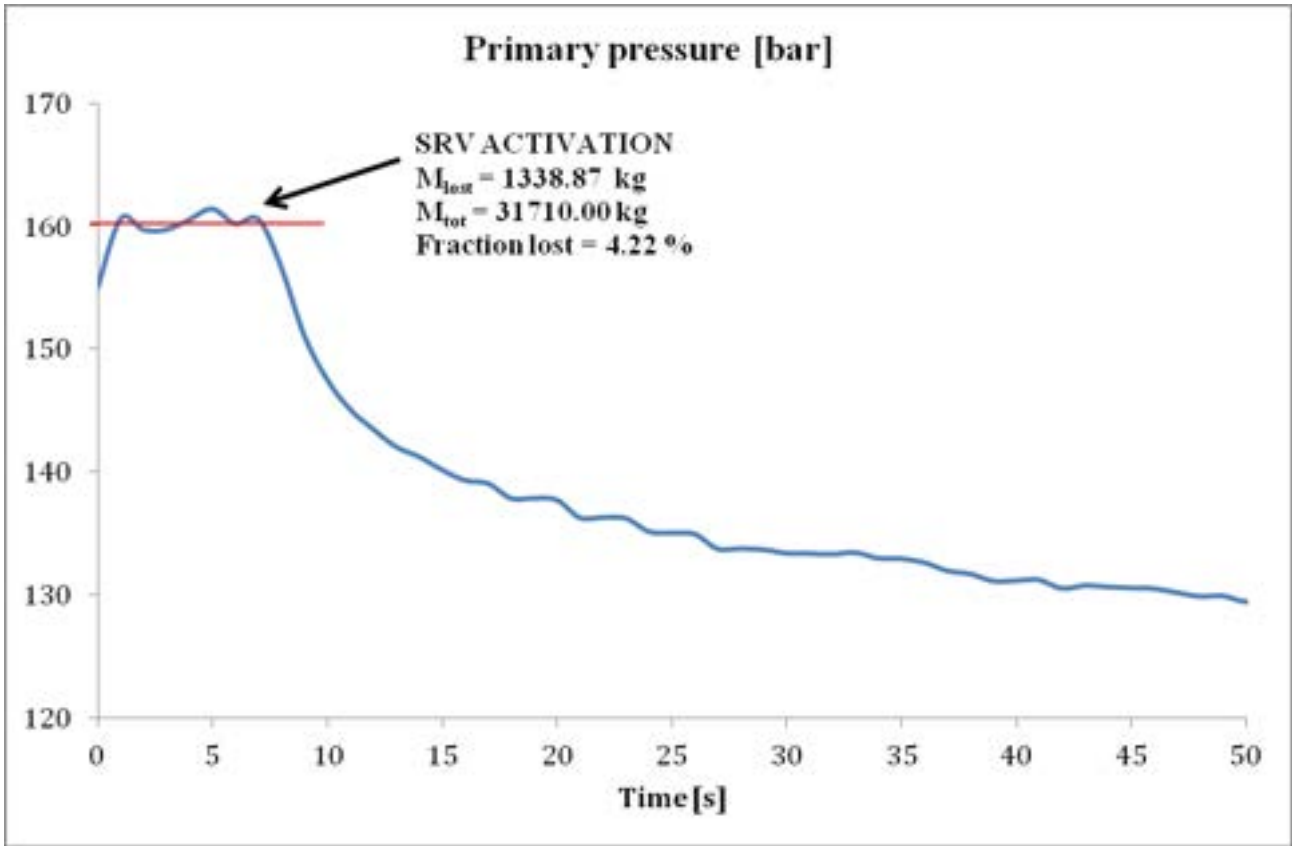

Figure 31. Primary pressure at the beginning of the transient (Case 1)

Figure 23 shows the primary pressure in the first 2 hours. In this part of the transient, several regions are of importance to be characterized. In the first 1000 seconds, a pressure plateau in the range of 120-140 bar is shown, and this is explained by the fact that during this part of the transient the intermediate loop is in hot temperature and pressure conditions but the power removed by the air heat exchanger is low. As the power removed by the air HX increases the energy starts to be transferred to the environment and the primary system experiences a rapid pressure decrease down to the value of 40 bar. When the power produced by the decay heat and the power removed by the DHR first matches the pressure has a second plateau in the first hour of the transient.

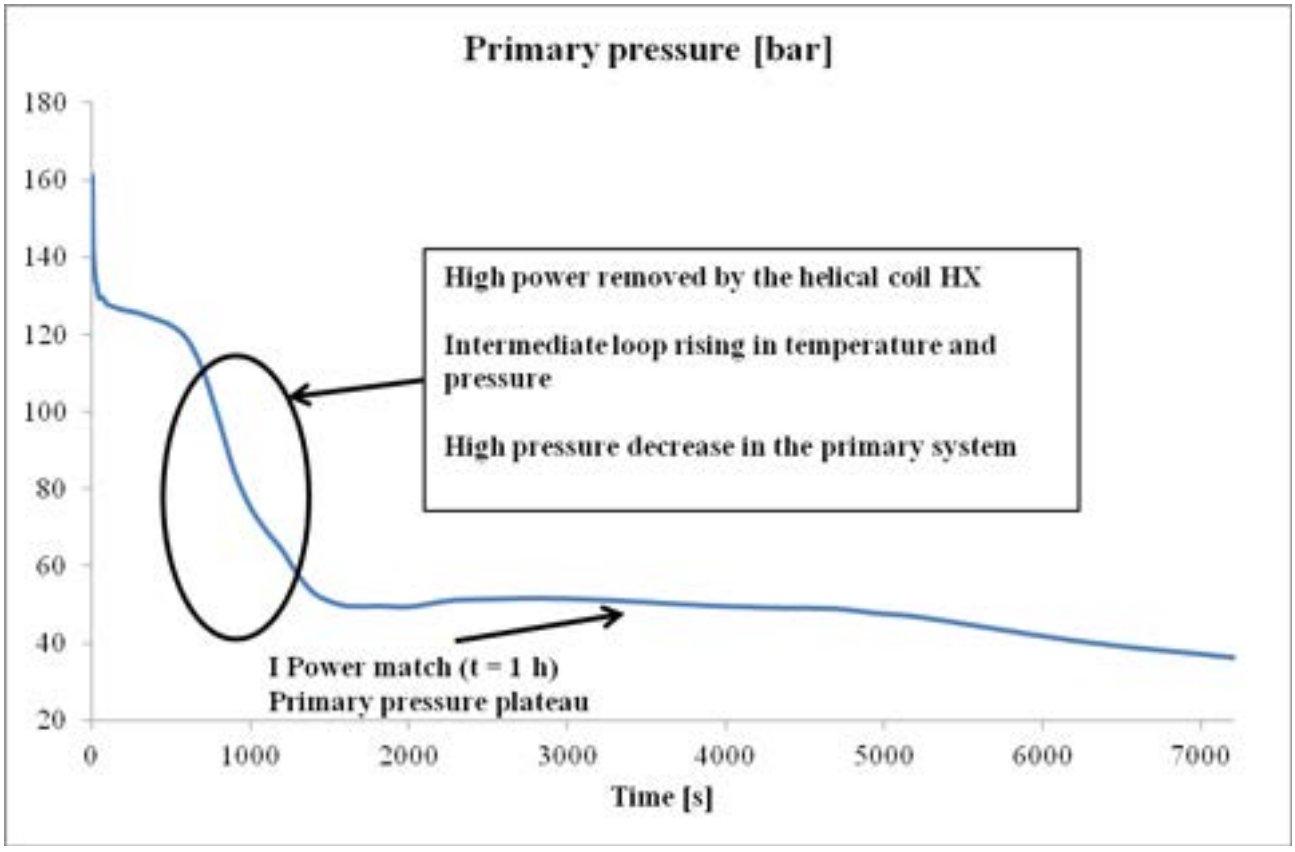

Figure 32. Primary pressure in the first 2 hours (Case 1)

Figure 24 shows the behaviour of the primary pressure during the total time of the transient. After the first 2 hours of the transient the pressure continues to decrease reaching the value of 1.5 bar after 72 hours.

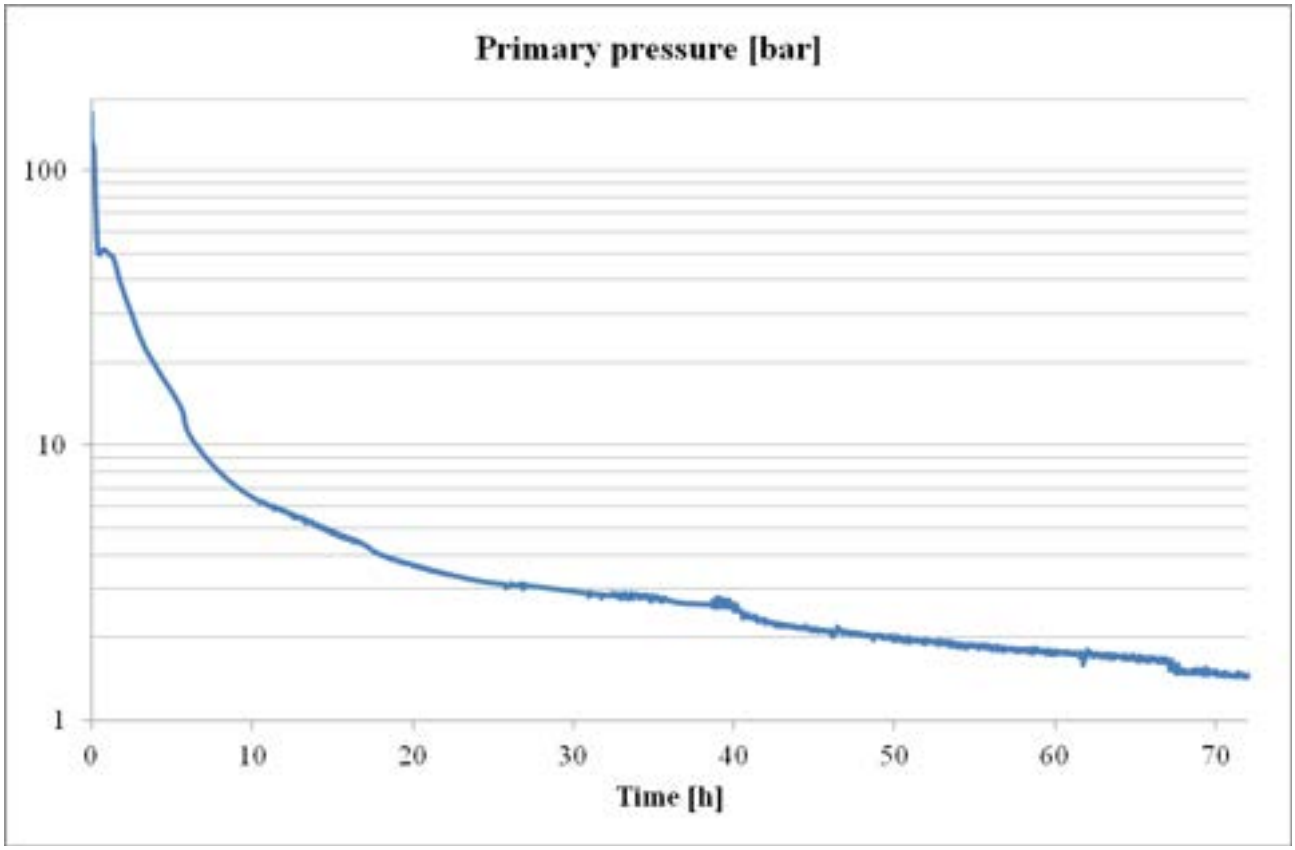

Figure 33. primary pressure (Case 1)

Primary temperature

Figures 25 and 26 shows the behaviour of the primary temperature. The first 10 hours of the transients are depicted in figure 25. As it can be seen, several regions can be found. From the very first moments of the transient the outlet temperature reaches the saturation temperature and steam is produced inside the core. The inlet temperature experiences a very high decrease due to the cold water storage inside the DHR. After that the inlet temperature starts increasing as the power removed by the DHR is lower than the power produced. After the first hour the power removed increases and this provide a second inlet temperature decrease. The outlet temperature decreases with the saturation temperature as the pressure is reduced. In the long term of the transient (figure 26), inlet and outlet temperature decreases and the steam produced is reduced. In the very last part of the transient, inlet temperature approaches the saturation temperature and small amounts of steam are produced in the bottom region of the core.

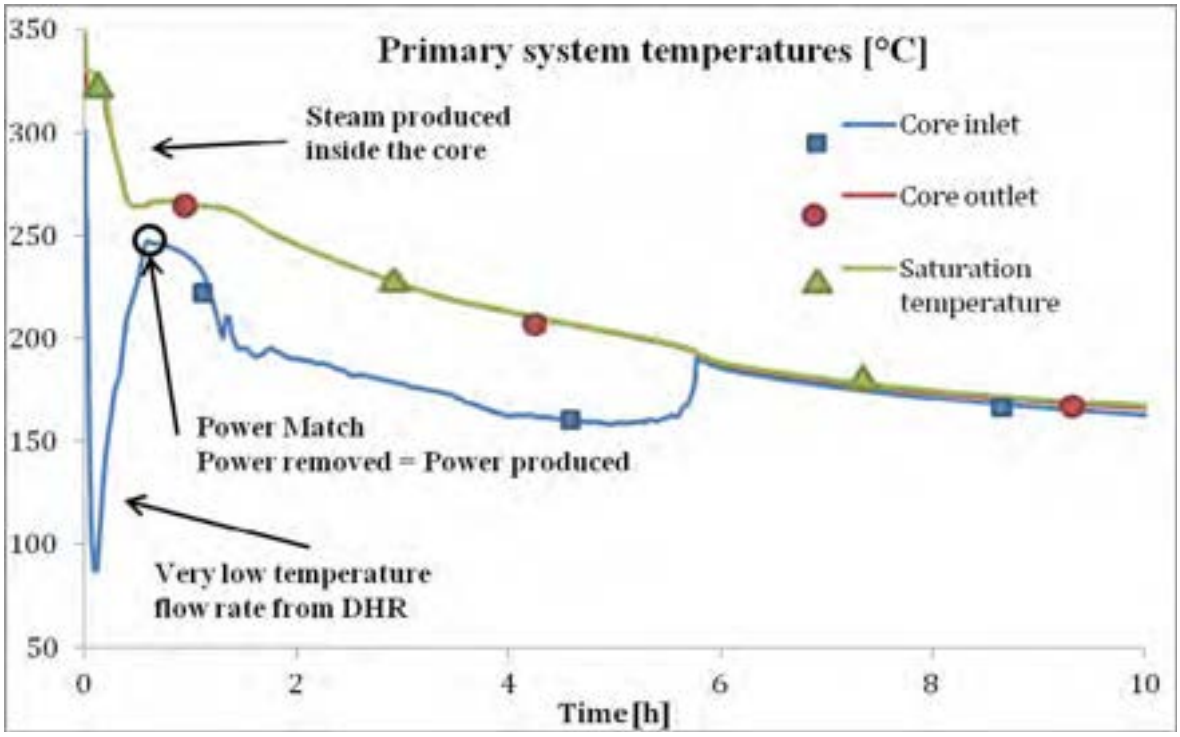

Figure 34. Core temperatures in the first 10 hours of the transient (Case 1)

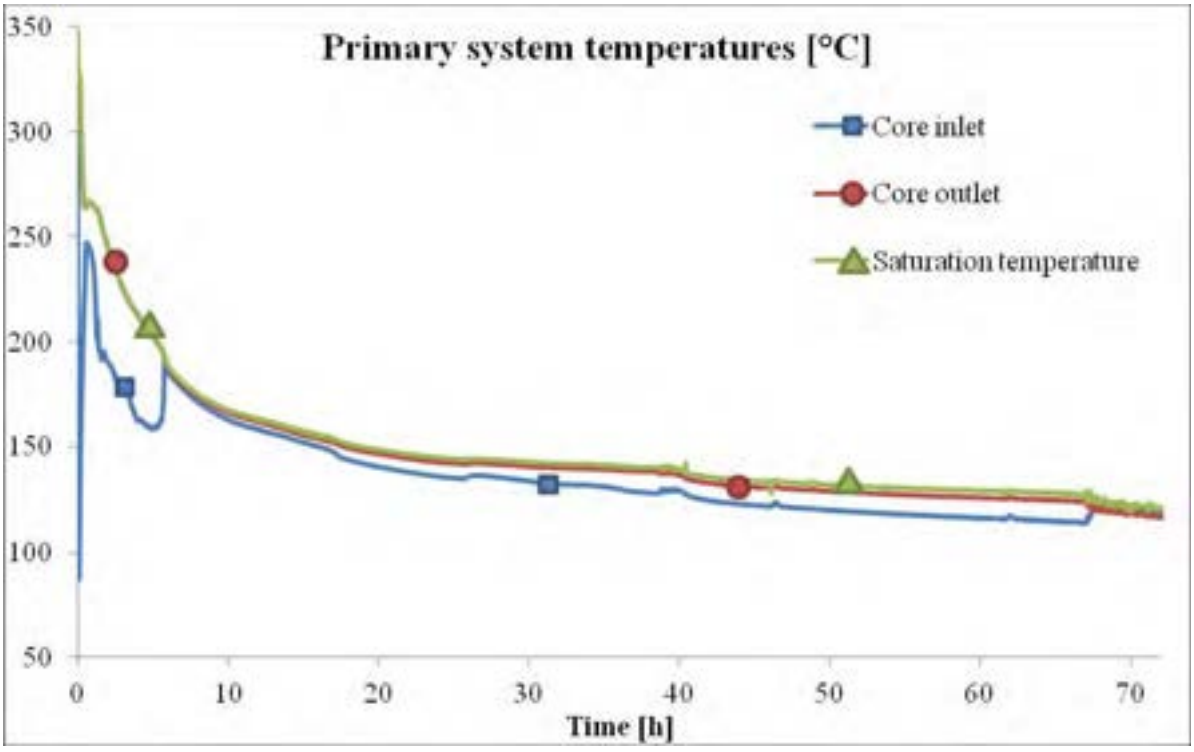

Figure 35. Primary temperatures during the transient (Case 1)

Primary flow rate

Figures 27 and 28 shows the behaviour of the core flow rate during the transient. In the first 10 hours of the transient (figure 27) the flow rate has two characteristic regions: a first one where the higher subcooling produces a low natural circulation head inside the core, and a second one where the enthalpy increase is reduced and the increase of steam production provides a larger density variation between hot leg and cold leg. These two regions can be distinguished by two different flow rate average values.

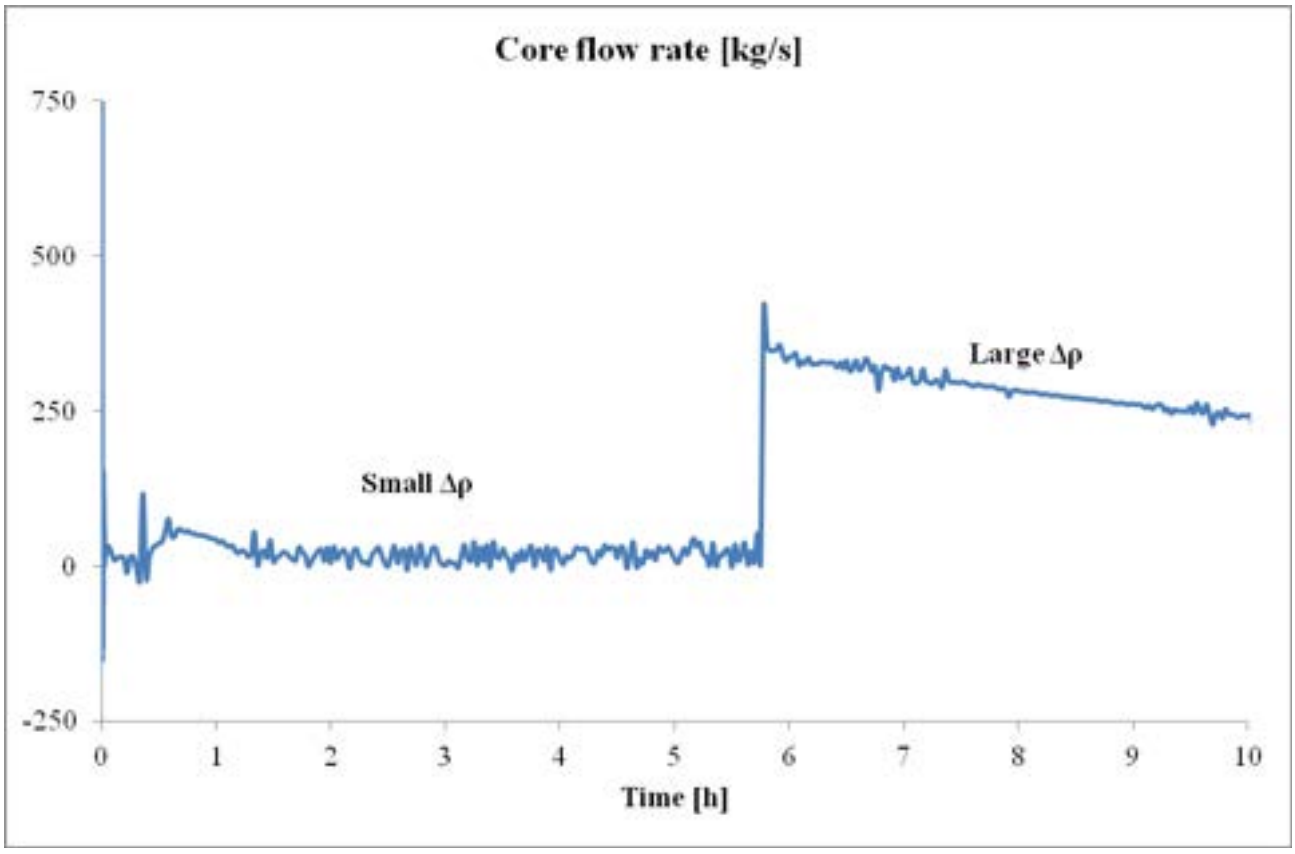

Figure 36. Core flow rate in the first 10 hours (Case 1)

As the transient continues (figure 28), the flow rate at the inlet of the core shows an unstable behaviour due to complex effects of steam production, condensation and pressure change. As the pressure is reduced, in the last part of the transient flow rate oscillations become higher.

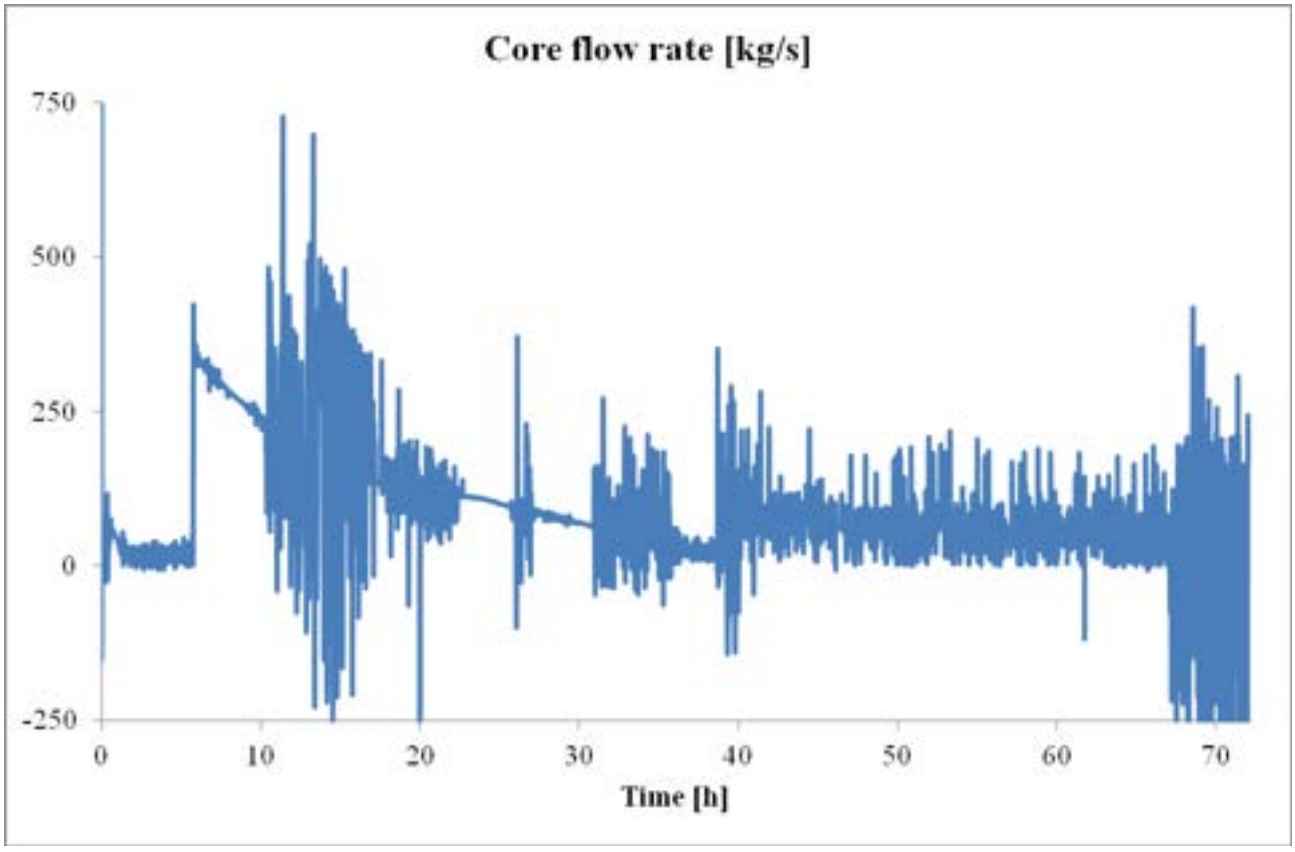

Figure 37. Core flow rate (Case 1)

Intermediate loop pressure

As far as the intermediate loop is concerned, the system experiences a rapid pressure increase in the first seconds of the transient with several oscillations starting from ambient conditions until it reaches the maximum value of 23.5 bar. Once the maximum pressure is reached the system starts its slow depressurization, and the lowest value obtained after 72 hours is the one of 11 bar (see figure 29).

The pressure oscillation at the start-up of the system can be seen in figure 30: the maximum recorded amplitude is in the order of 1.5 bar after 20 seconds from the scram. As the pressure increases the amplitude of the pressure waves reduces.

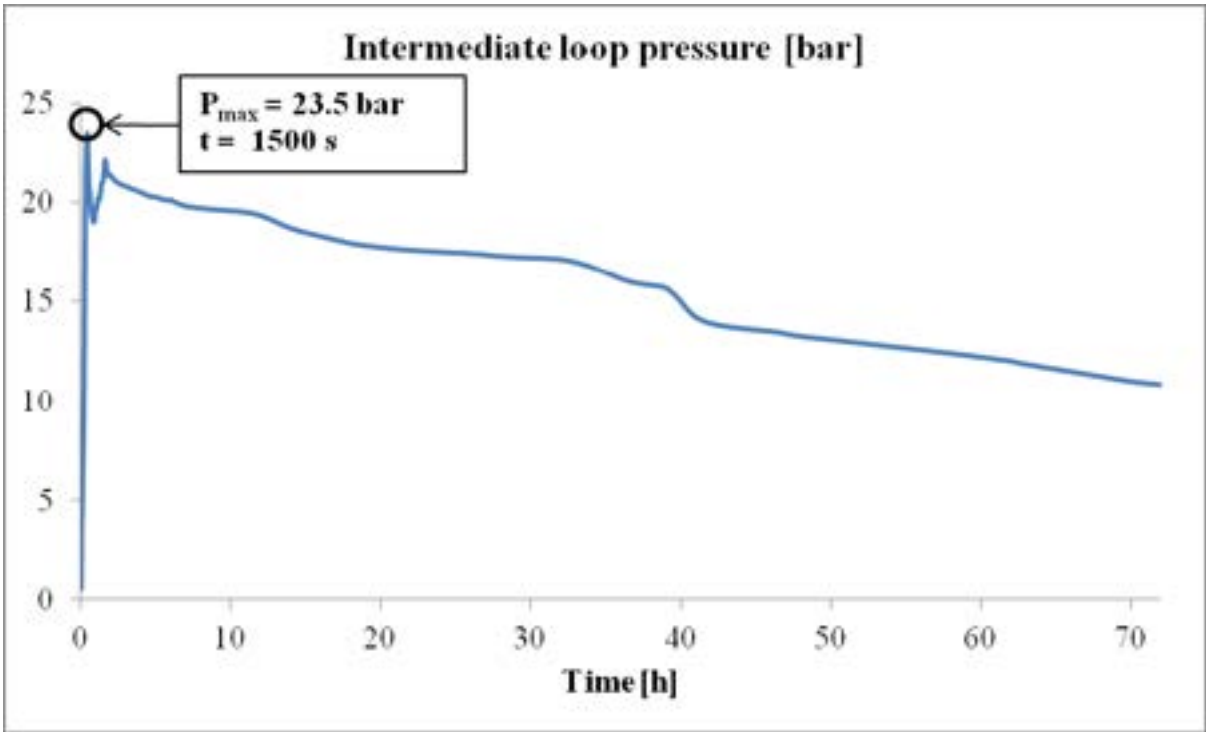

Figure 38. intermediate loop pressure (Case 1)

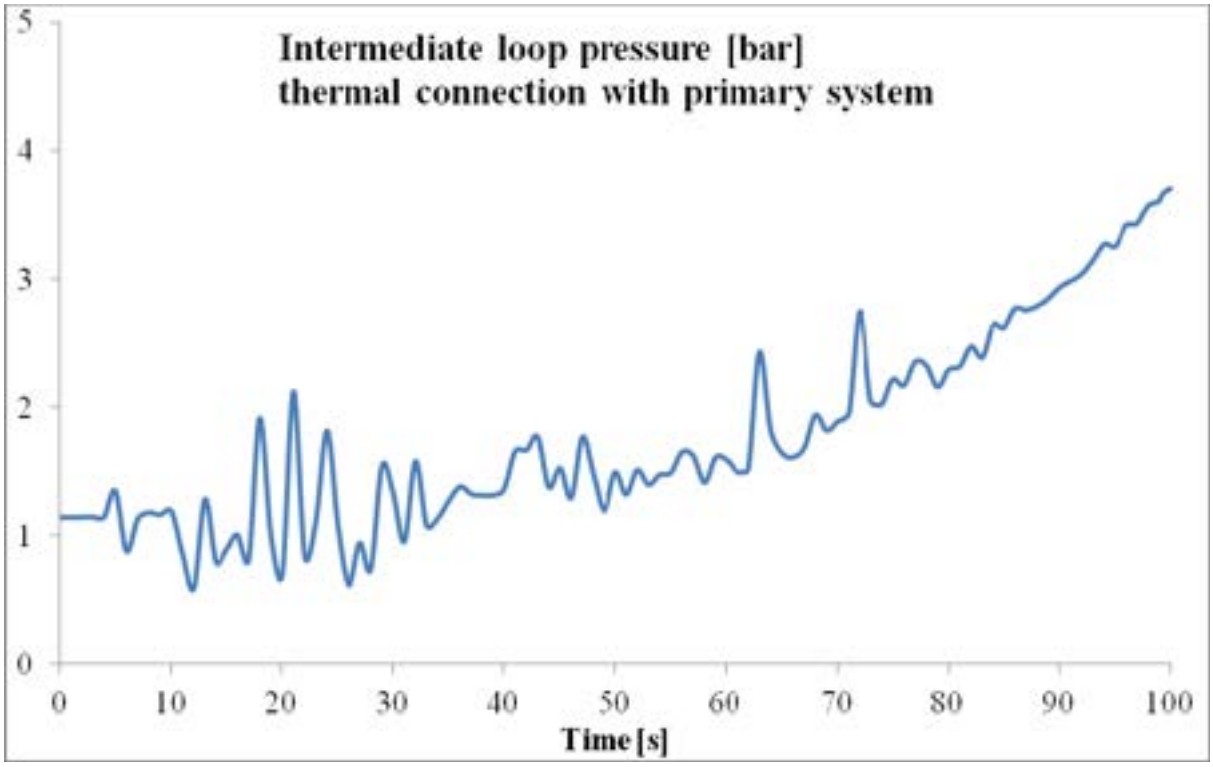

Figure 39. Intermediate loop pressure at start-up (Case 1)

Intermediate loop temperatures

The inlet and outlet temperatures of the helical coil heat exchanger in the intermediate loop side can be seen in figures 31 and 32. Figure 31 shows the behaviour of the temperatures at the beginning of the transient. Pressure wave oscillations affects the behaviour of the saturation temperature. The outlet temperature is firstly affected by the different values of power absorbed by the primary system, while the inlet temperature remains nearly constant until a first turn of the loop is done by the water; after the first turn the temperature starts increasing because the air heat exchanger is removing a lower power. As it can be seen the secondary loop remains in single phase condition.

Figure 32 depicts the behaviour of the intermediate loop temperatures during the whole transient. As the maximum value is reached in the first half an hour of the transient, the temperatures starts decreasing in parallel keeping a nearly constant temperature difference of 20°C. During the whole transient the maximum temperature remains lower than the saturation temperature.

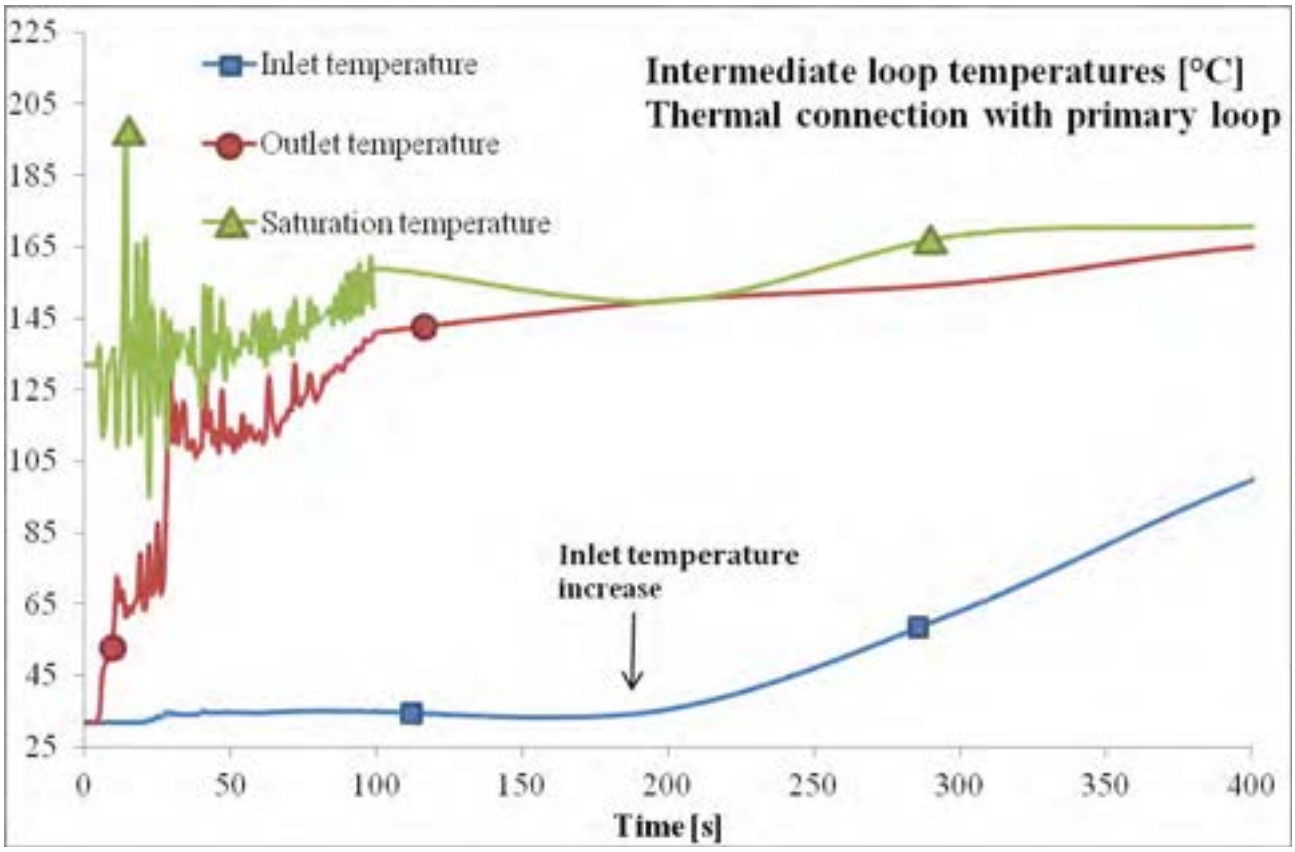

Figure 40. Intermediate loop temperatures at start-up (Case 1)

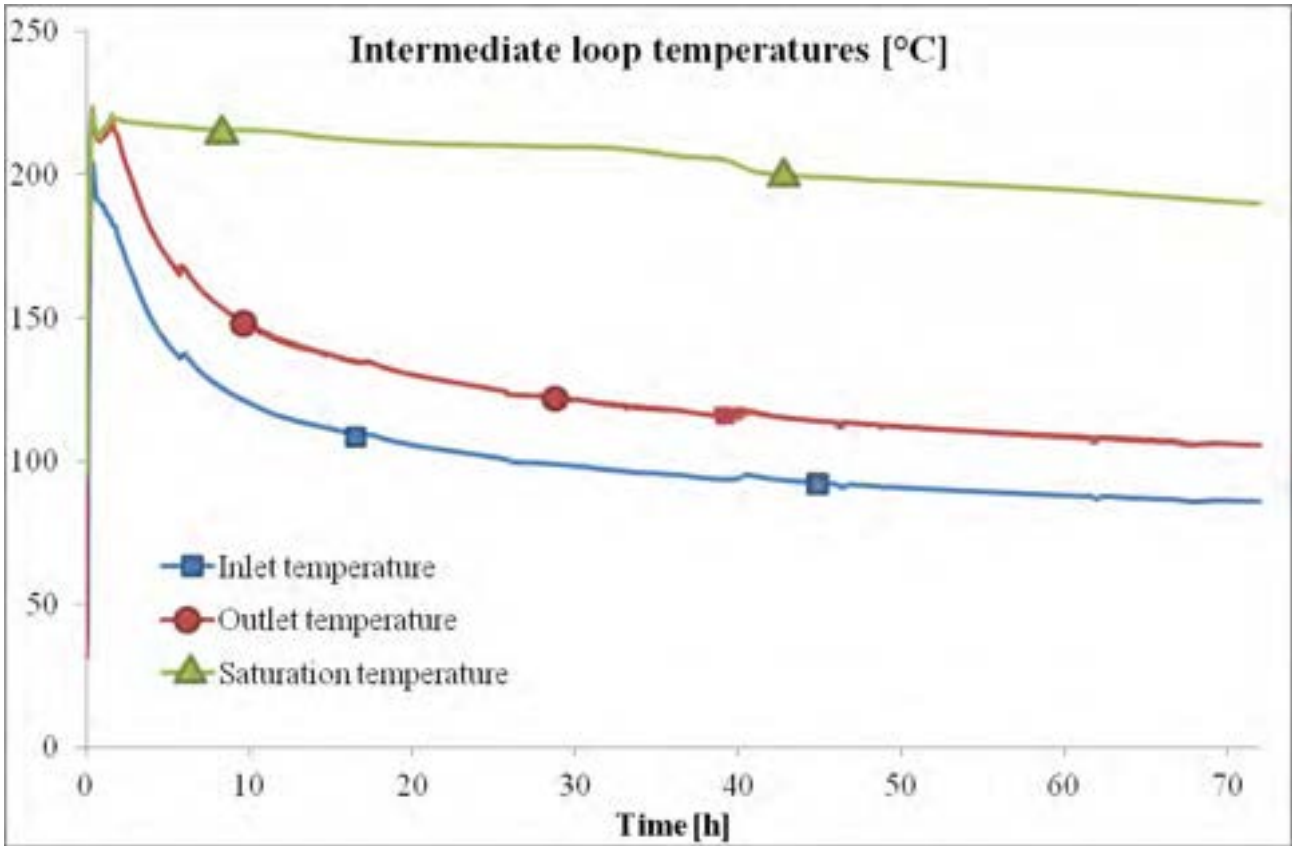

Figure 41. Intermediate loop temperatures (Case 1)

Intermediate loop flow rate

Figures 33 and 34 show the behaviour of the intermediate loop flow rate at the beginning and during the whole transient. Figure 33 shows the beginning of the transient. For the first 3 seconds from the time the system is linked to the reactor there is no fluid in motion. After that, high flow rate oscillations are recorded until the beginning of a stable natural circulation after 17 seconds from the beginning of the transient.

In the long term of the transient the intermediate loop flow rate decreases with an exponential form as the power is reduced, and this behaviour finds a confirmation on the fact that a constant difference is established between the minimum and the maximum temperature.

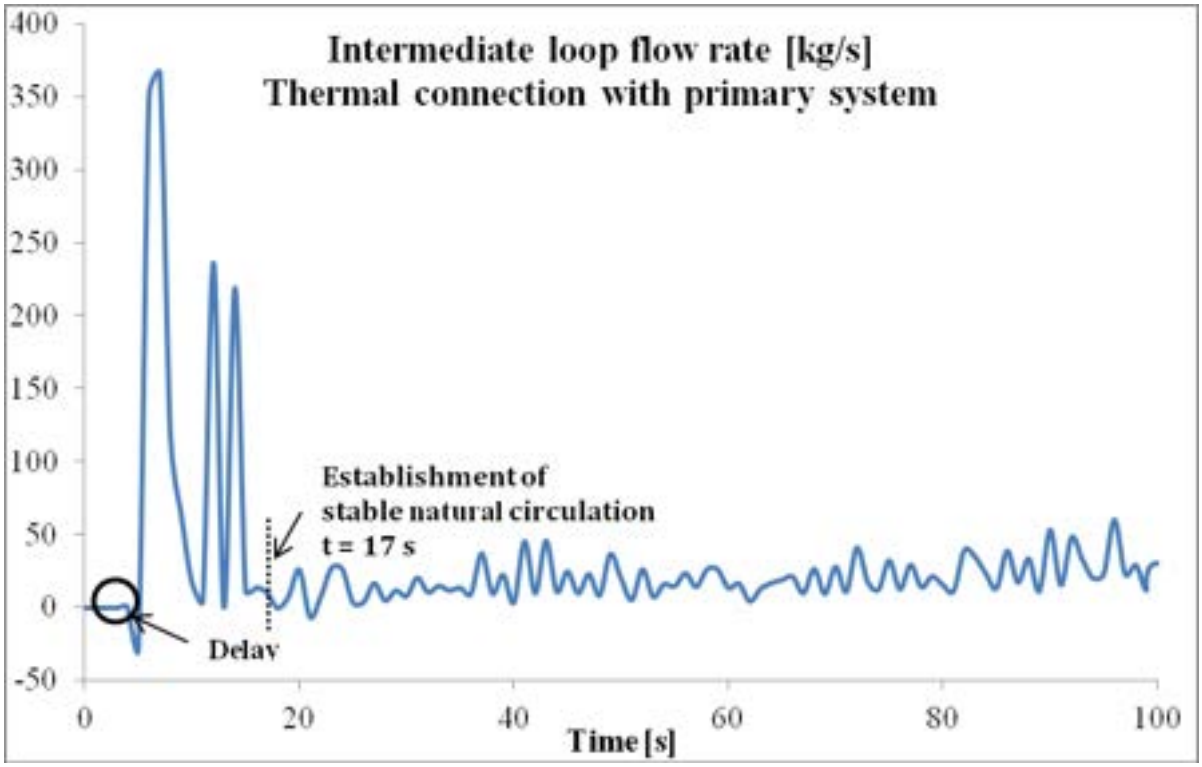

Figure 42. Intermediate loop flow rate at start-up (Case 1)

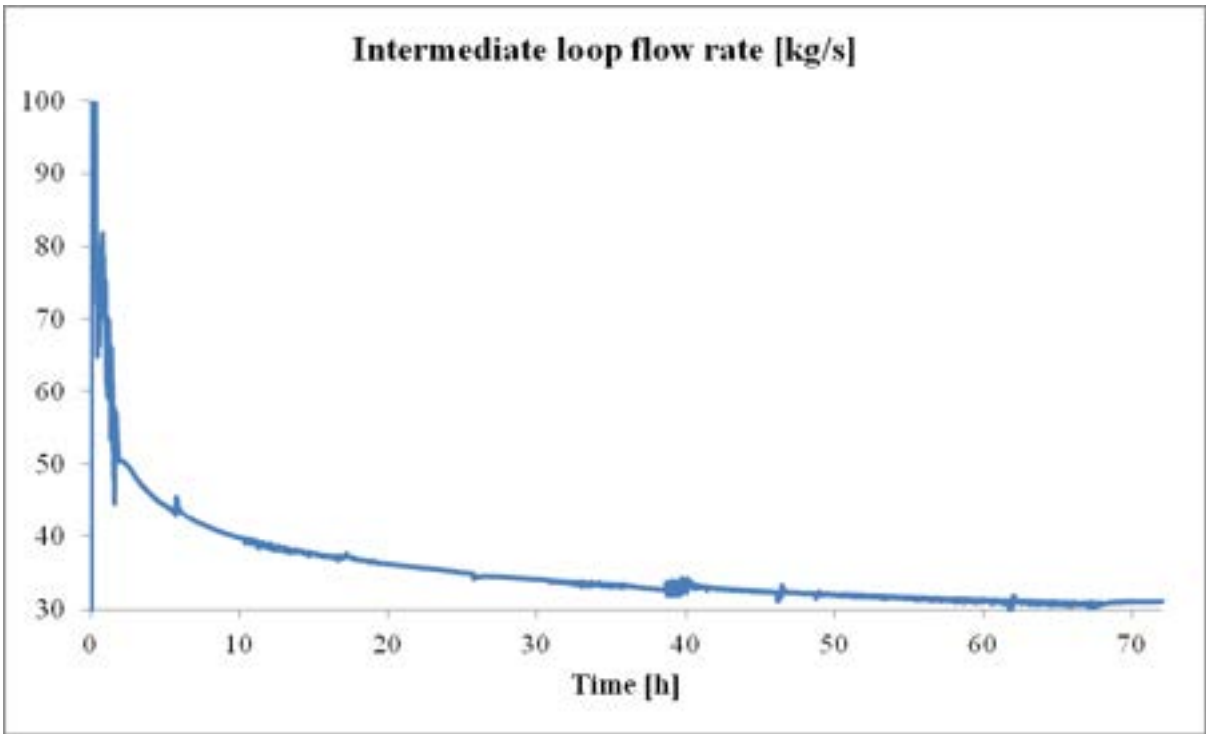

Figure 43. Intermediate loop flow rate (Case 1)

Air heat exchanger temperatures

The ultimate heat sink starts the transient in a total equilibrium condition with the environment. As the hot fluid from the intermediate loop reaches its heat exchanger an air flow rate is established and the outlet temperature starts increasing while the inlet temperature remains at the constant value of 30 °C. Figure 35 shows the behaviour of the temperature in the air heat exchanger at the beginning of the transient. The delay time is the time needed by the intermediate loop to transport the heat from the helical coil heat exchanger to the air heat exchanger. The maximum temperature is reached after 1400 seconds at the value of 212.83 °C.

As the transient evolves, the outlet temperature after 1400 seconds follows a decreasing curve reaching the value of 100°C at the end of the transient (figure 36).

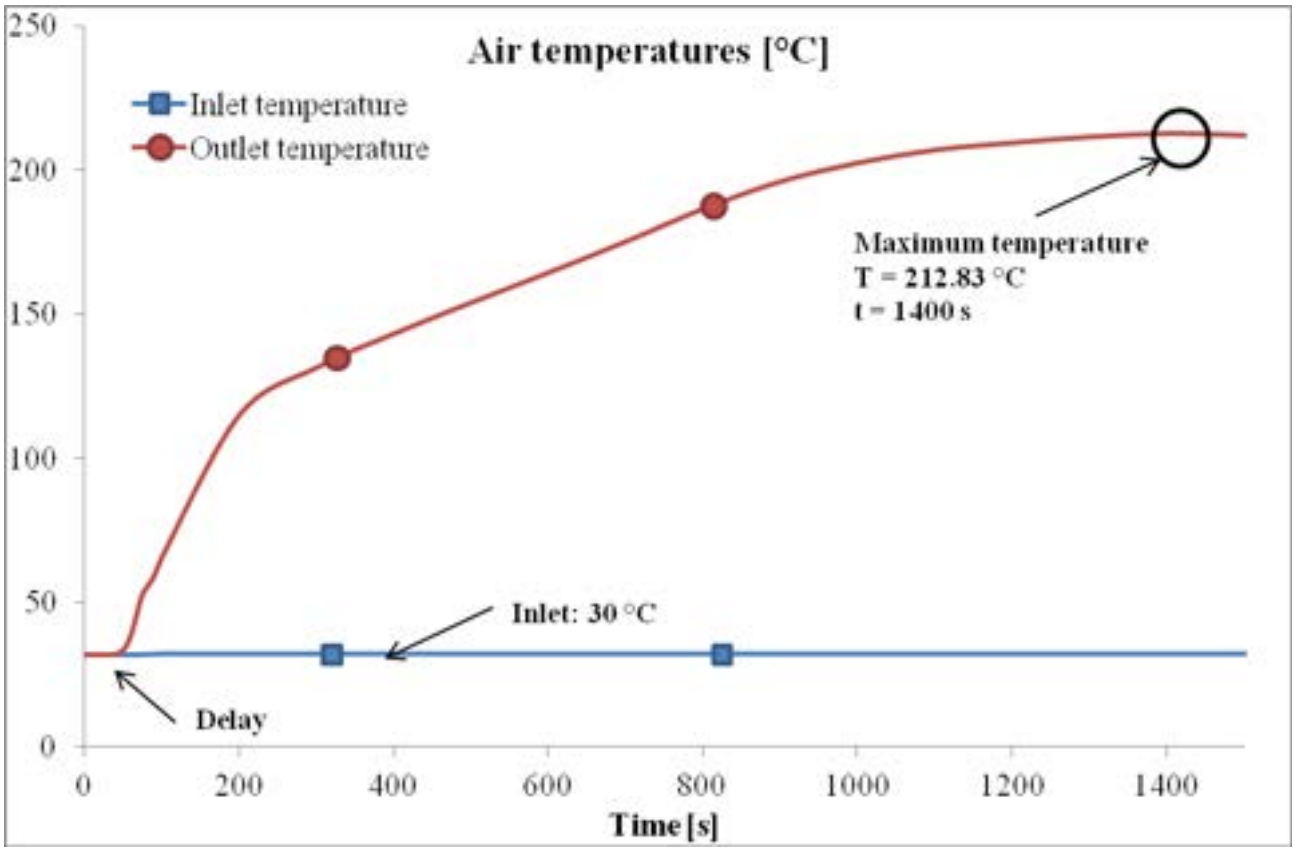

Figure 44. Air temperatures at start-up (Case 1)

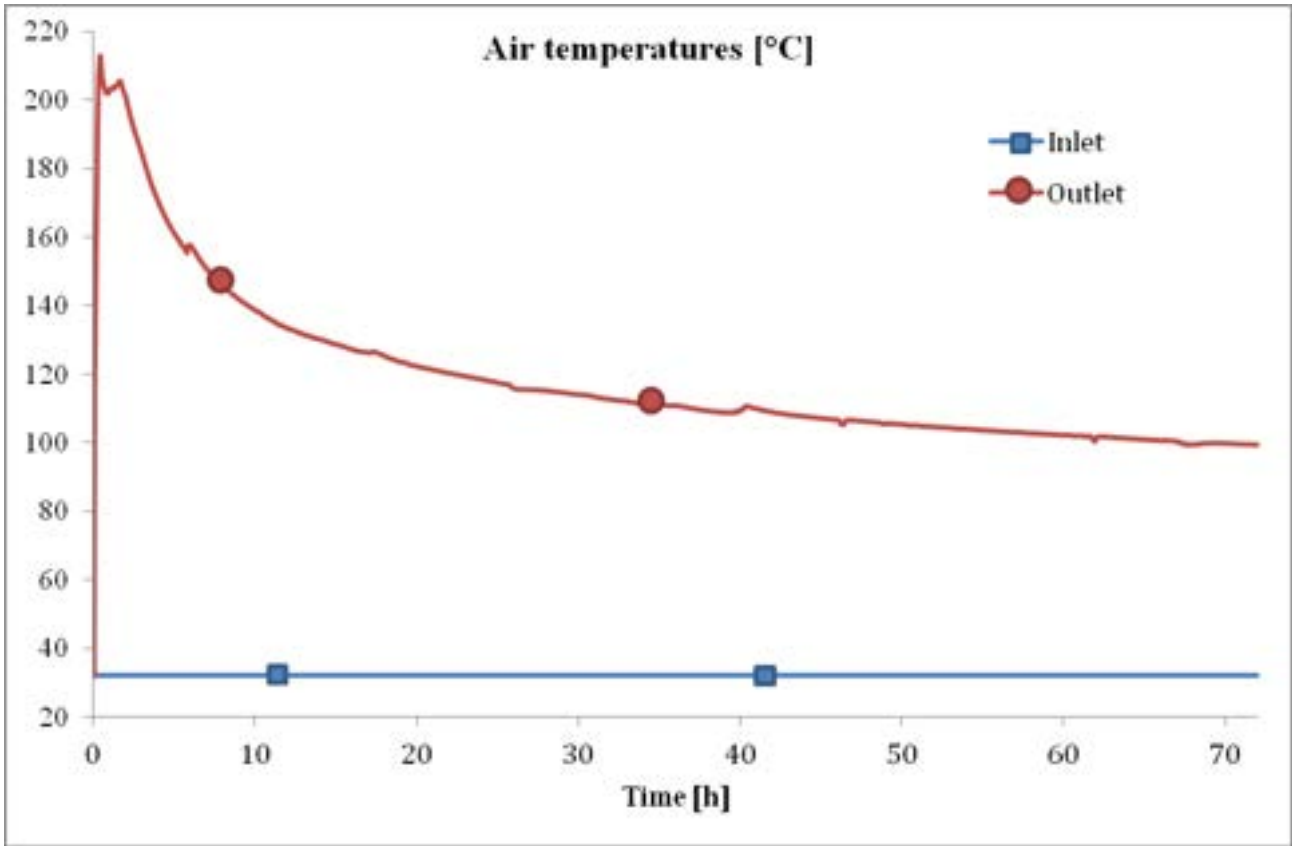

Figure 45. Air temperatures (Case 1)

Air heat exchanger flow rates

The air flow rate during the start-up and the whole time of the transient can be seen in figures 37 and 38. Figure 37 reports the air flow rate at the beginning of the transient. Natural circulation is established after the first 50 seconds. The total behaviour of the air flow rate can be seen in figure 38. The maximum flow rate recorded is of 47.25 kg/s after 5900 from the beginning of the transient, while the flow rate obtained after 72 hours is of 36.75 kg/s. No flow rate oscillations have been recorded in the final heat sink.

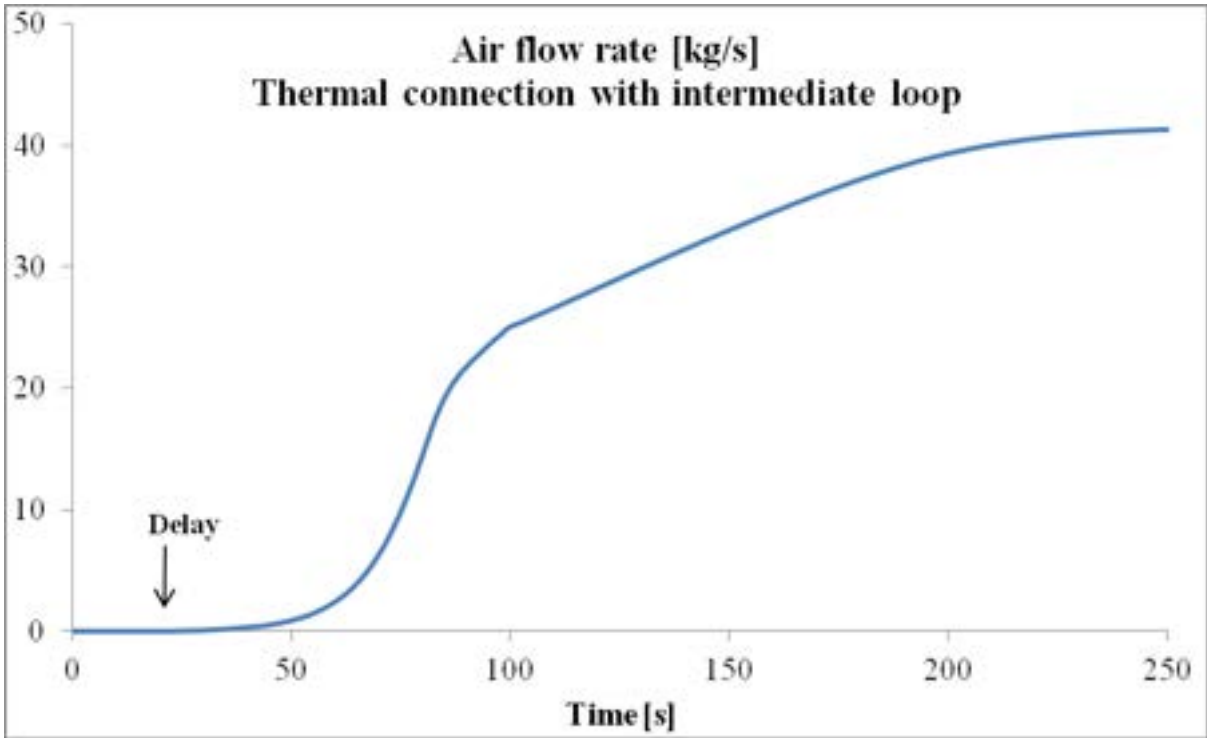

Figure 46. Air flow rate at start-up (Case 1)

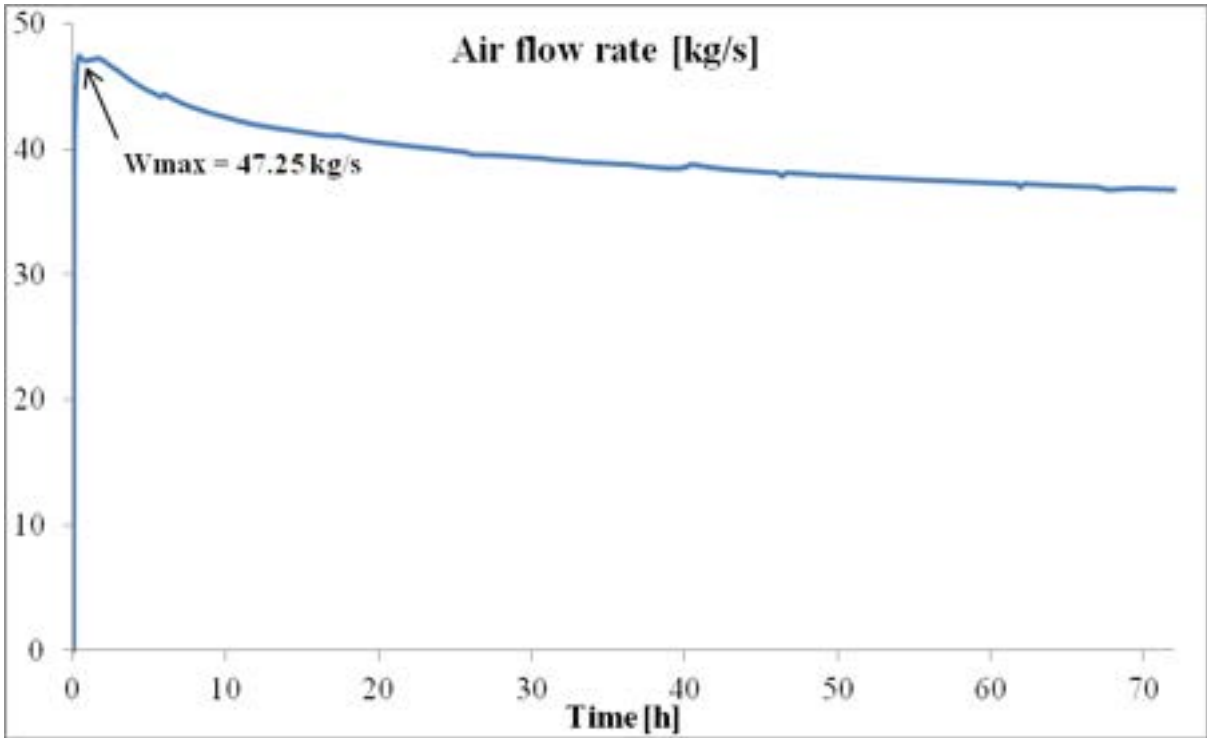

Figure 47. Air flow rate (Case 1)

Heat transfer

From the point of view of the heat transfer, the power exchanged between the primary system, the intermediate loop and the final heat sink is depicted in figures 39, 40 and 41. Figure 39 shows the power exchanged at the beginning of the transient. The helical coil heat exchanger has a fast and oscillatory behaviour as the intermediate loop rises in temperature and pressure: the power removed overcomes the decay heat curve in the first 50 seconds of the transient. The air heat exchanger has a slower behaviour due to the time needed by the heat to be transported in the intermediate loop.

The power removed in the first 30 hours is shown in figure 40. Two power match can be identified in the figure, one in the first hour and the other one after 25 hours. In the meantime, the intermediate loop and the final heat sink reduce the internal energy of the primary system reducing its pressure and temperature. After nearly 25 hours the power produced by the decay heat is equalled by the power removed by the safety system and quasi-stationary conditions are established. The helical coil heat exchanger is characterized by an oscillatory behaviour of the power removed even though a precise behaviour can be observed and these oscillations decreases as the transient evolves.

In the long term, the heat removed by the system decreases as the decay heat is reduced, and the primary system is successfully cooled for 72 hours.

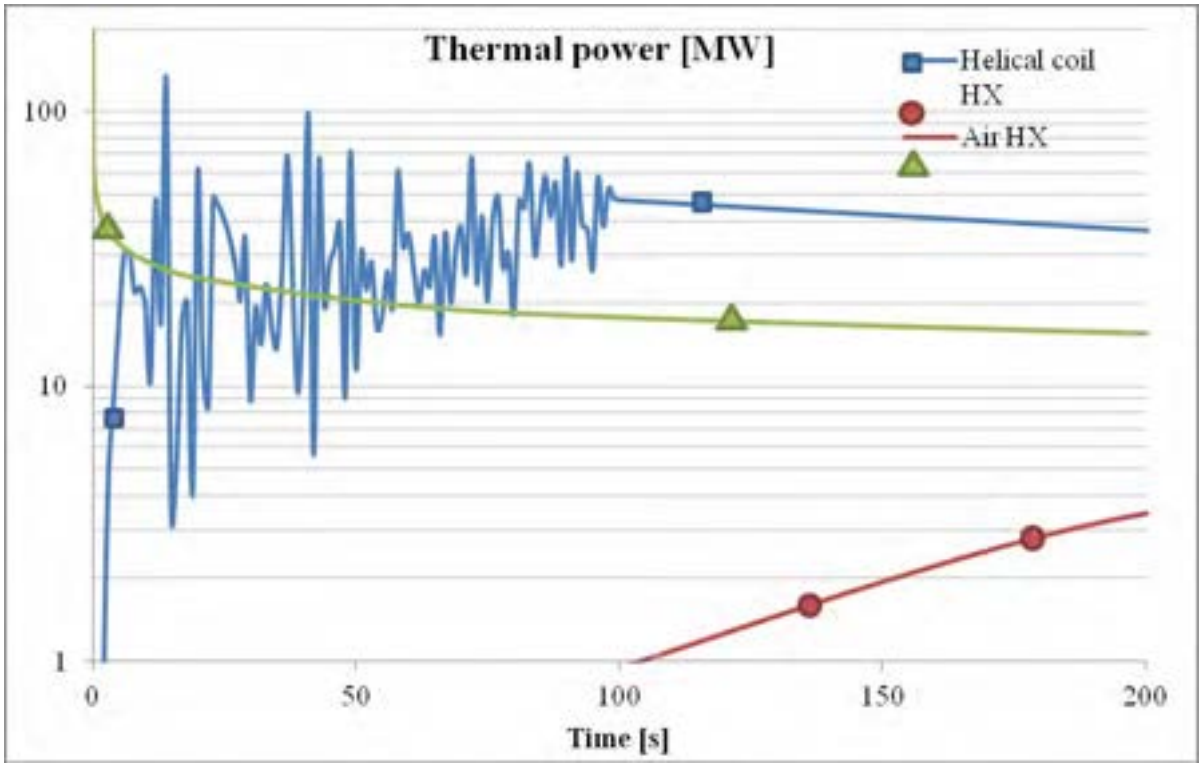

Figure 48: Thermal power at the beginning of the transient (Case 1)

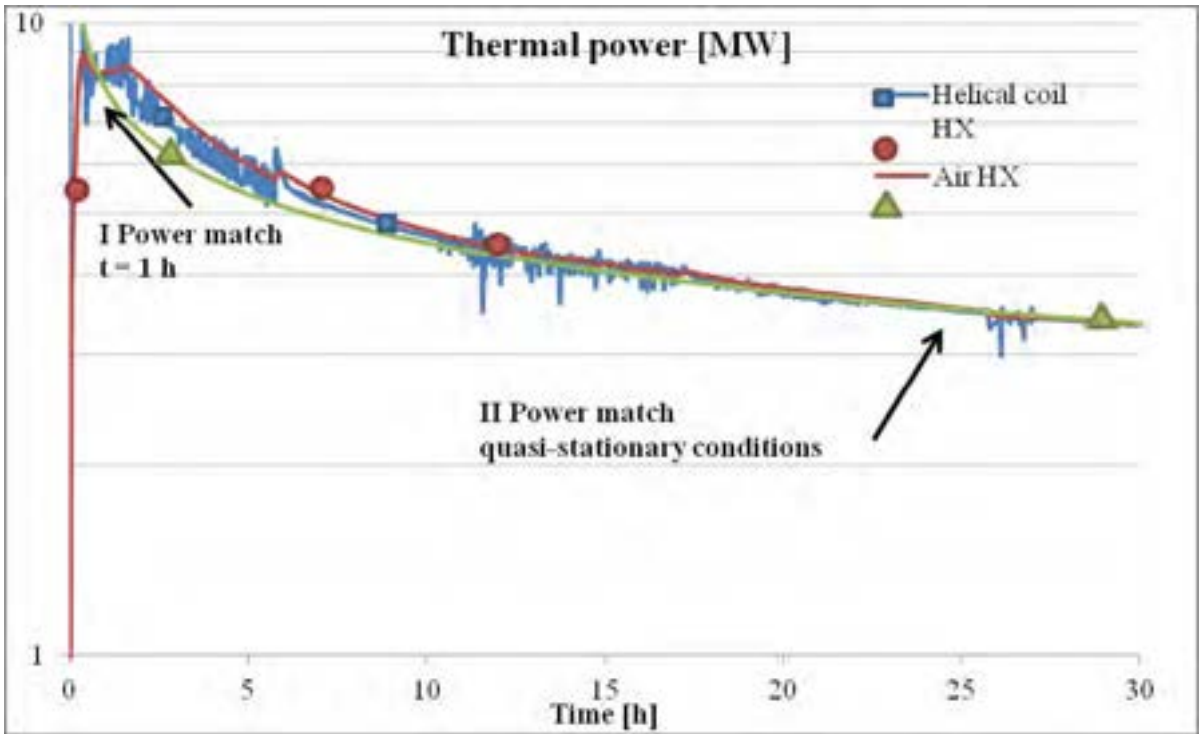

Figure 49. Power removed in the first 30 hours (Case 1)

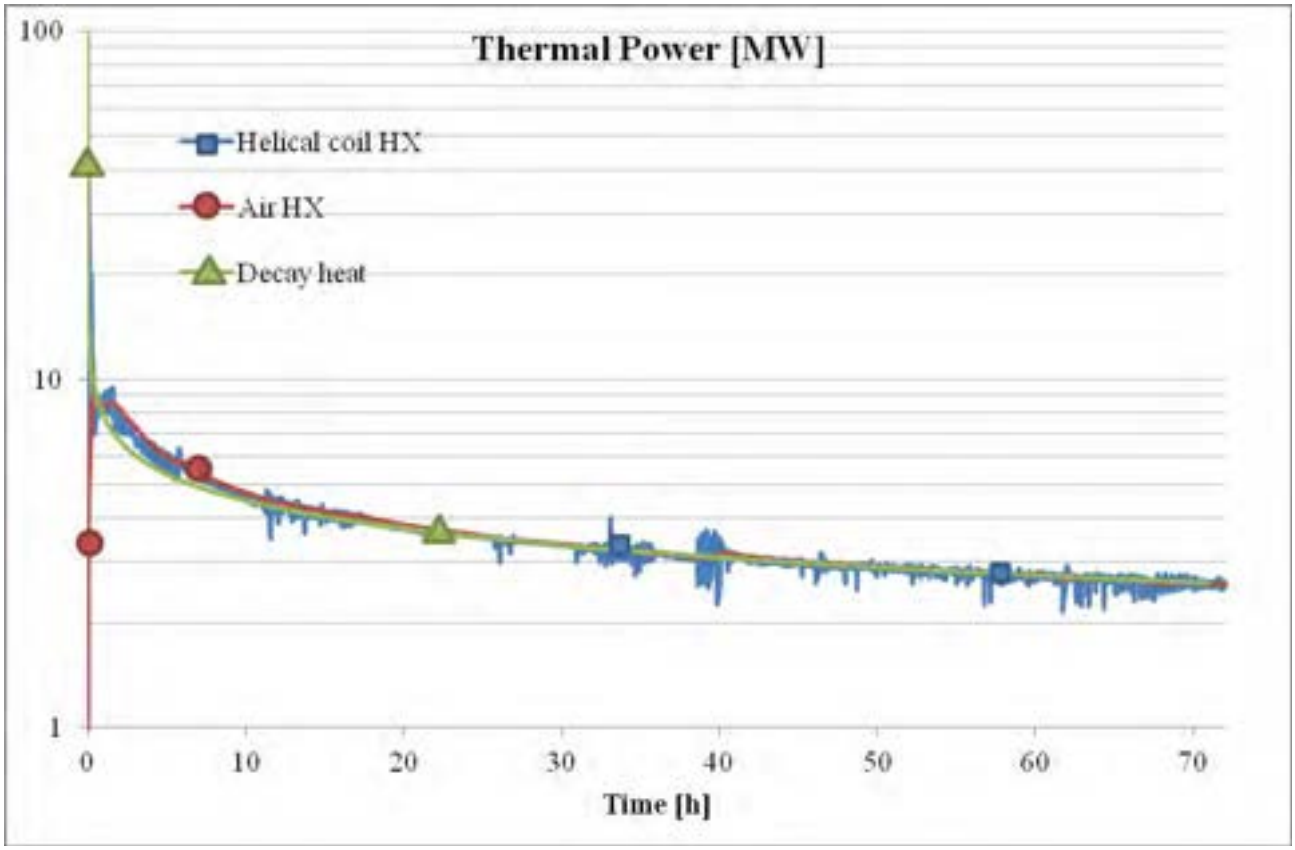

Figure 50. Power removed in the long term (Case 1)

7.2 Case 3: Helical Coil Heat Exch. (A) and Isolation Condenser (D)

In this second case analysed, a helical coil heat exchanger shroud constitutes the DHR, while the ultimate heat sink is made of a vertical pipe bundle inside a pool at ambient pressure and temperature.

Primary pressure

Figures 42, 43 and 44 reports the primary pressure behaviour in different phases of the transient. In the first seconds of the transient the DHR system is not able to remove the thermal power of the system and for this reason a pressure increase is experienced by the primary system which causes the safety relief valves to open and release part of the water inventory in the containment. The amount of water released is in the order of the 4.6%. After this first 10 seconds of the transient the intermediate loop is able to start the heat removal and the pressure starts decreasing. After 400 seconds the isolation condenser starts its effect and the heat is removed completely from the system. This event causes a rapid pressure reduction in the primary system reaching the value of 7.6 bar after one hour. After 1 hour the heat produced by the decay is in the same order of the one transmitted to the environment, and this causes the primary system to reduce its pressure very slowly during the whole time of the accident, coming to the ending vale of 2.4 bar after 72 hours. After 5 hours from the beginning of the transient the isolation condenser experiences an increase in the power transferred to the water inside the pool. This effect is caused by a local increase in boiling.

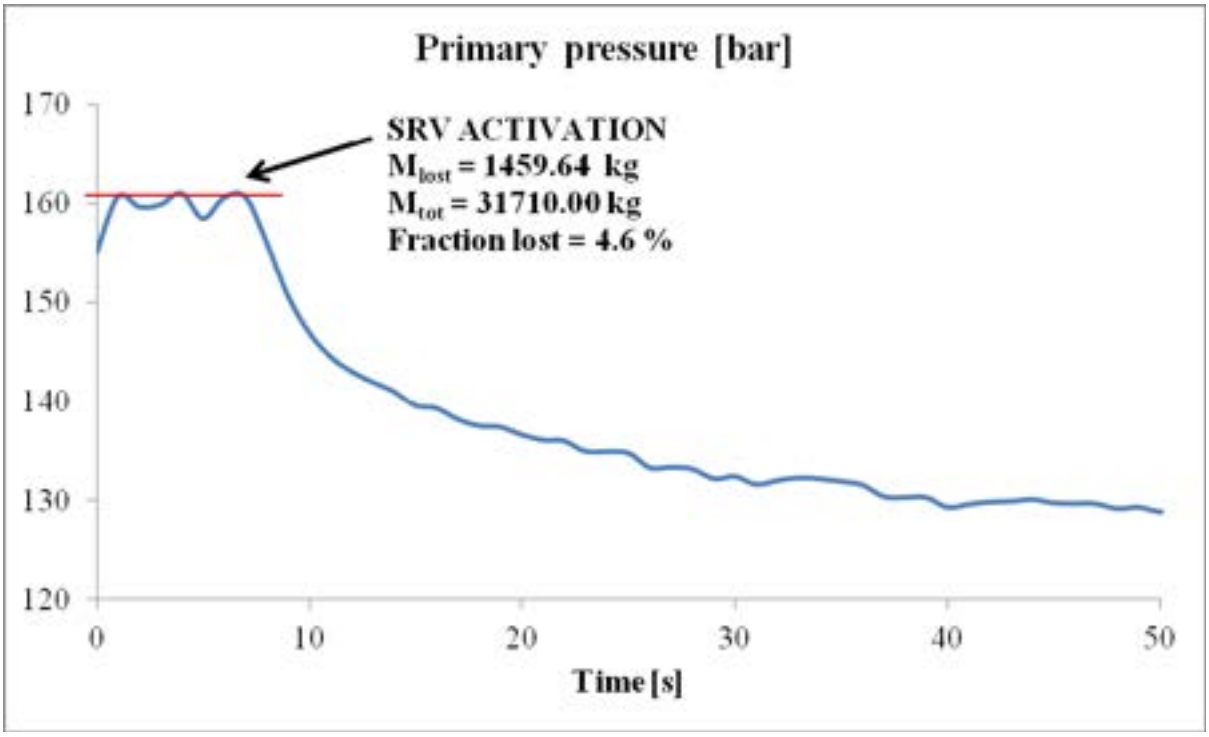

Figure 51. Primary pressure at start-up (Case 3)

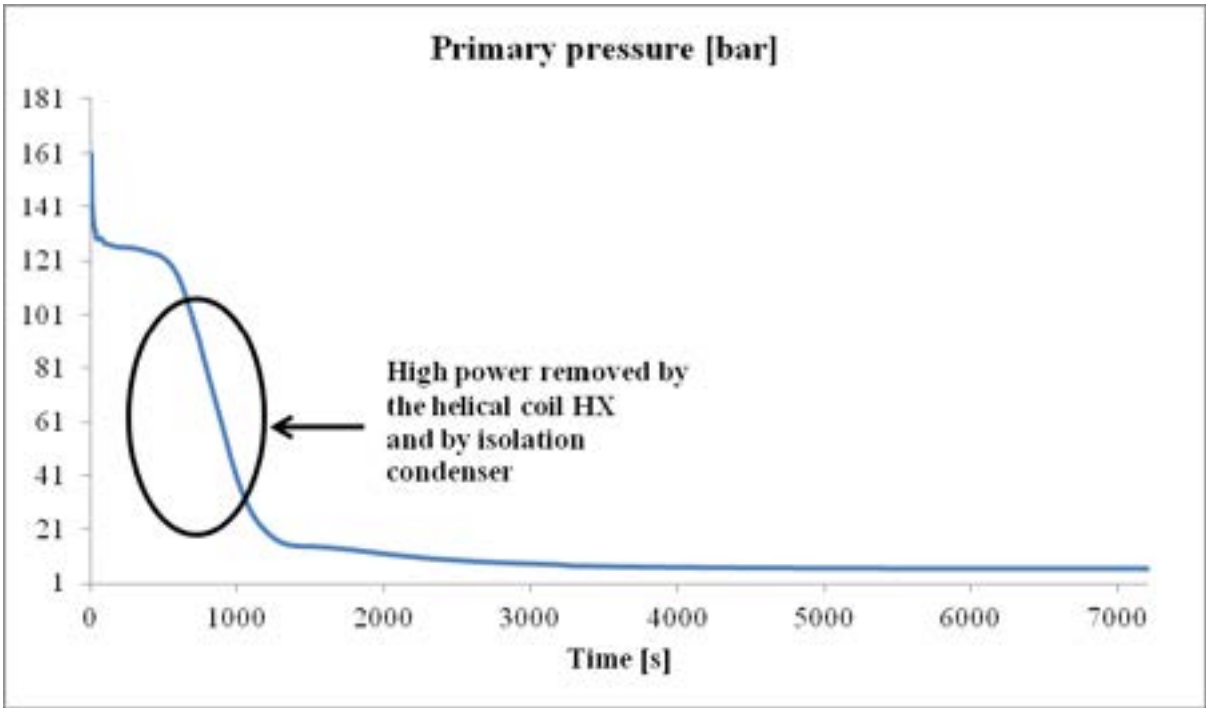

Figure 52. Primary pressure after 2 hours (Case 3)

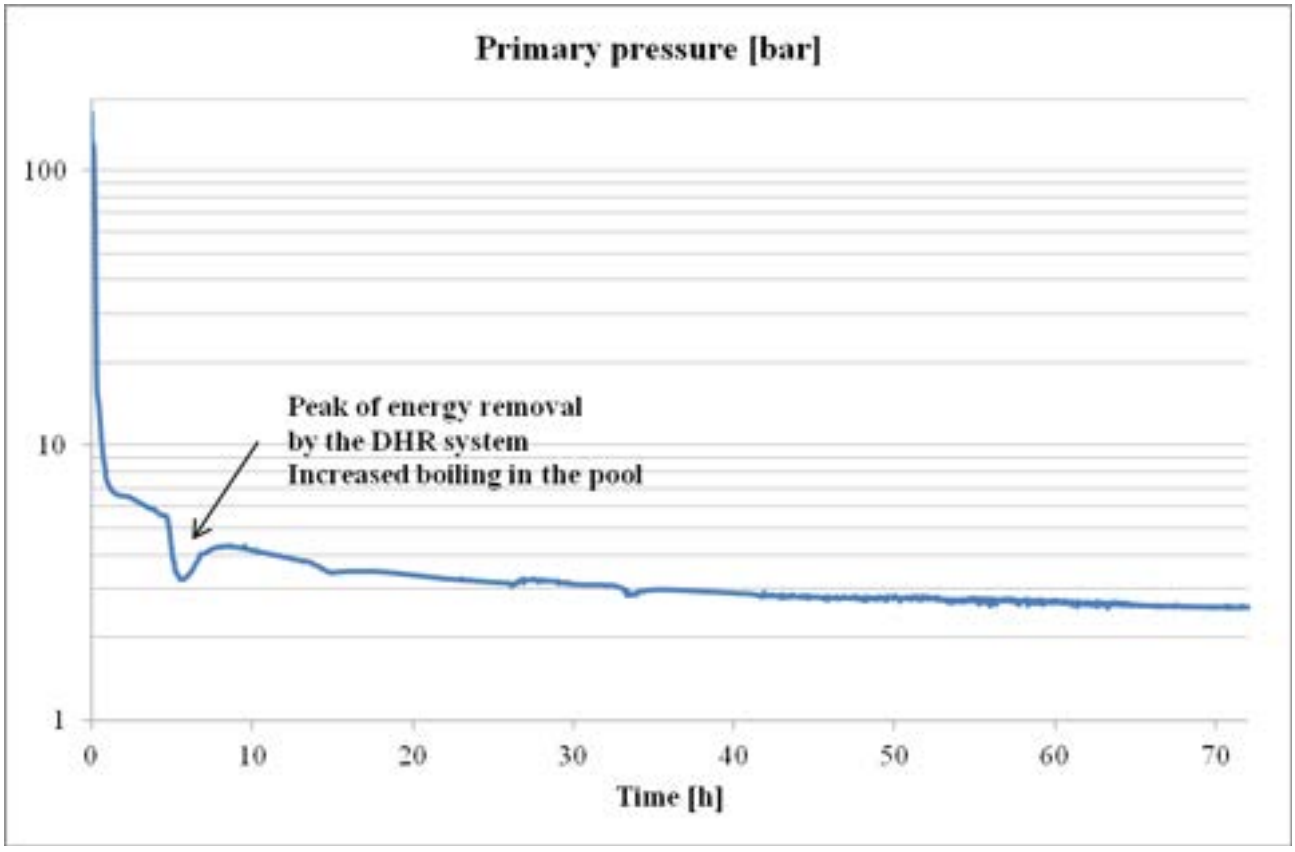

Figure 53. Primary system's pressure (Case 3)

Primary temperatures

As the DHR system is connected with the primary system the injection of cold primary water in thermal equilibrium with the intermediate loop causes a conspicuous reduction in the inlet temperature of the core. In a second part of the transient during the first hour the inlet temperature increases again until a power match is established. From that point, the DHR system removes more power than the one produced inside the core and the inlet temperature starts decreasing again. After the first hour the thermal inertia of the primary system is completely removed and the temperature difference between the inlet and the outlet of the core is reduced. From the point of view of the outlet temperature, the core generates small amounts of steam in the upper part, and this causes the outlet temperature to follow the saturation temperature.

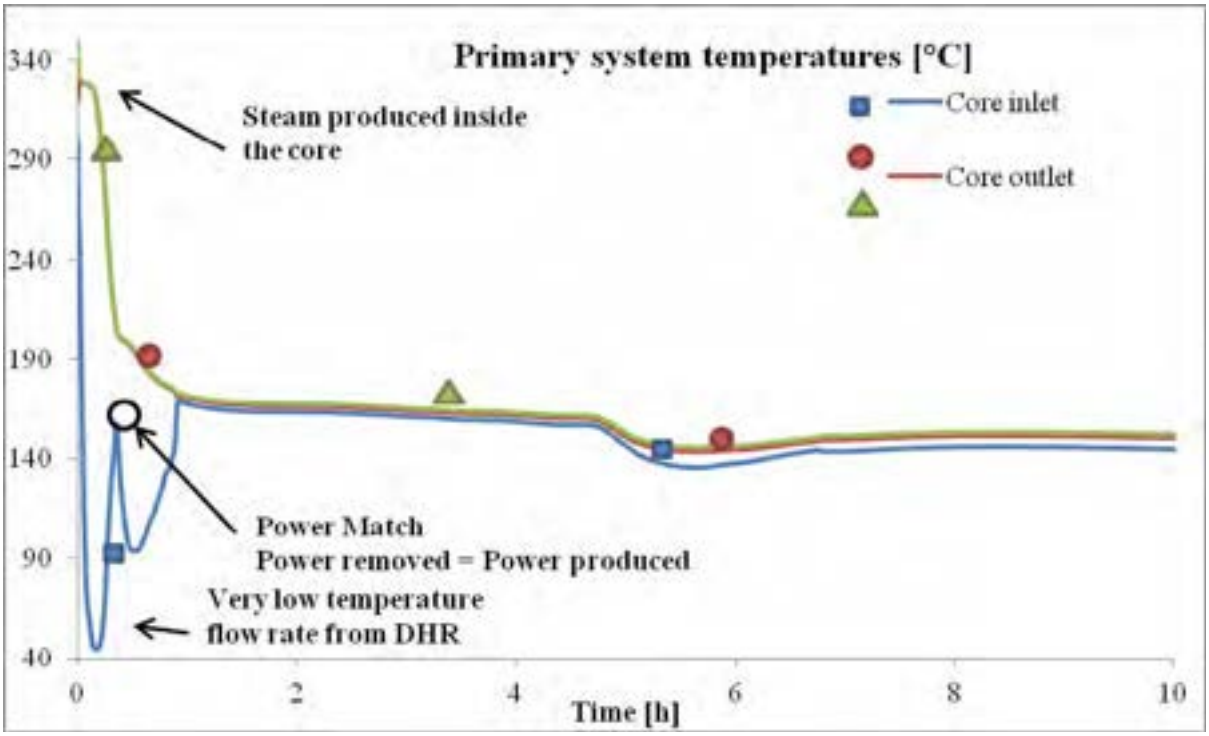

Figure 54. Primary system's temperatures – start-up (Case 3)

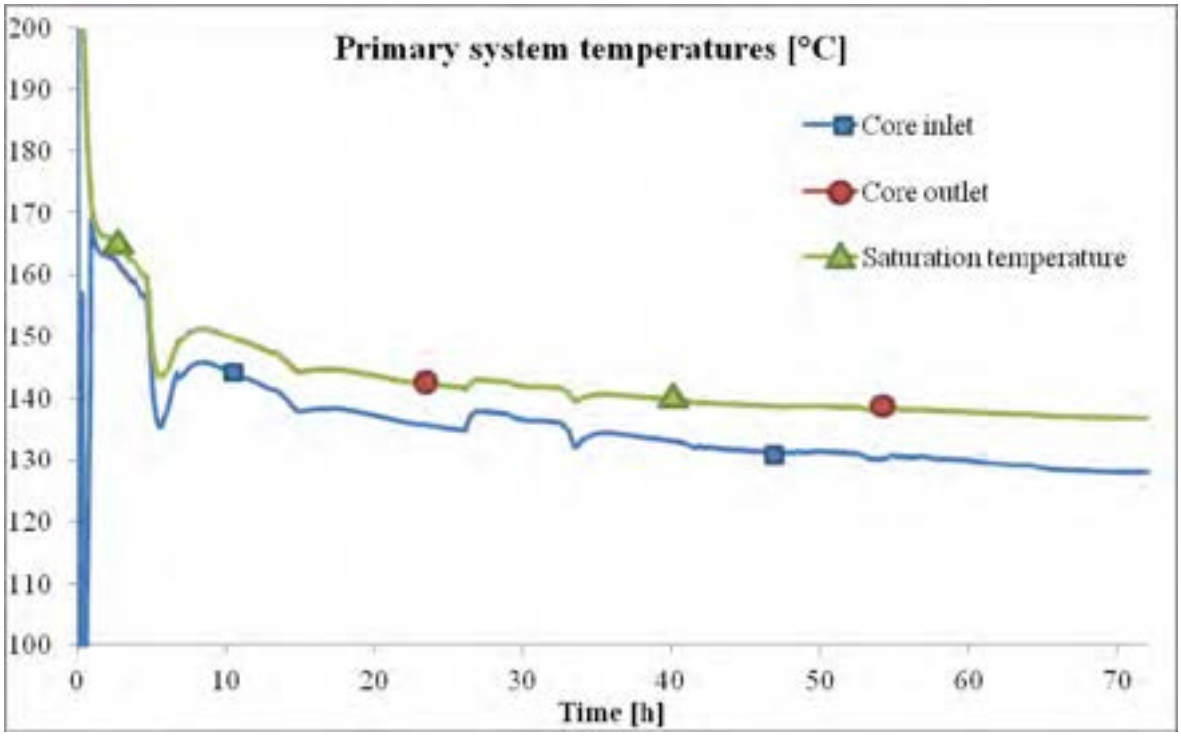

Figure 55. Primary system temperatures in the long term (Case 3)

Primary system flow rate

Figures 47 and 48 reports the behaviour of the core flow rate during the transient. In the first hours of the transient the flow rate is subjected to the variation of density difference between hot and cold leg and as the amount of steam produced increases a large variation of flow rate is established. This event happens around the end of the first hour. After that, the flow rate starts decreasing as the power of the decay heat is reduced. The behaviour of the flow rate follows the decay heat as the temperature difference between inlet and outlet remains unchanged after the complete removal of the primary system thermal inertia.

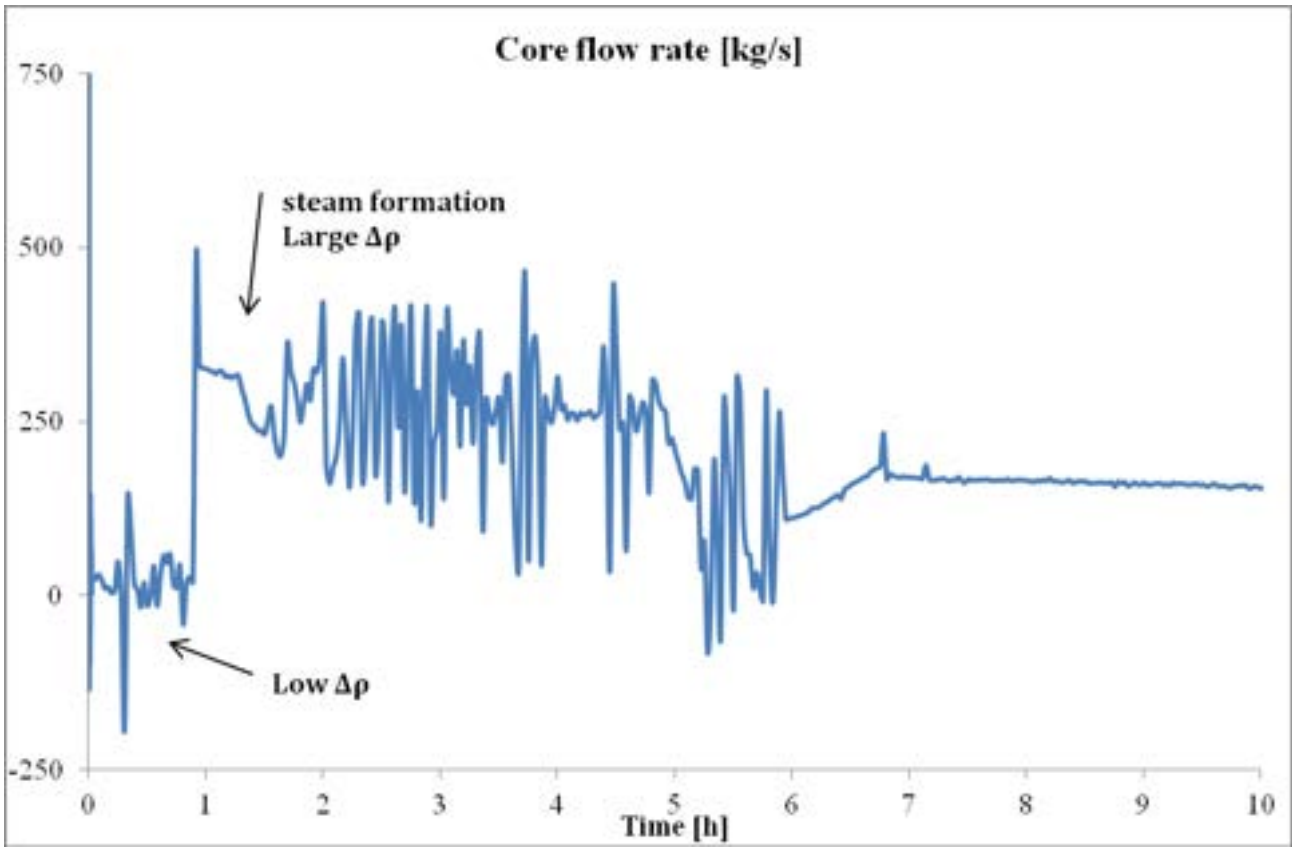

Figure 56. Primary flow rate at start-up (Case 3)

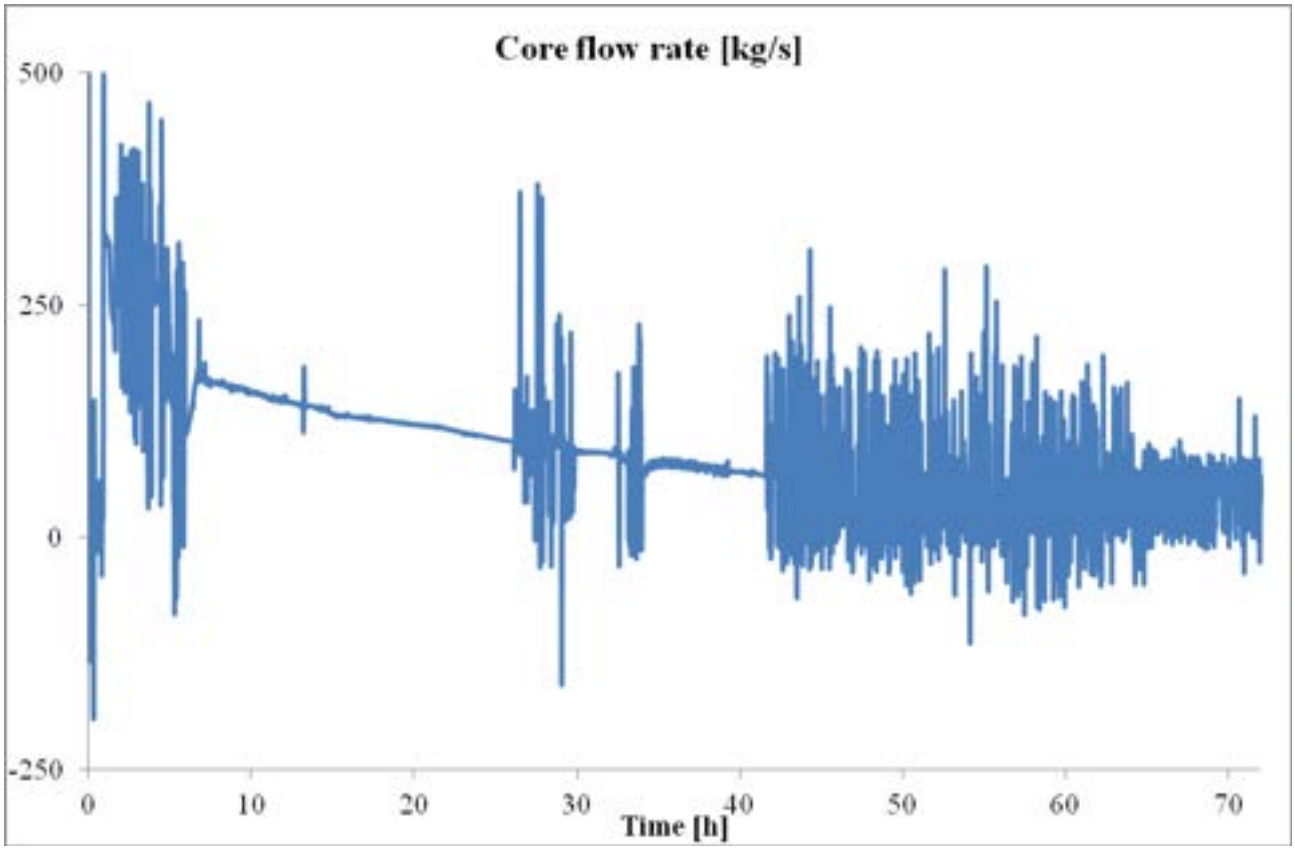

Figure 57. Primary flow rate (Case 3)

Intermediate loop pressure

Figure 49 and 50 shows the behaviour of the intermediate loop pressure. As the intermediate loop is connected to the primary system, heat is transferred and pressure oscillations are recorded in the heat exchanger with a general increase in the mean value. After the first 50 seconds the amplitude of the pressure oscillation decreases as the mean value of the pressure increases until 900 seconds where the maximum value of 7.6 bar is reached. From that point the pressure of the intermediate loop remains nearly constant during the whole time of the transient, reaching the value of 6 bar after 72 hours.

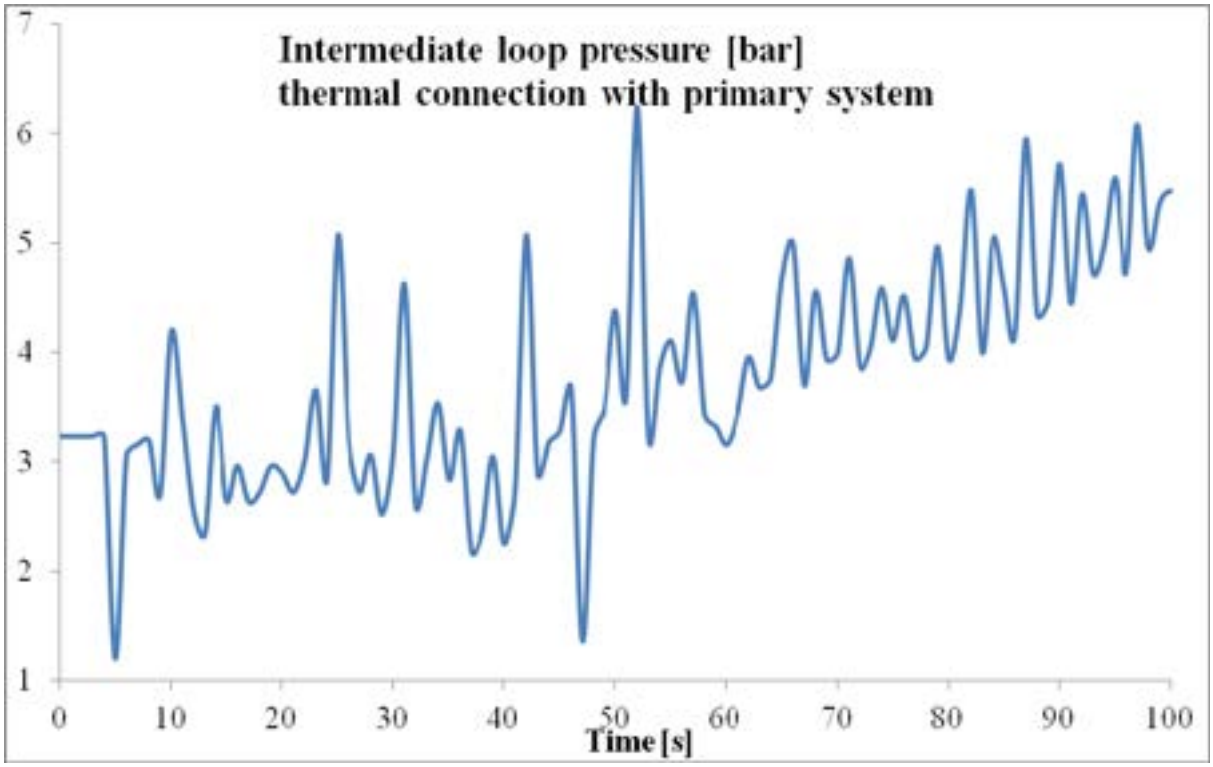

Figure 58. Intermediate loop pressure at start-up (Case 3)

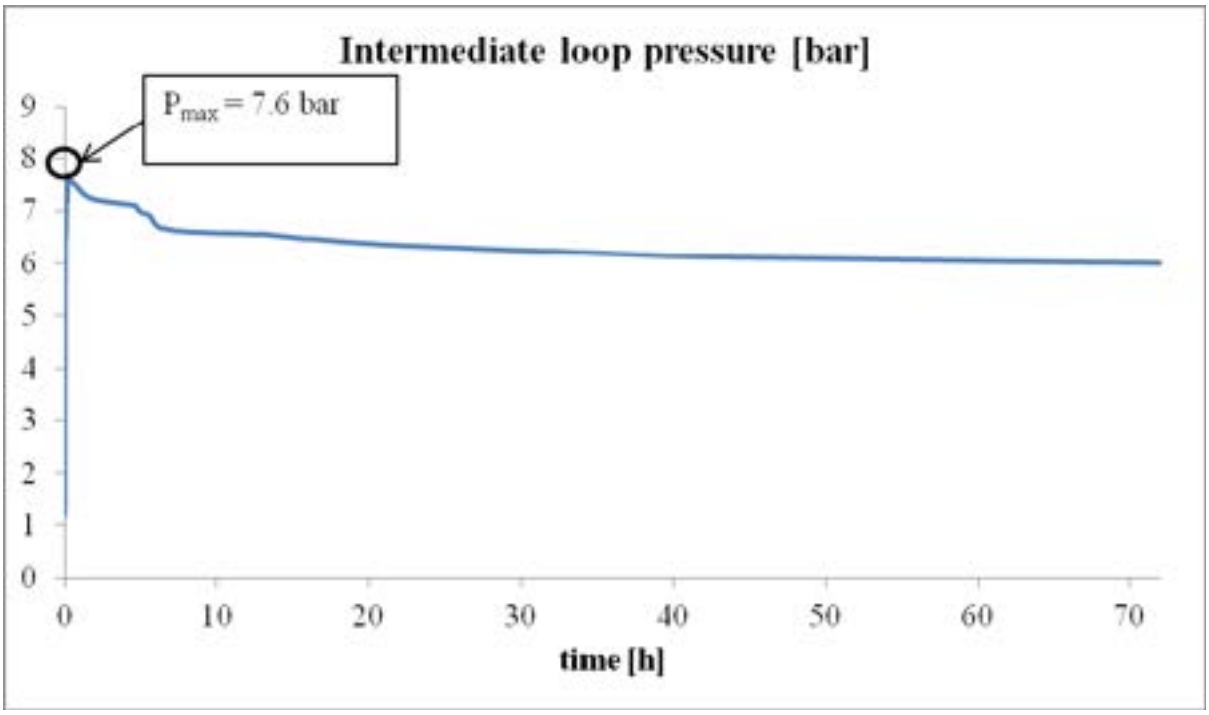

Figure 59. Intermediate loop pressure (Case 3)

Intermediate loop temperatures

As the intermediate loop is connected to the primary system the heat exchanged causes the outlet temperature on the intermediate side to increase. In the first seconds of the transient the outlet temperature is subjected to fluctuations which reduces over time during the first minutes. As the transient continues the oscillations are eliminated. The inlet temperature of the heat exchanger is nearly constant in the first part of the transient, which is the effect of the rapid heat transfer within the isolation condenser. The maximum temperature reached by the system during the incidental sequence does not reach the saturation temperature and no steam is formed. The heat transfer conditions of the loop are of a single phase convection during the whole transient. In the long term period of the transient the temperature difference between the inlet and the outlet of the helical coil does not change in an appreciable way.

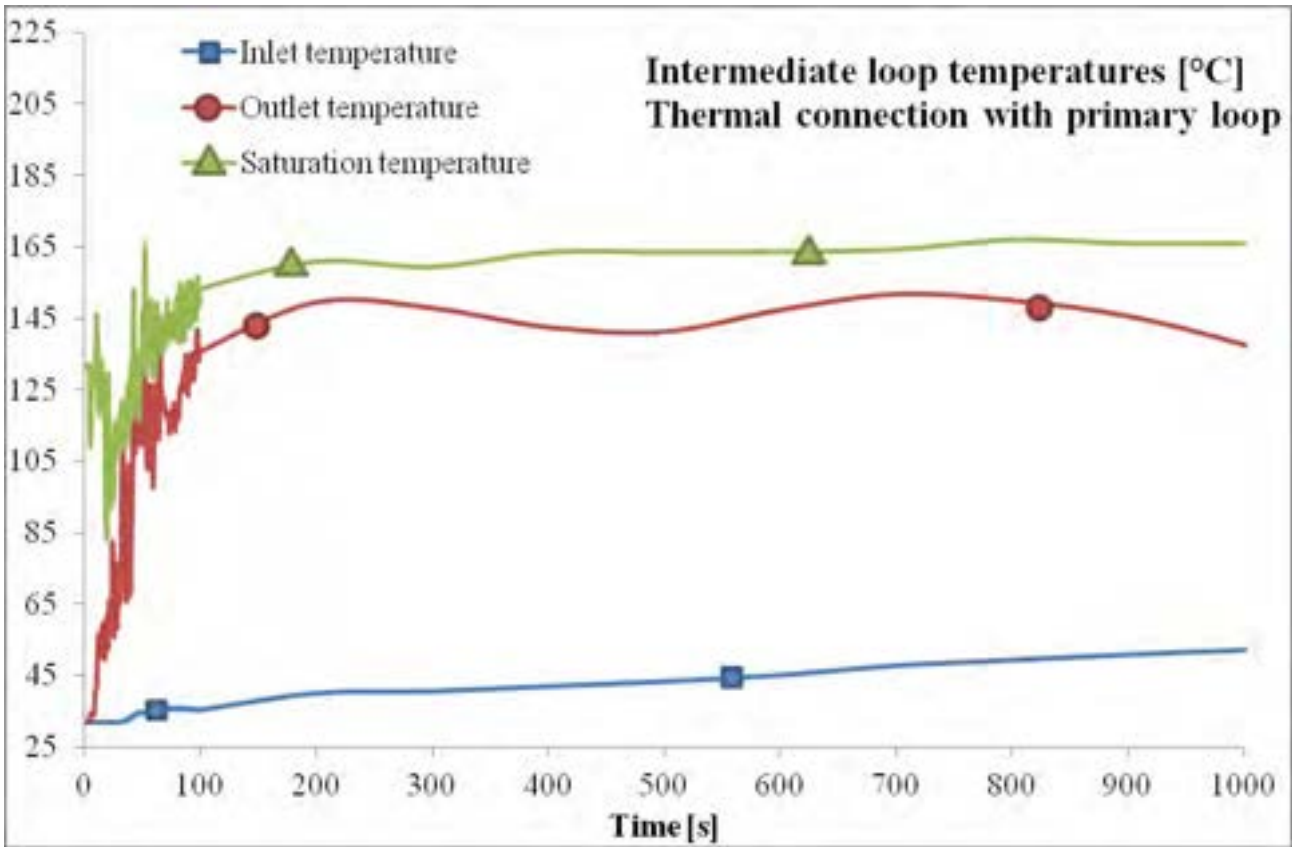

Figure 60. Intermediate loop temperatures at start-up (Case 3)

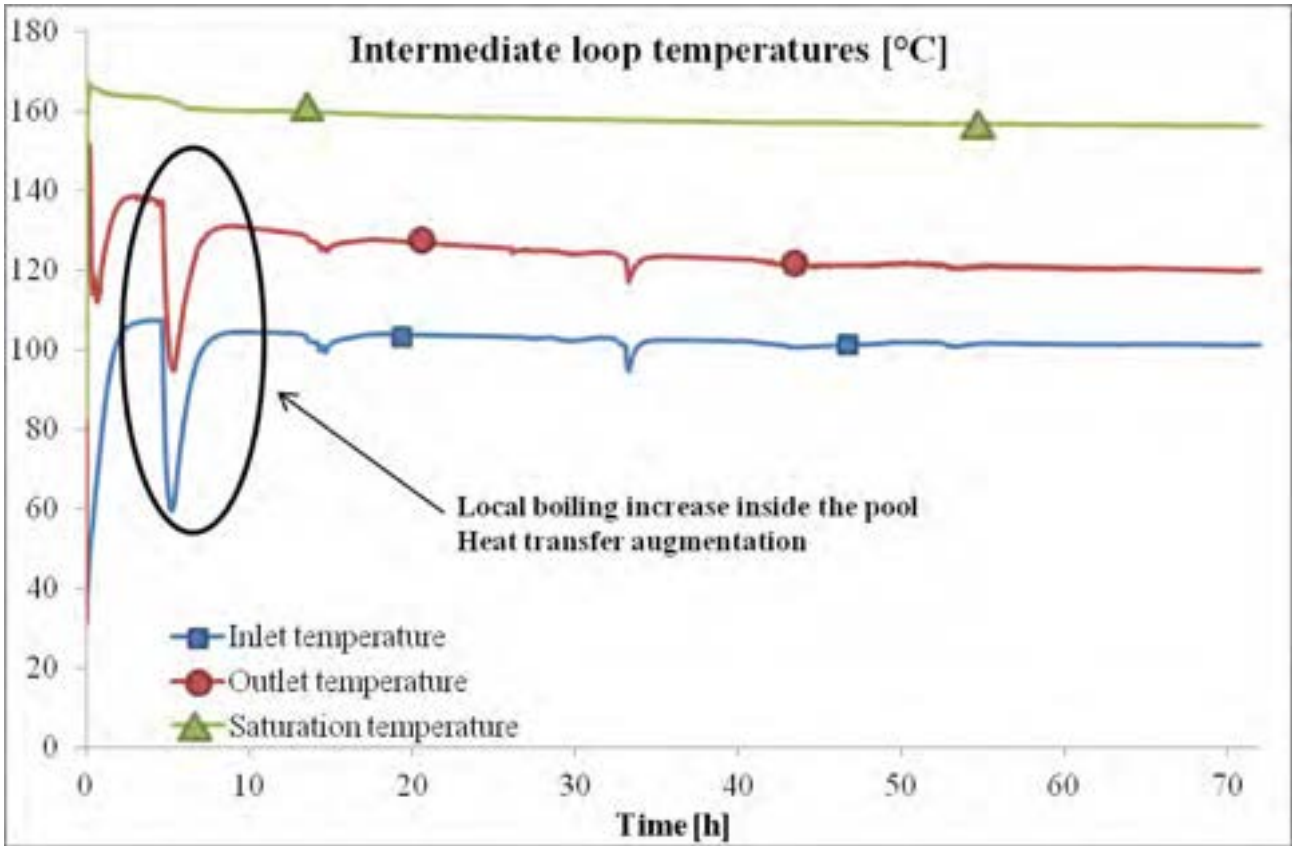

Figure 61. Intermediate loop temperatures (Case 3)

Intermediate loop flow rate

The absence of steam formation inside the intermediate loop causes heavy flow oscillation at the beginning of the transient as it can be seen in figure 53. By the time the flow is stabilized it behaves as the decay heat curve profile as the temperature difference inside the loop is nearly constant in the long terms of the transient.

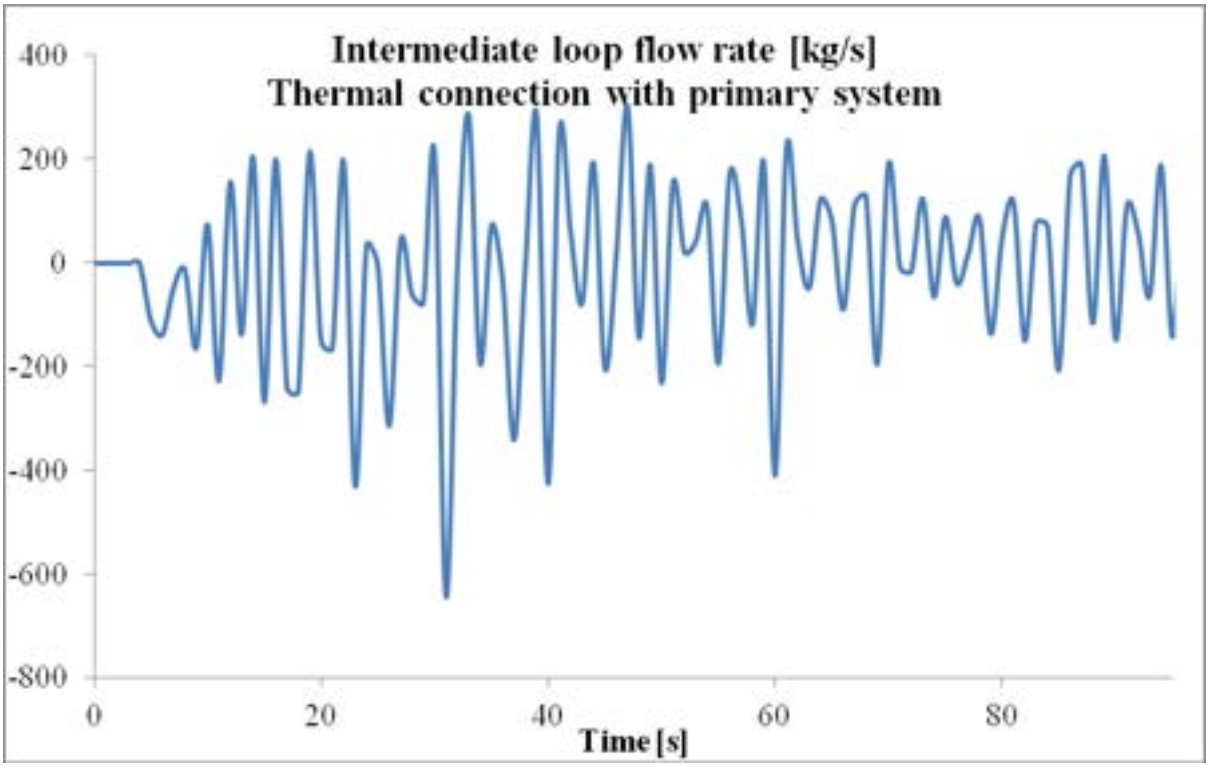

Figure 62. Intermediate loop flow rate at start-up (Case 3)

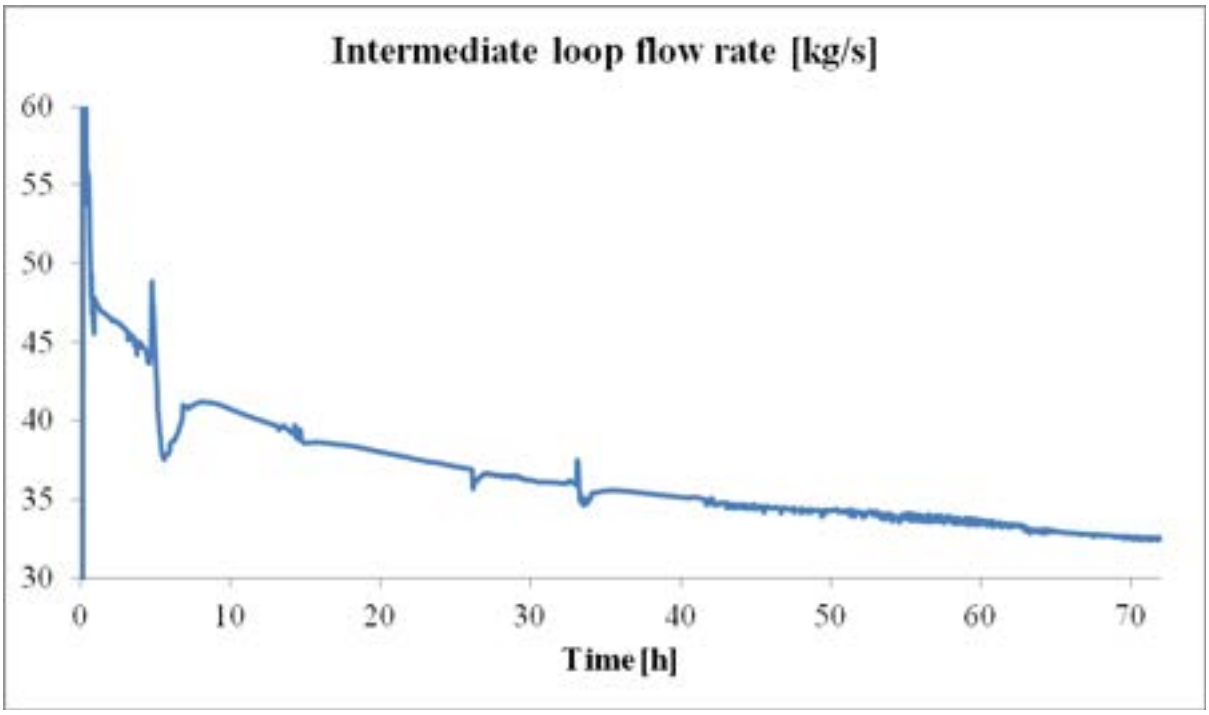

Figure 63. Intermediate loop flow rate (Case 3)

Heat transfer

Last results obtained during the simulation regards the heat transfer between the systems. Figures from 55 to 57 highlight the power removed by the system during the transient. During the first 100 seconds of the transient both the isolation condenser and the secondary loop match the decay heat curve and start to remove more power than the one produced. During the first hour the thermal inertia of the system is completely removed and after that quasi-static conditions of heat transfer are established. Figure 57 gives the opportunity to highlight the power increase after 5 hours by the isolation condenser system. Both the helical coil heat exchanger experiences a power increase thanks to its minimum temperature decrease.

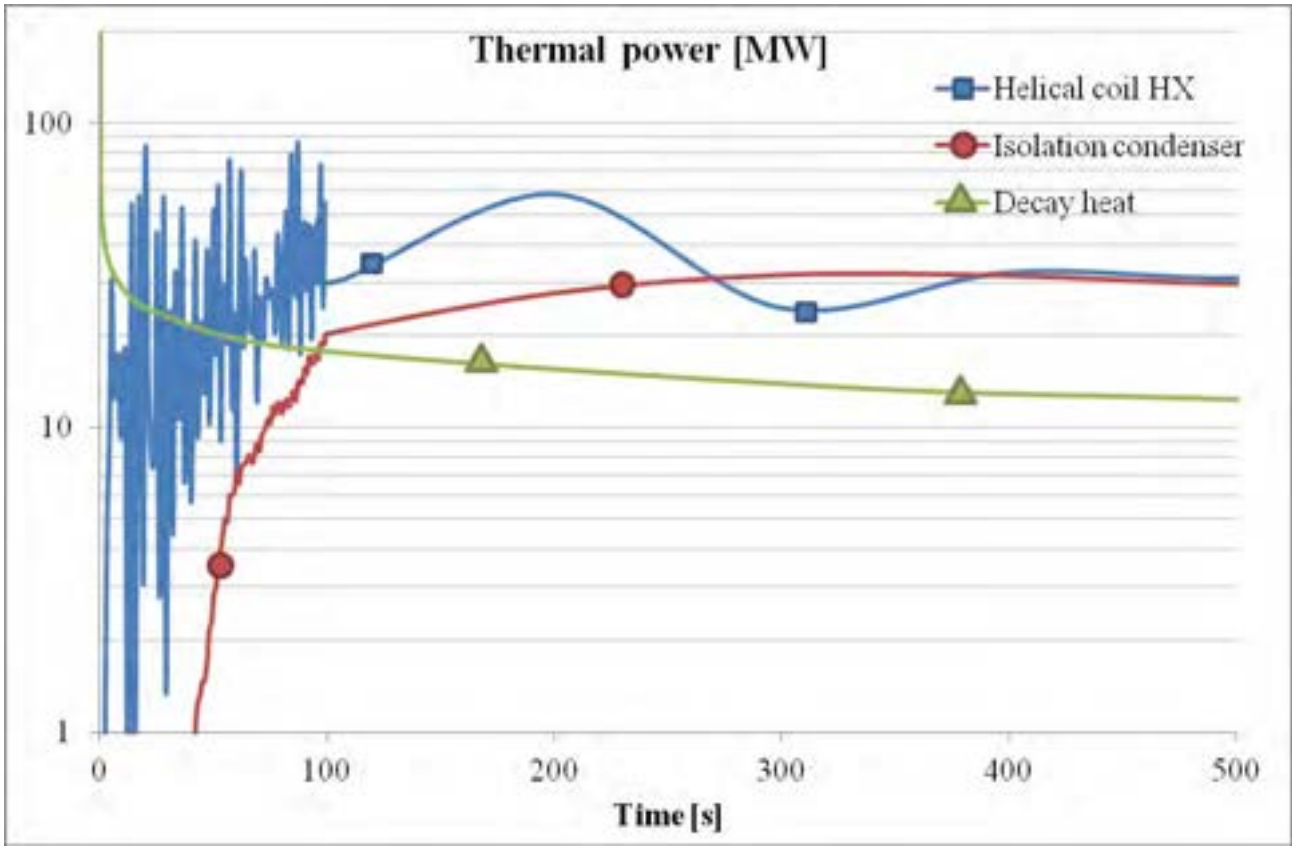

Figure 64. Power removed at the system start-up (Case 3)

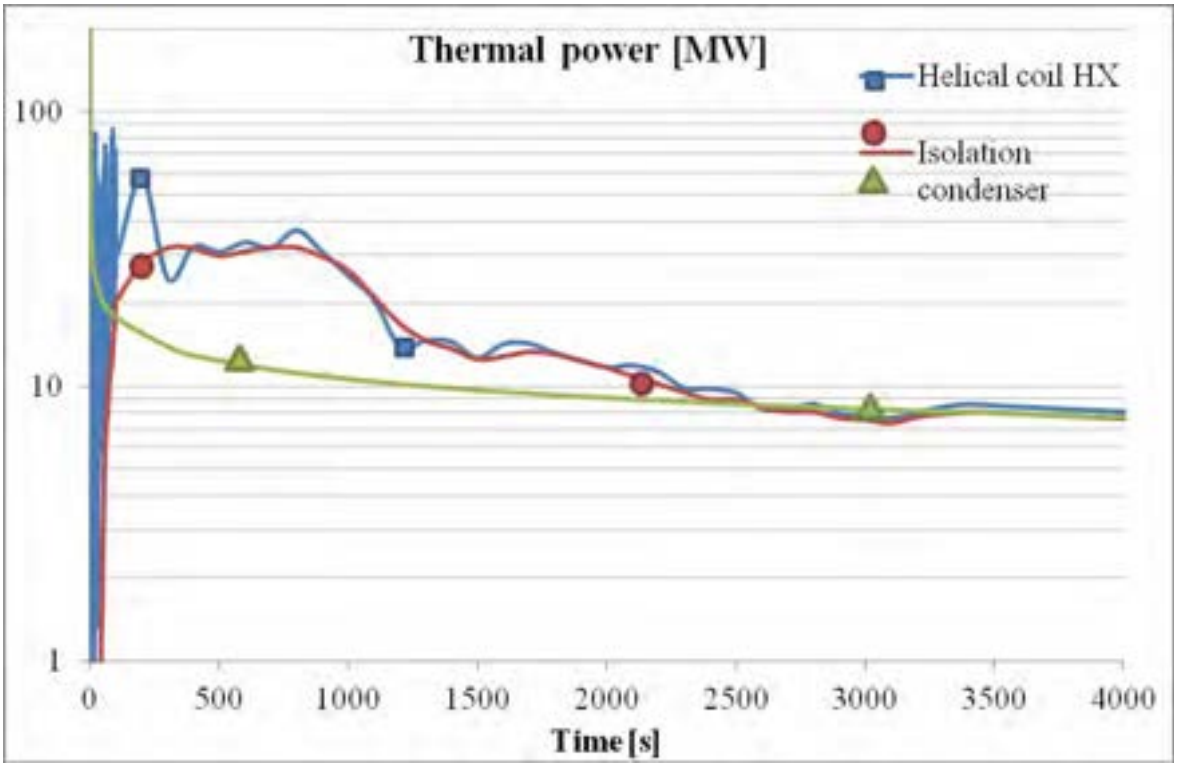

Figure 65. Power removed during the first hour (Case 3)

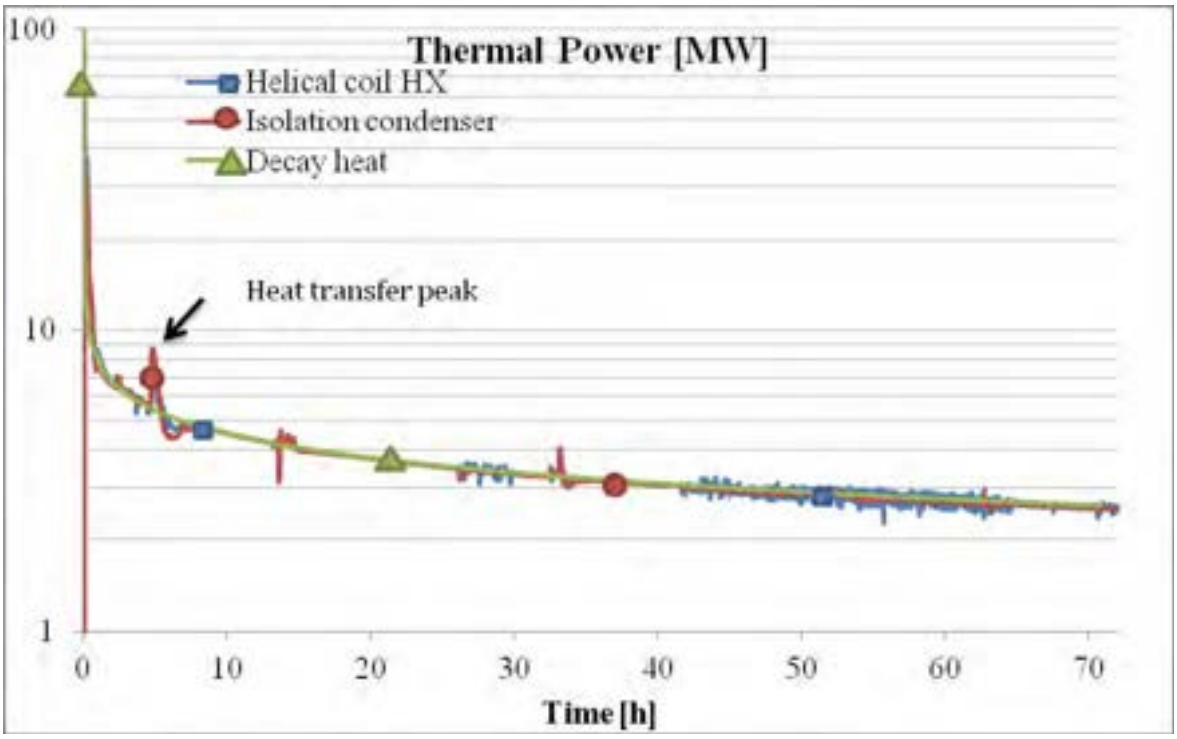

Figure 66. Power removed in the long term (Case 3)

8 Simulations results: accident conditions with pump inertia effect

In this chapter the results obtained considering the effect of pump inertia for the first 100 seconds of the transient will be shown. The detailed description of the accidental sequence is reported in chapter 5. The four simulations are grouped in two couples depending on the final heat sink in order to perform a comparison between the two configurations: Table 8 reports the simulations reported in this chapter.

Table 8. Simulations performed

DHRS configuration	In-vessel HX (DHR heat exchanger)	External HX (Ultimate heat sink)
Case 1 (A+C)	Helical Coil Heat Exchanger (A)	Air Cooled Heat Exchanger (C)
Case 2 (B+C)	Microchannel Heat Exchanger (B)	Air Cooled Heat Exchanger (C)
Case 3 (A+D)	Helical Coil Heat Exchanger (A)	Isolation Condenser (Pool) (D)
Case 4 (B+D)	Microchannel Heat Exchanger (B)	Isolation Condenser (Pool) (D)

The inertia of the primary pump and of the pump of the secondary system is taken into account by using the flow rate curve reported in figures 67 and 68.

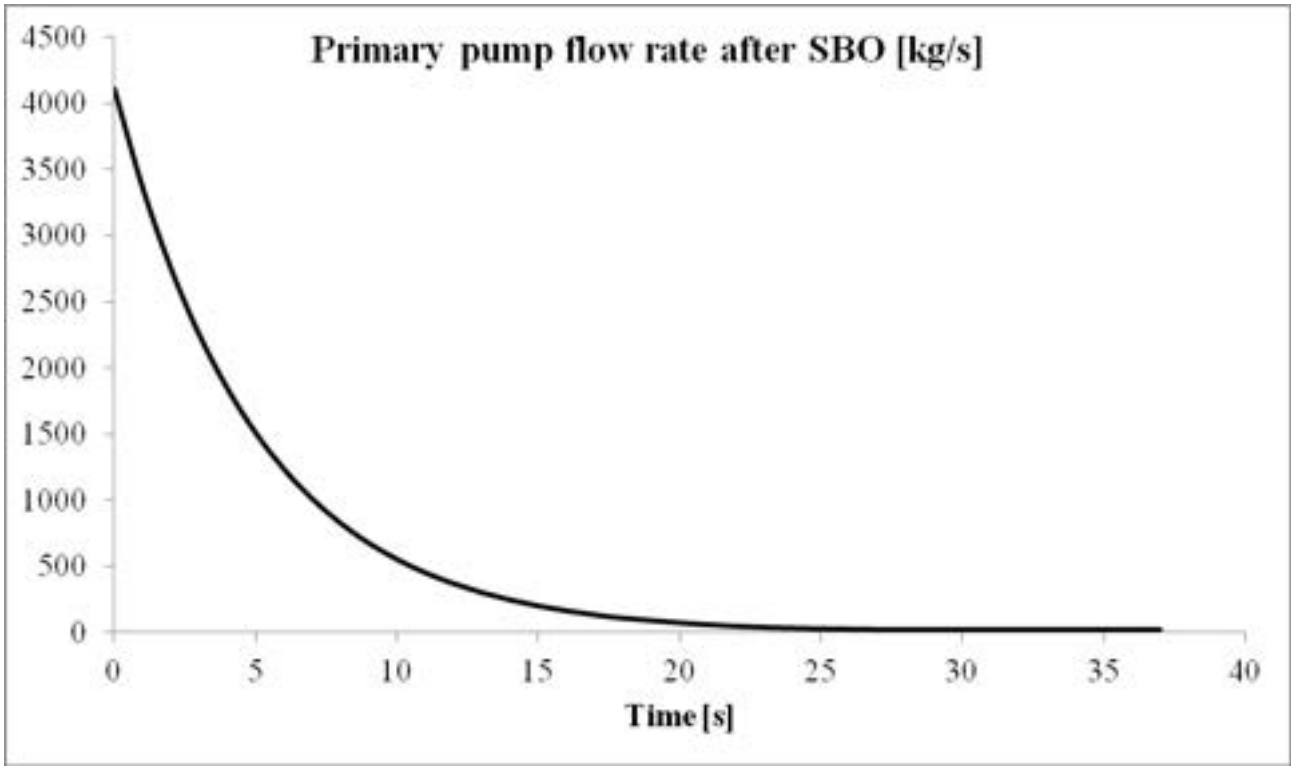

Figure 67. Primary pump flow rate after SBO

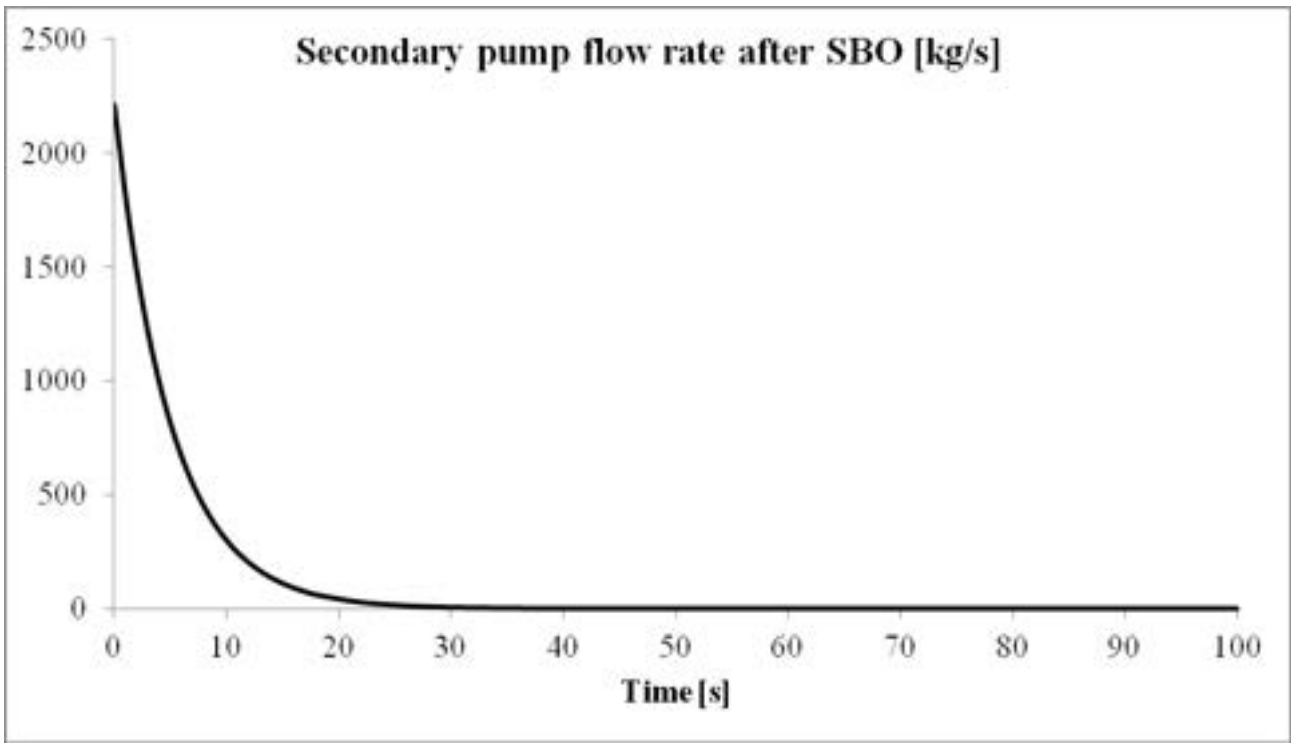

Figure 68. Secondary pump flow rate after SBO [kg/s]

8.1 Case 3+4: Isolation Condenser (Pool) as final heat sink

This paragraph is devoted to the description of the results obtained during the simulations that uses the pool heat exchanger as the final heat sink.

Primary pressure

Figure 69 and 70 report the behaviour of the pressure in the primary system. From figure 70 it is possible to observe a different behaviour in the cases taken into account. During the first hour the microchannel configuration is able to reduce the primary pressure with an higher speed than the helical coil configuration. After the first hour the pressure in the primary system in the case of the microchannel configuration stabilize near the value of 20 bar and remains nearly constant during the whole time of the transient. After 72 hours the pressure in the primary system reaches 16 bar. In the case of the helical coil configuration the pressure continues decreasing after the first hour. The stabilization level is reached after 10 hours at the value of 4 bar, while 2 bar of pressure are reached after 72 hours. No SRV are opened during the transients.

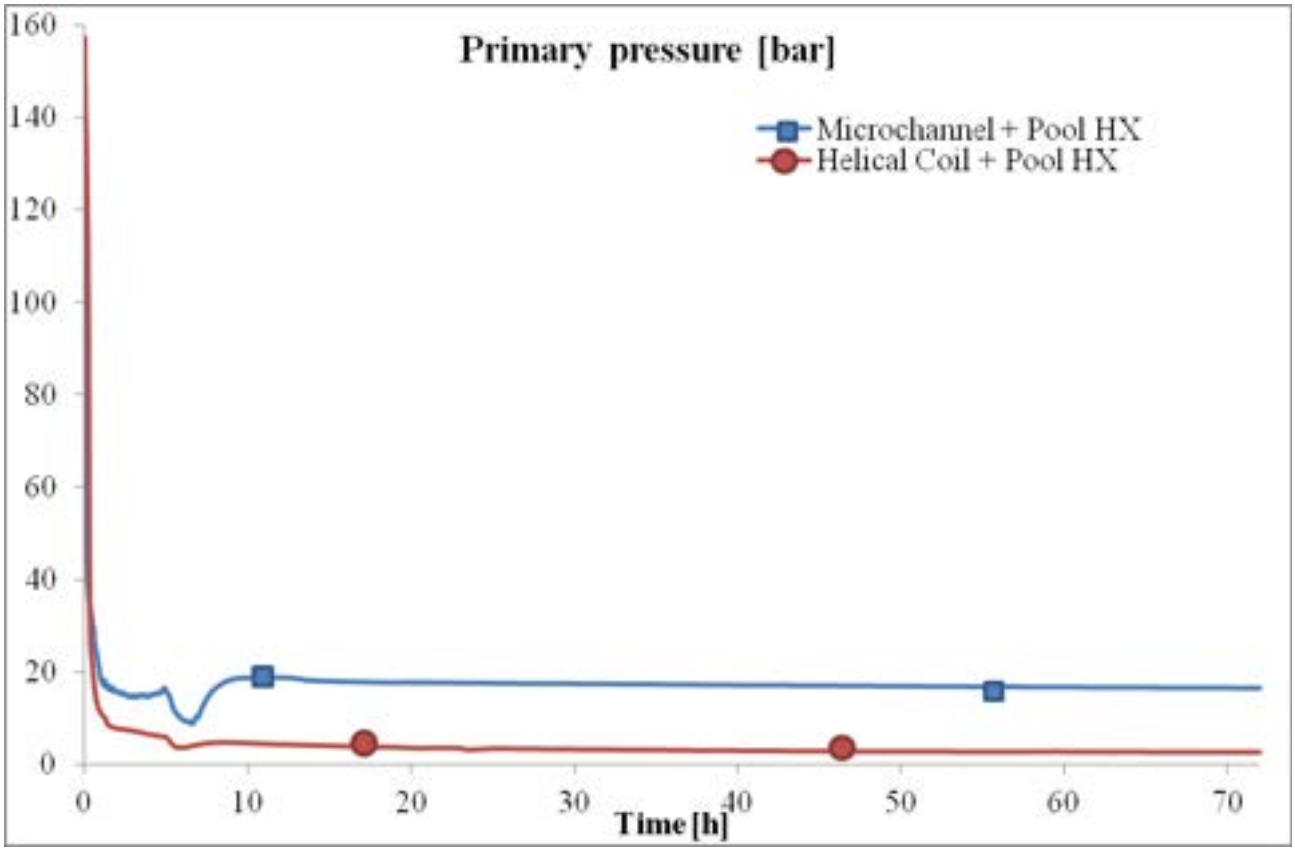

Figure 69. Primary pressure (Case 3+4)

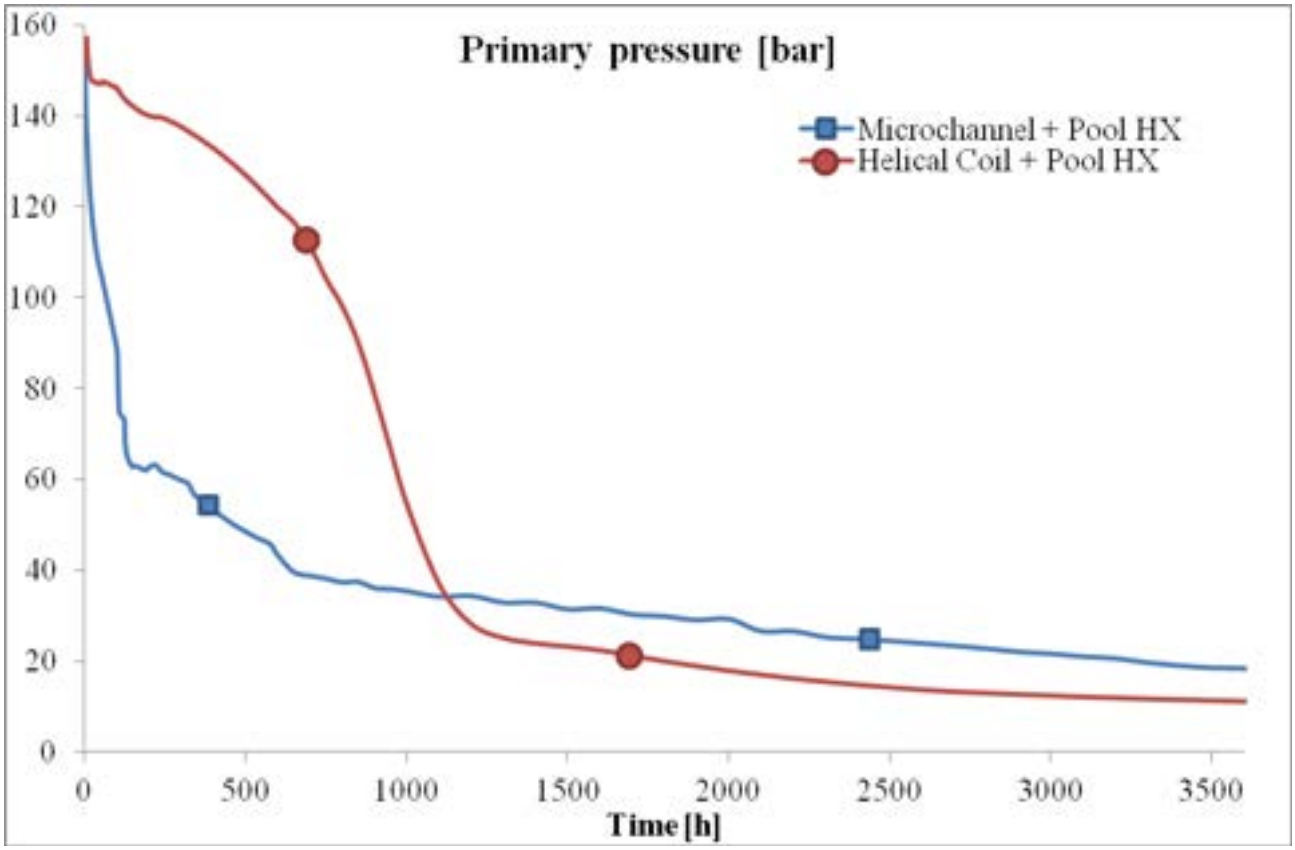

Figure 70. Primary pressure at the beginning of the transient (Case 3+4)

Primary temperatures

Figures 71, 72 and 73 show the behaviour of the primary system temperature. Figure 71 reports the temperature behaviour during the first hour. In the case of the microchannel configuration the inlet temperature reaches a minimum value of 100 °C after the cold water injection from the DHR system. The outlet temperature quickly reaches the saturation temperature and a time region is found where the steam formation in the core is intermittent. In the case of the helical coil configuration the inlet temperature's minimum after the DHR cold water injection is of 50°C. The outlet temperature is more stable with respect to the microchannel configuration and after the saturation condition is reached the outlet temperature is kept constant at the saturation temperature.

Figure 72 and 73 report the temperature behaviour during the first 10 hours and during the whole transient. An non-negligible difference exists between the two cases in the temperature difference between the inlet and the outlet of the core, which is in the order of 40 °C for the microchannel configuration and of few °C in the case of the helical coil configuration.

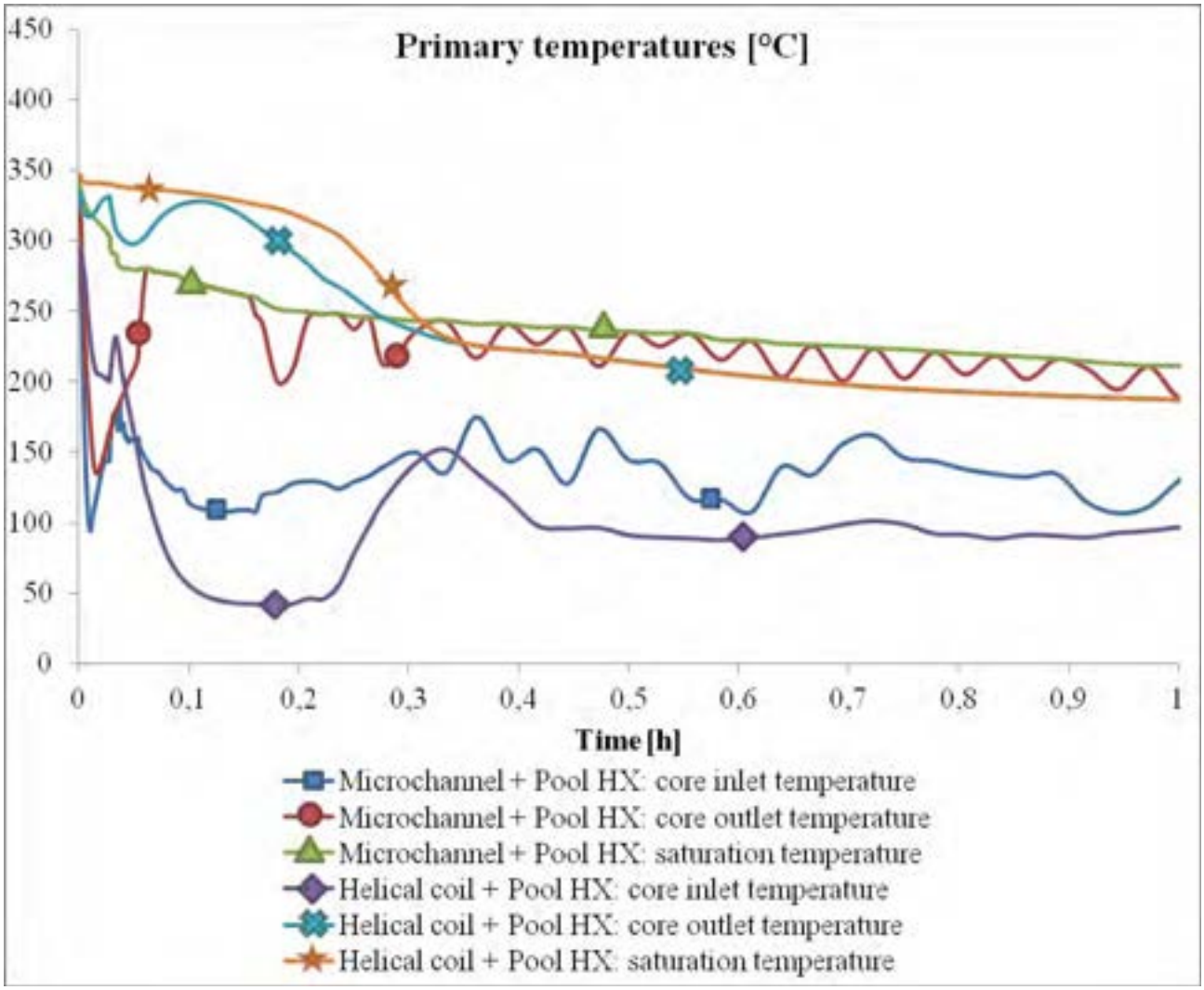

Figure 71. Primary system's temperatures in the first hour (Case 3+4)

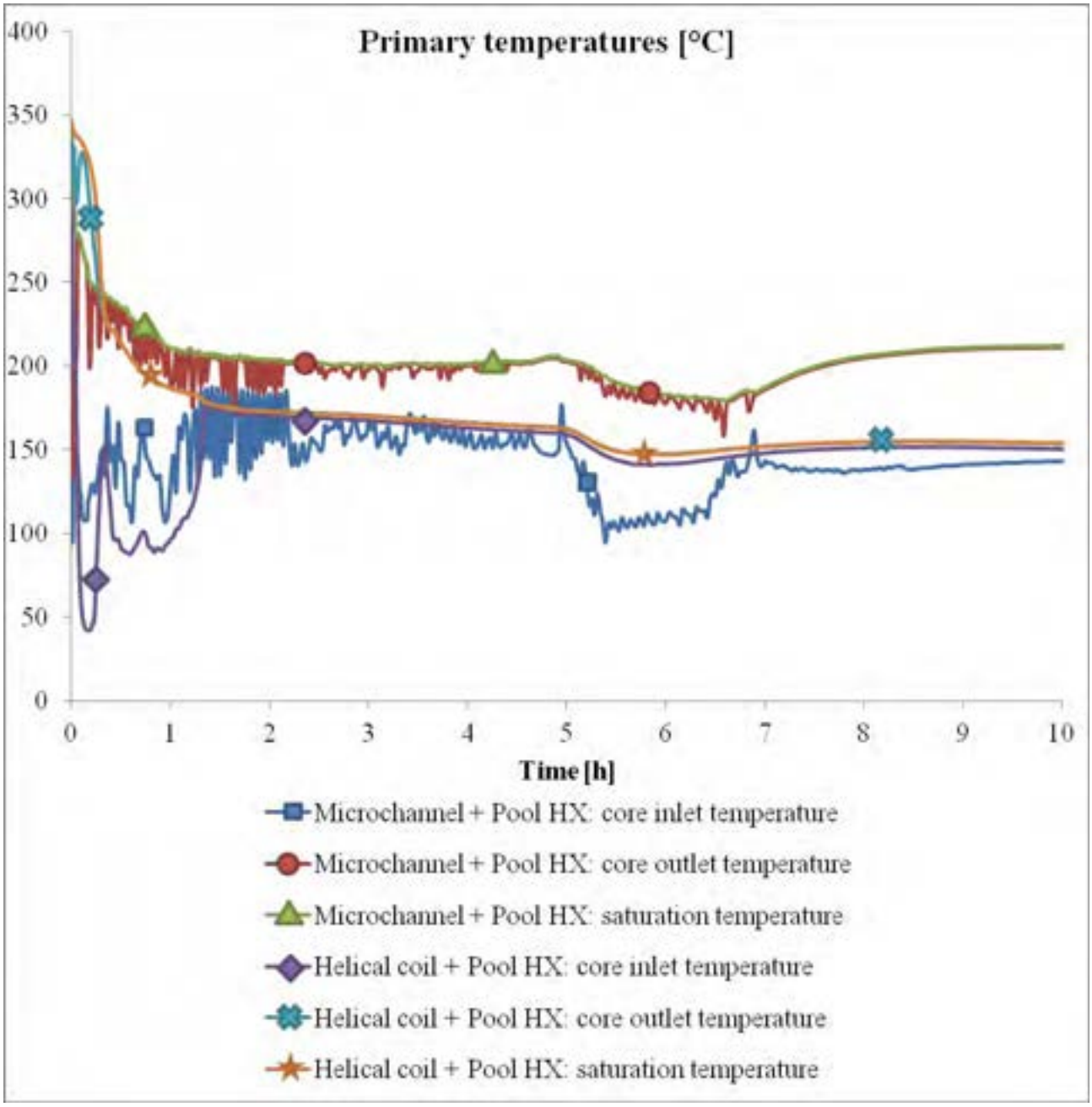

Figure 72. Primary system's temperatures during the first 10 hours (Case 3+4)

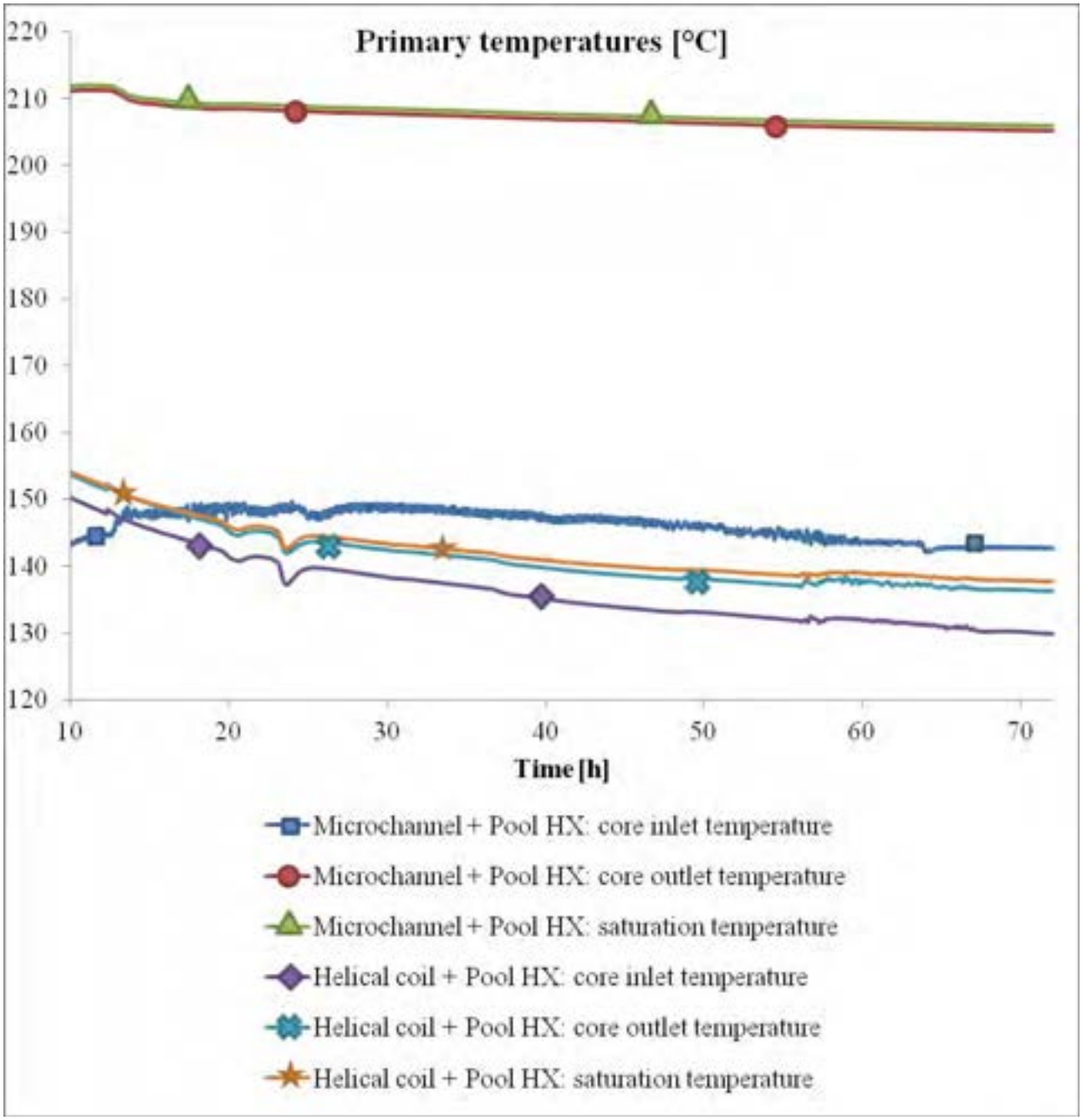

Figure 73. Primary system's temperature (Case 3+4)

Primary flow rates

Figures 74, 75 and 76 show the primary flow rate. The flow rates calculated result to be different in the two cases during the long term of the transient, and this finds a correspondence in the high difference of the temperature difference in the core. In this case, the flow rate circulating in the helical coil configurations is higher. In the first 10 hours (figure 75) the flow rate within the core in the case of the helical coil configuration has a rapid increase after the first hour: this event correspond to an increase in the density difference between the hot leg and the cold leg of the loop as the steam produced inside the core increases. During the long term, the flow rate in the helical coil configuration is higher than one order of magnitude on the flow rate in the microchannel configuration. At the beginning of the transient (figure 76) the flow rate inside the core decreases more rapidly in the helical coil configuration rather than the microchannel configuration.

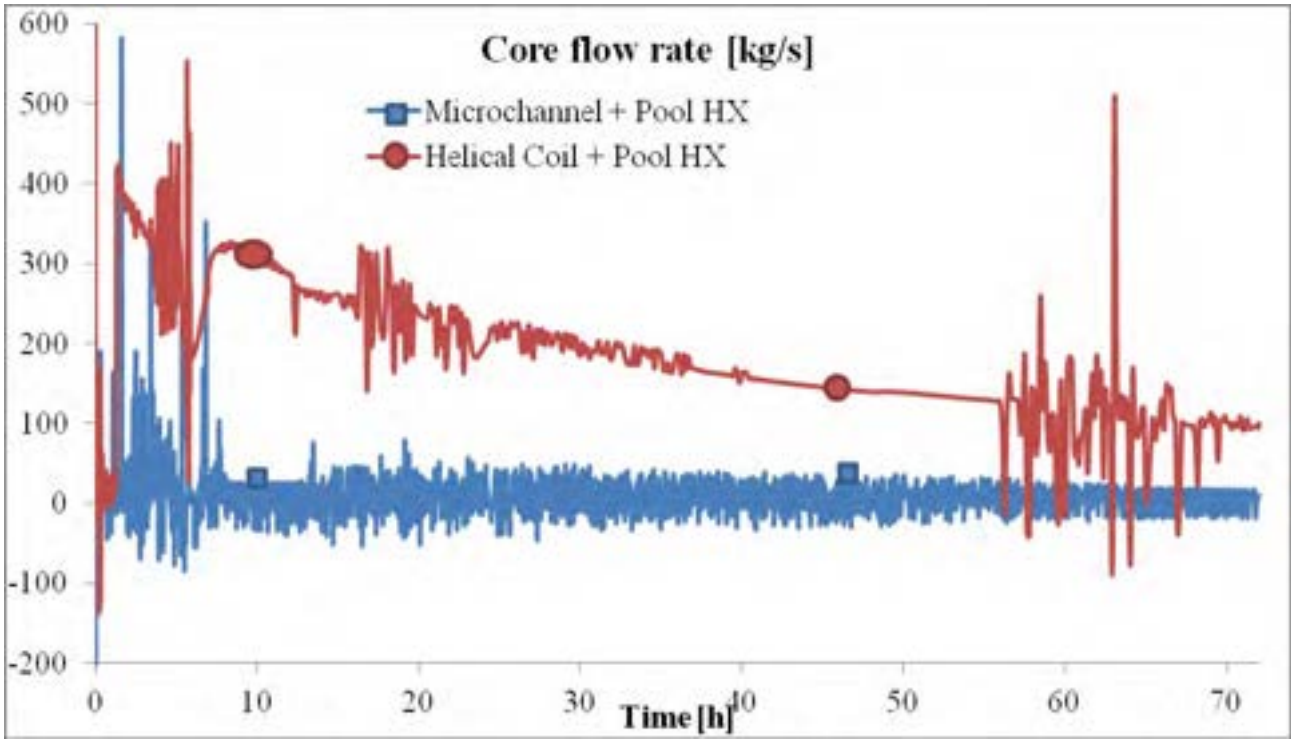

Figure 74. Core flow rate (Case 3+4)

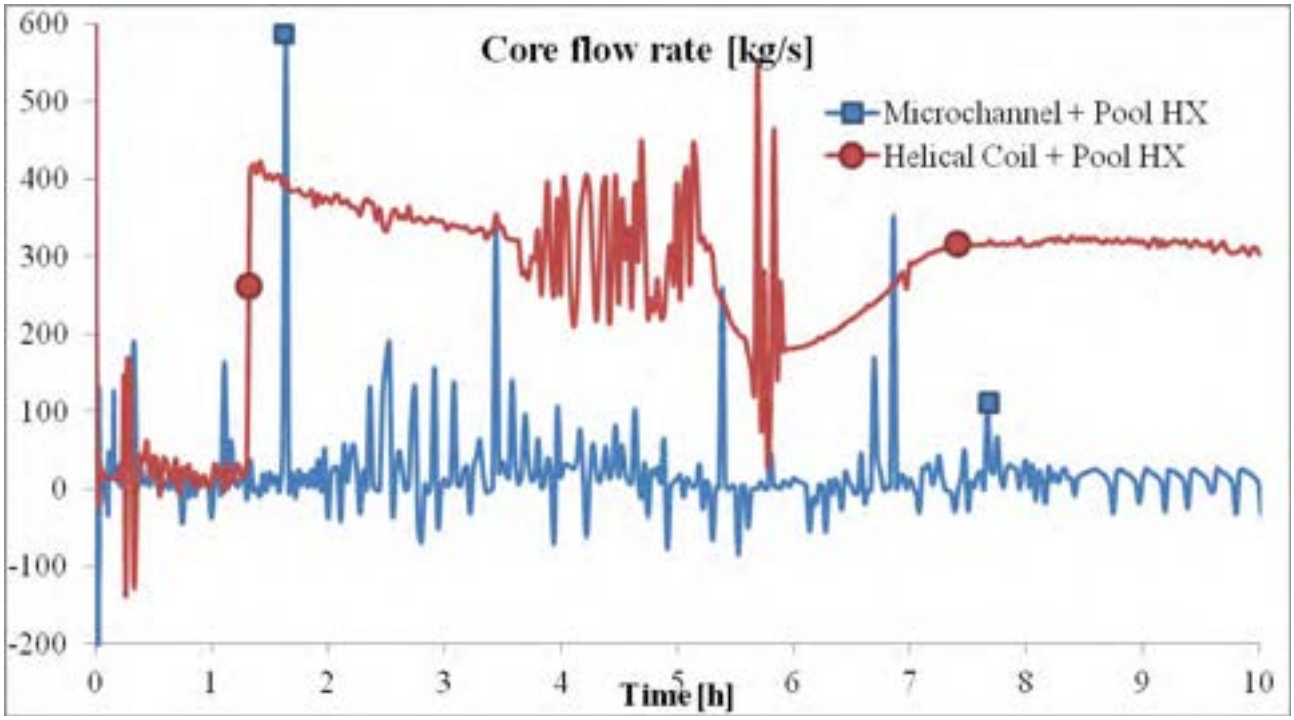

Figure 75. Core flow rate (Case 3+4)

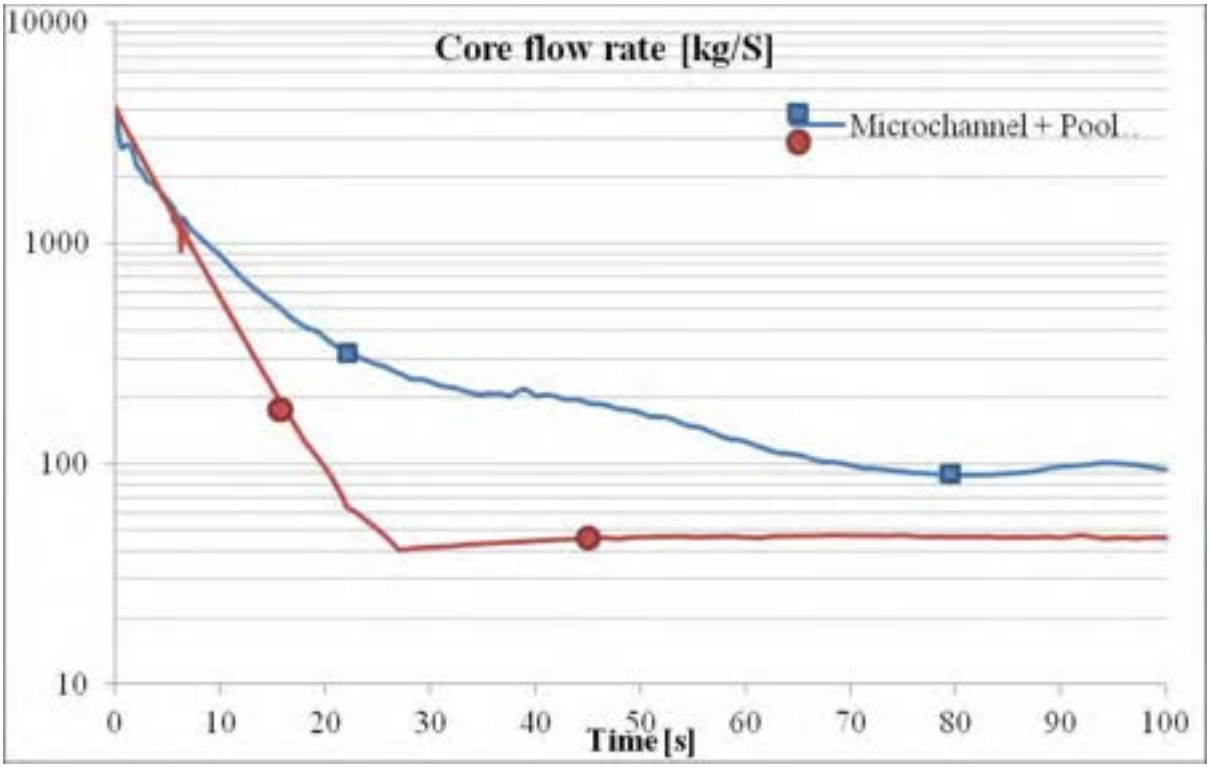

Figure 76. Core flow rate at the beginning of the transient (Case 3+4)

Intermediate loop pressure

Figures 77, 78 and 79 report the pressure behaviour in the intermediate loop. As the loop is set in thermal contact with the primary system, pressure wave oscillations take place in the intermediate loop because of density changes and un-match between absorbed and released power. These density waves last for a couple of minutes and they decrease in time. As natural circulation is established inside the loop pressure increases up to a stable value which is kept nearly constant for the whole transient. The pressure of the second loop is in both cases around 4.8 bar after 10 hours from the beginning of the transient. Due to thermal inertia the thermal contact between the primary and secondary loop has a delayed effect on pressure of nearly 10 seconds in both cases (figure 78).

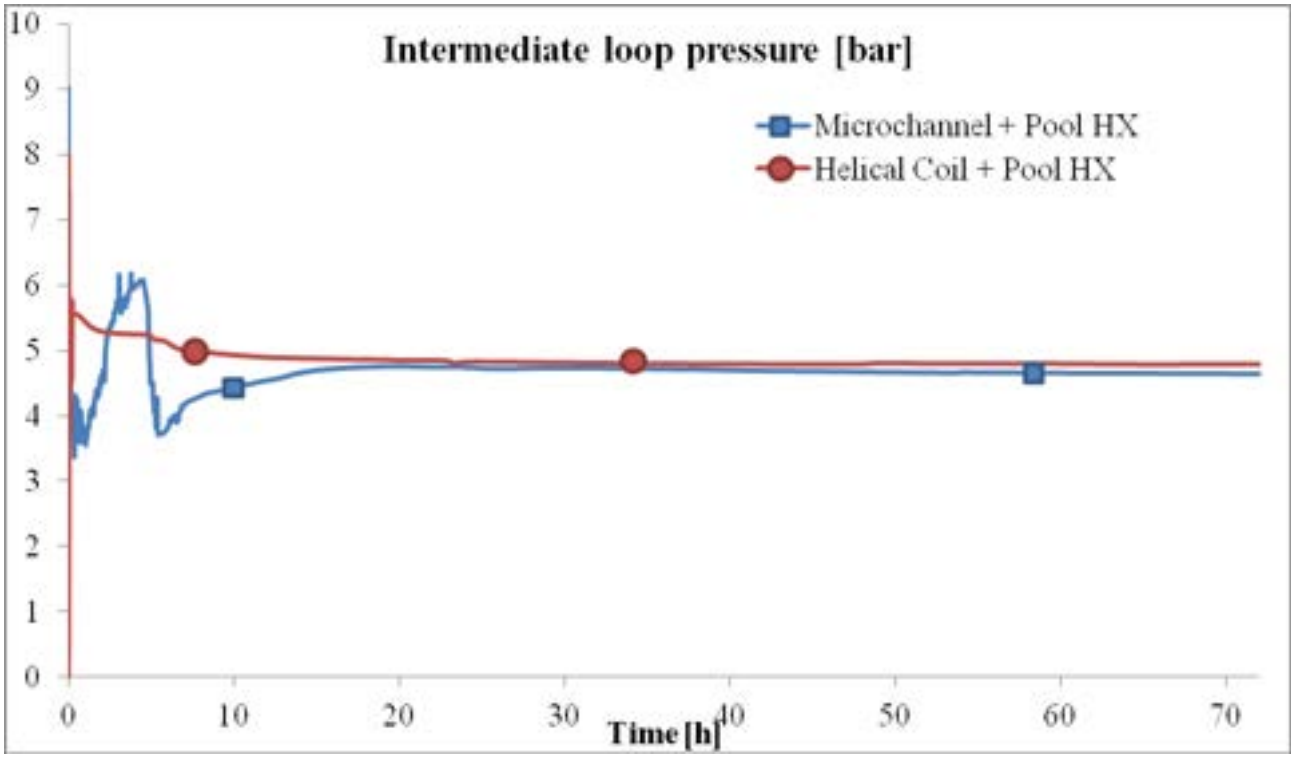

Figure 77. Intermediate loop pressure (Case 3+4)

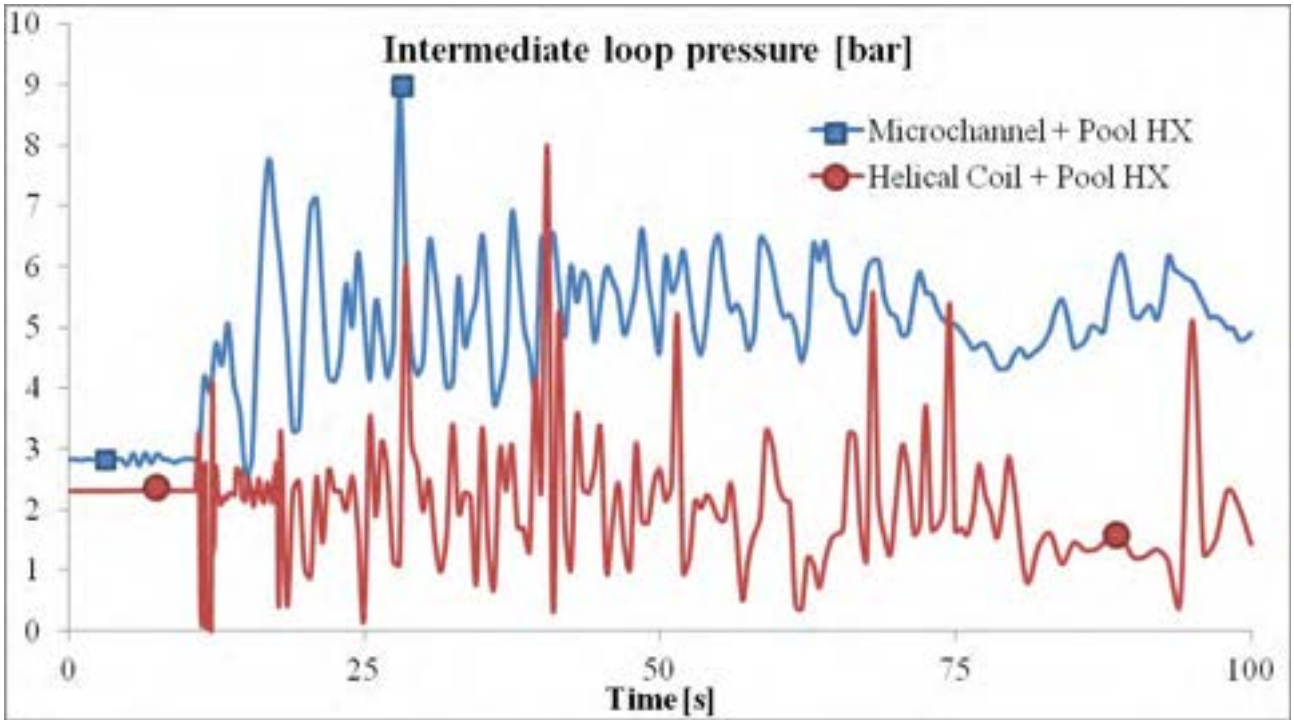

Figure 78. Intermediate loop pressure at the beginning of the transient (Case 3+4)

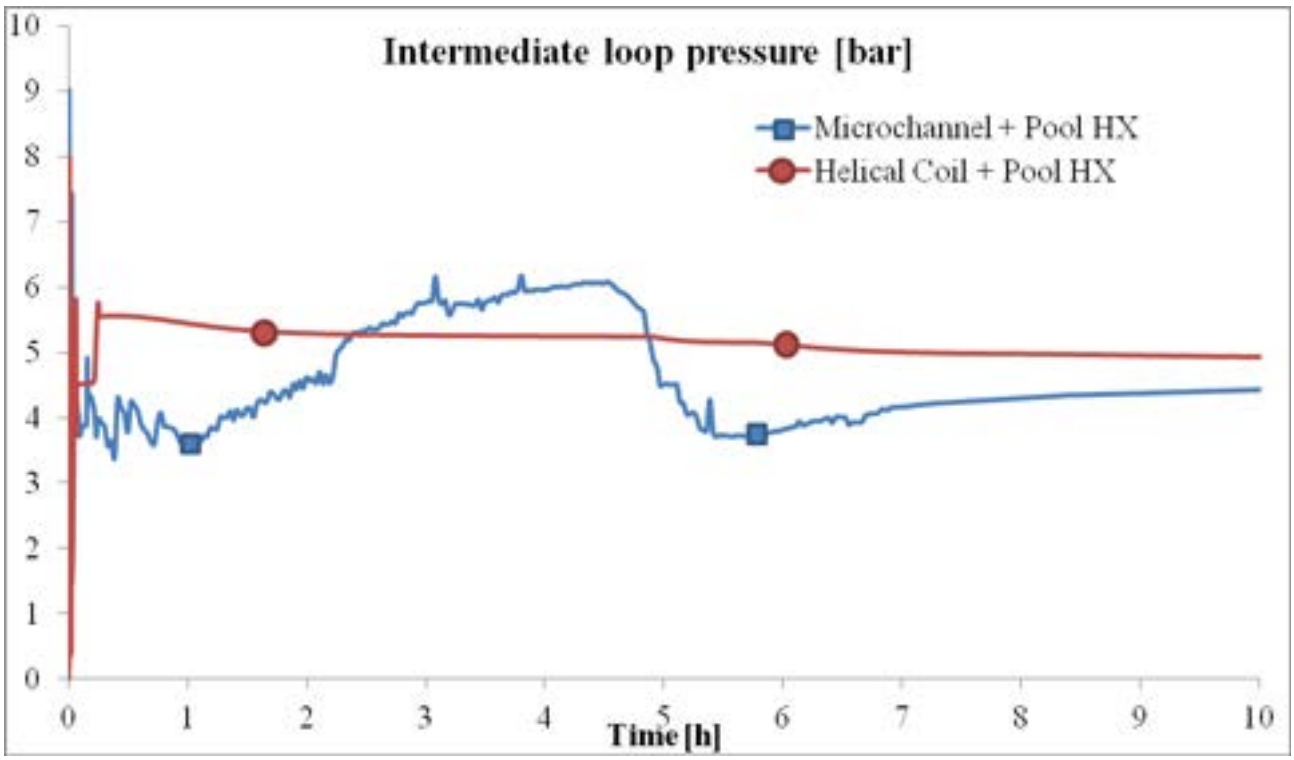

Figure 79. Intermediate loop pressure in the first 10 hours (Case 3+4)

Intermediate loop temperatures

Figures 80 and 81 report the behaviour of temperatures in the intermediate loop. The predicted outlet temperature in the case of the microchannel configuration shows an alternate behaviour with high oscillations during the whole transient. This effect may be explained by local numerical errors and code difficulties in predicting the heat transfer inside the microchannel geometry. Further studies both in the comprehension of modelling and numerical precision will be required to assess Relap5 capabilities to model microchannel heat exchangers.

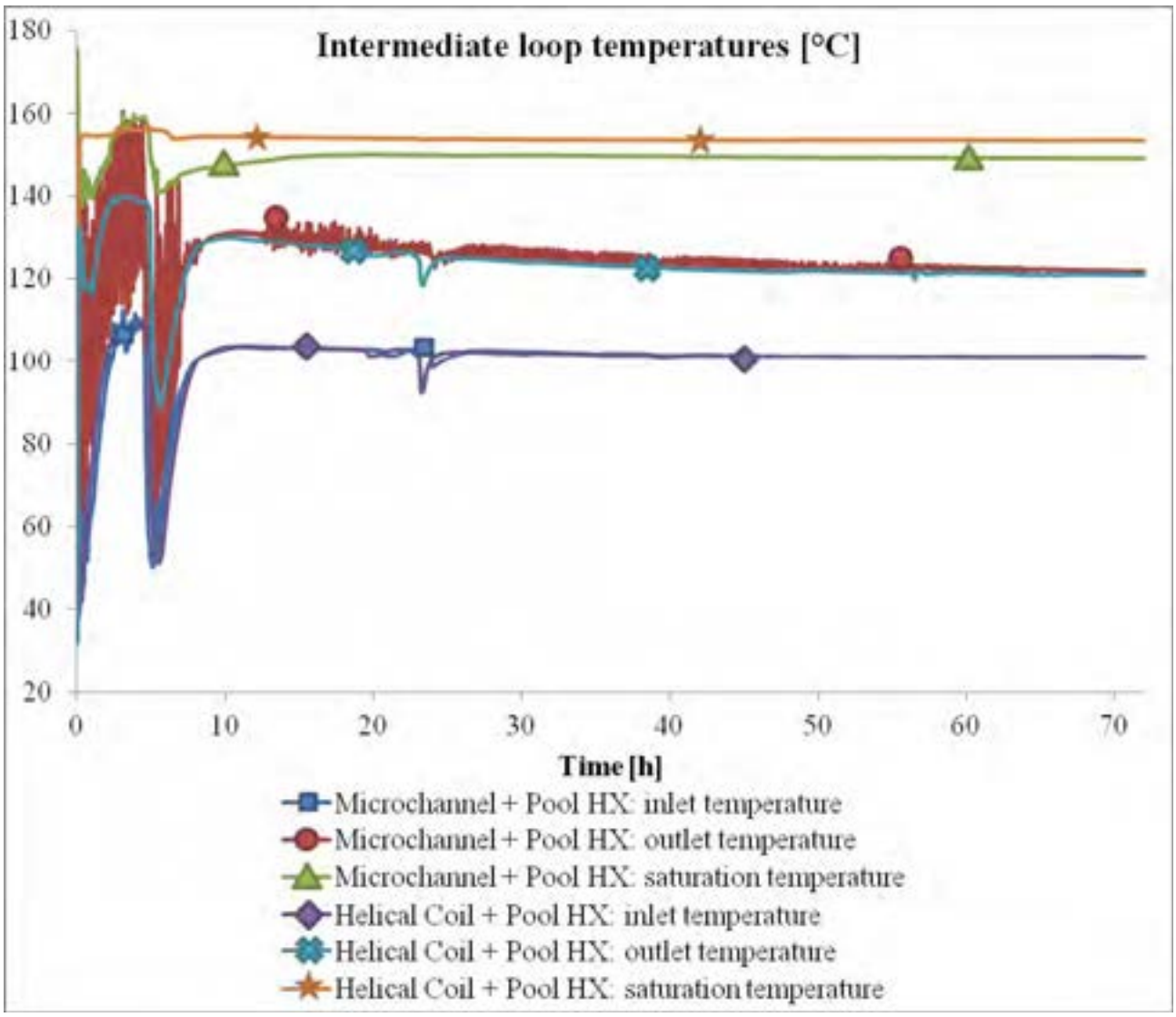

Figure 80. Intermediate loop temperatures (Case 3+4)

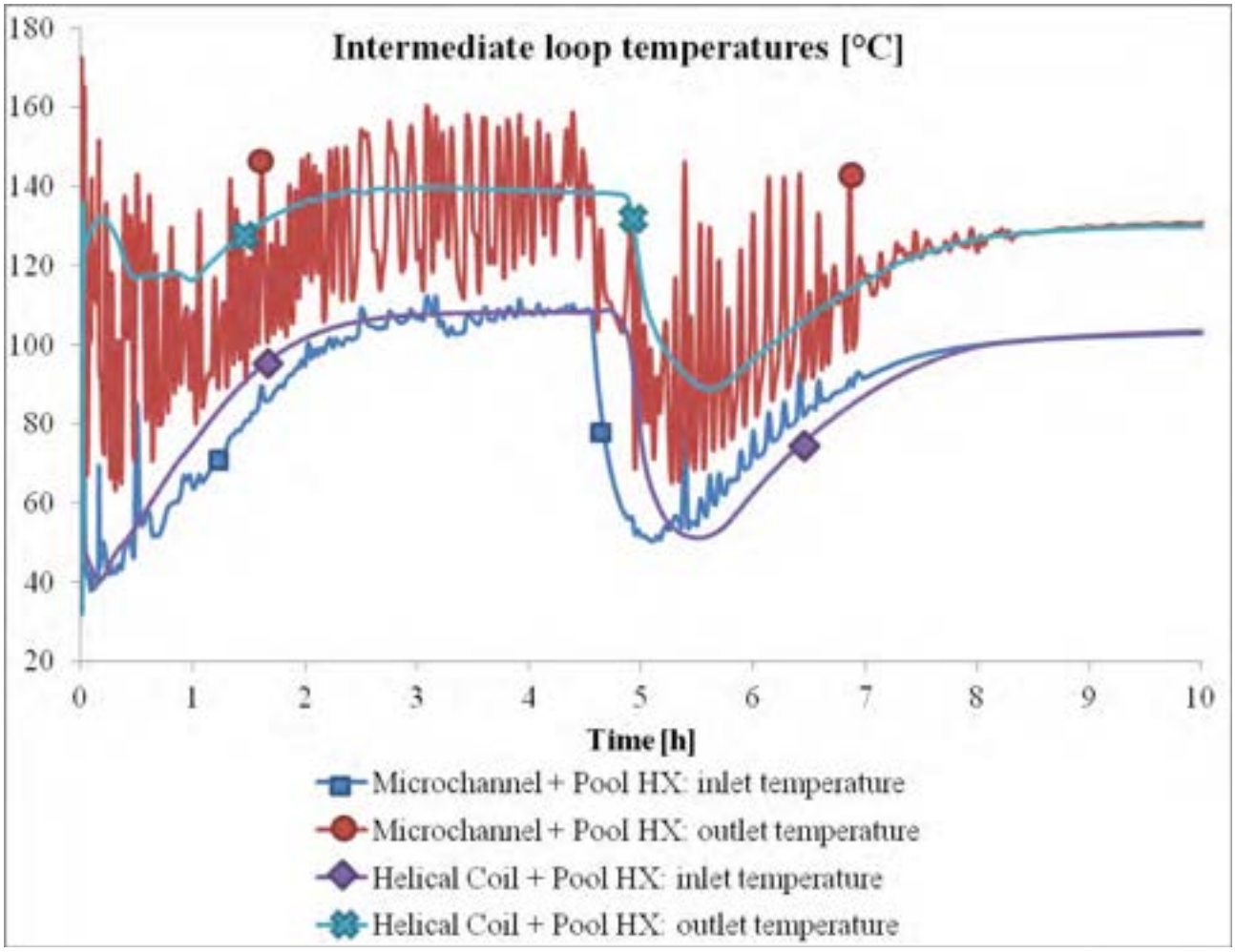

Figure 81. Intermediate loop temperatures (Case 3+4)

The general behaviour of the temperatures computed in the two cases is comparable, as it is the temperature difference between inlet and outlet. Local boiling phenomena are present in the first minutes of the transient, but in the long term the flow conditions of the loop are of completely single phase.

Intermediate loop flow rates

Figures 82, 83 and 84 report the behaviour of the flow rate in the intermediate loop. In the first seconds of the transient (figure 84) the thermal contact with the primary system causes flow rate oscillations similar to the ones obtained in the pressure behaviour. As natural circulation is established a comparable flow rate is predicted in both cases analysed. The helical coil configuration is characterized by a slight higher flow rate with a relative difference below 10%.

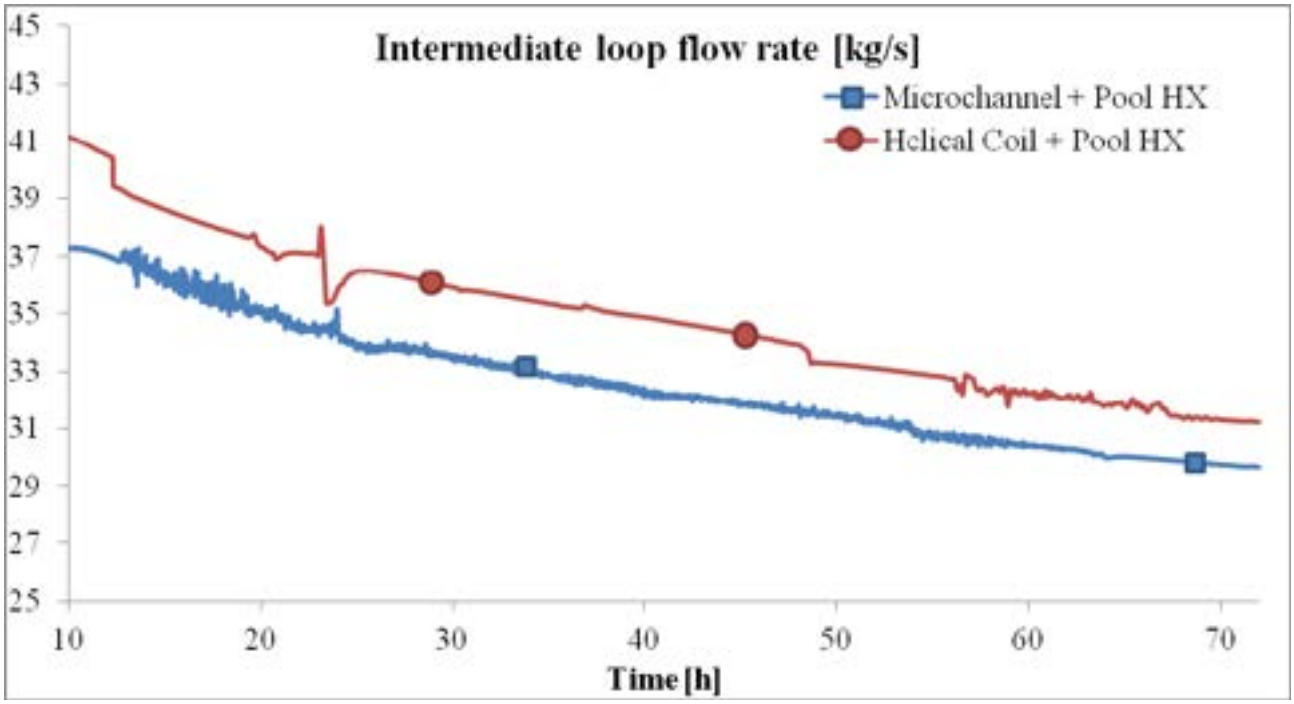

Figure 82. Intermediate loop flow rates in the long terms (Case 3+4)

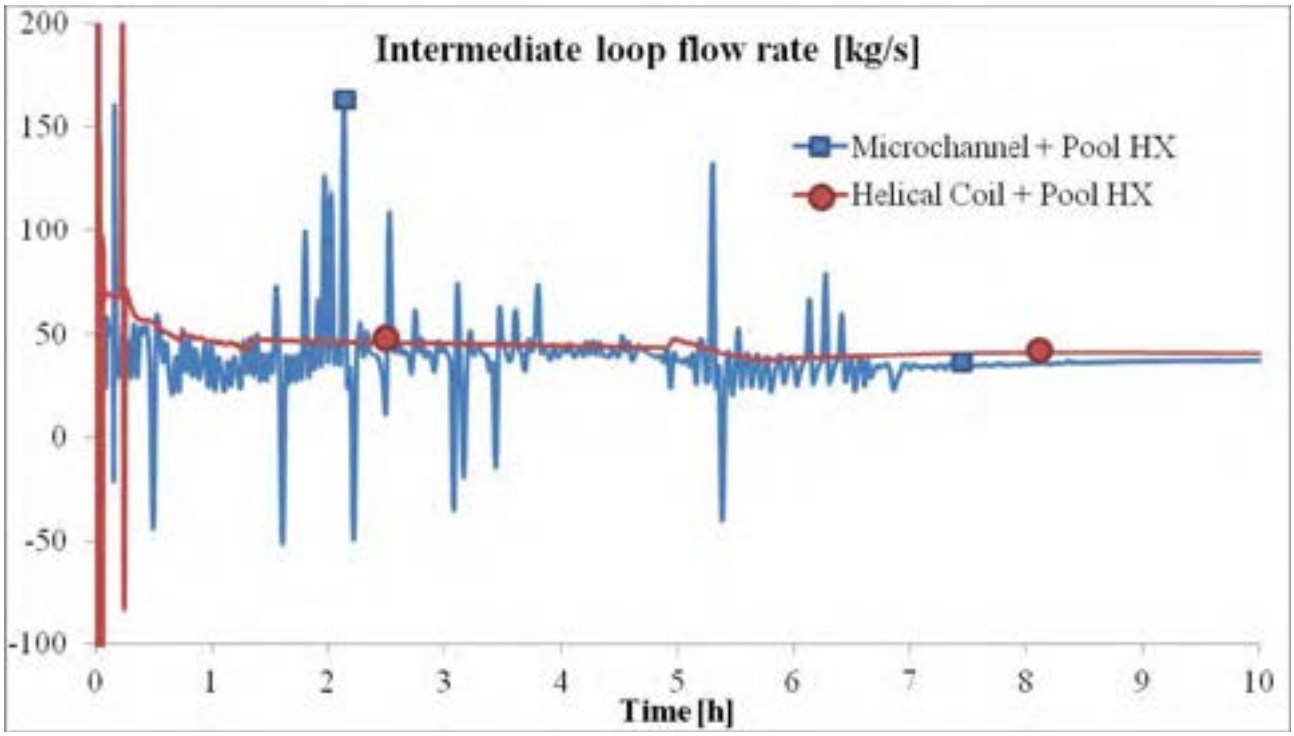

Figure 83. Intermediate loop flow rates in the first 10 hours (Case 3+4)

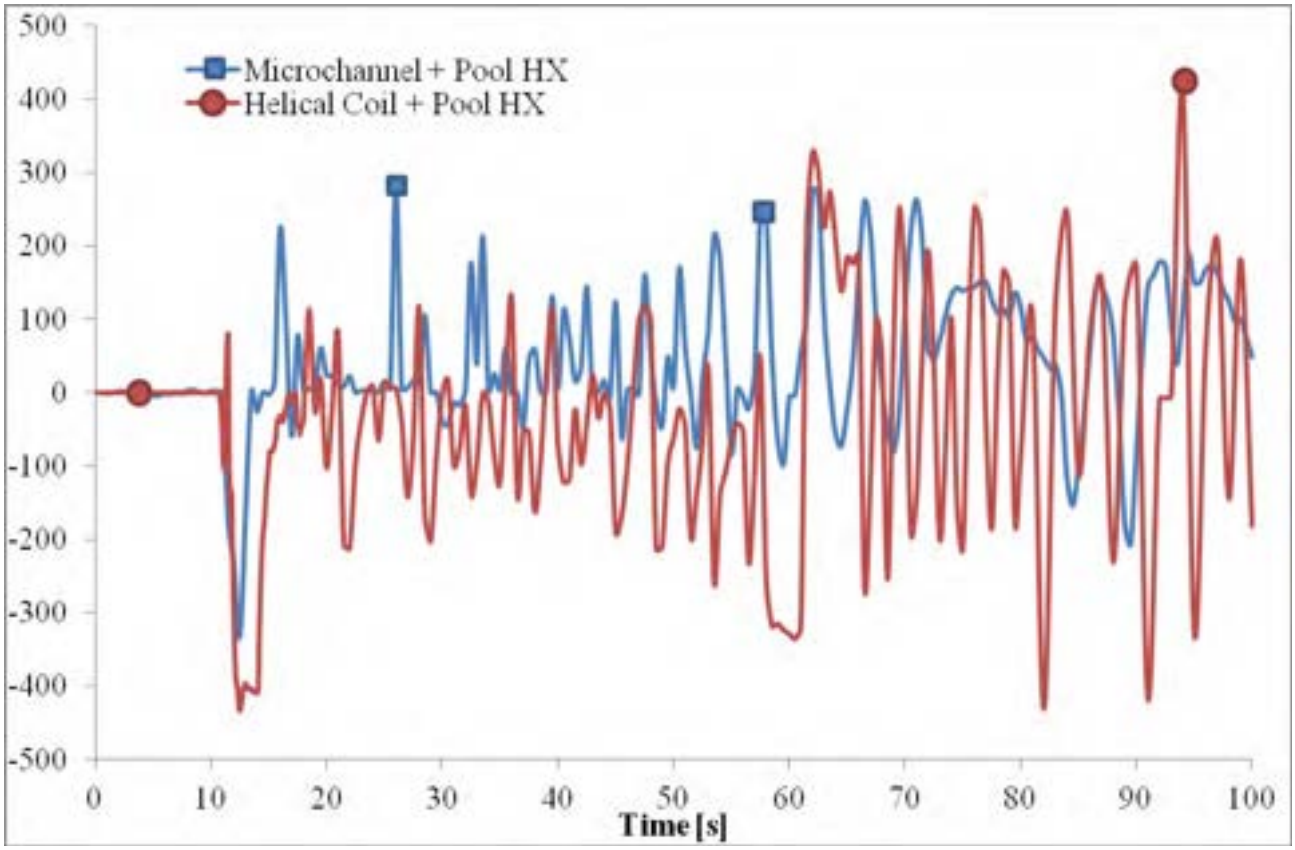

Figure 84. Intermediate loop flow rates at the beginning of the transient (Case 3+4)

Thermal power

The thermal power exchanged inside the DHR is depicted in figures 85 and 86. As in the case of the outlet temperature for the microchannel configuration, in this case the power transferred by this component is affected by an high scattering during the first 10 hours of the transient. The helical coil configuration results in a more linear behaviour during the transient and it's power match with the decay heat curve is around the first hour. In the long term of the transient the power oscillations decrease and both in the helical coil and microchannel configuration the decay heat curve is followed and a quasi-static heat transfer condition is established.

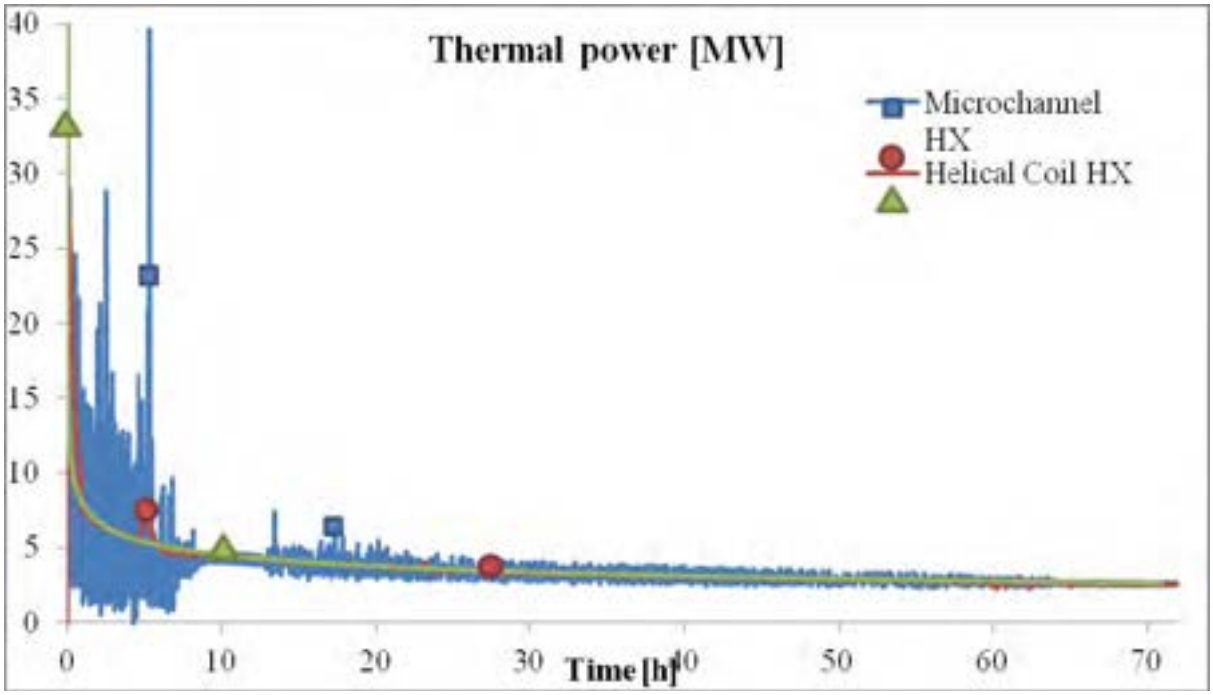

Figure 85. Thermal power (Case 3+4)

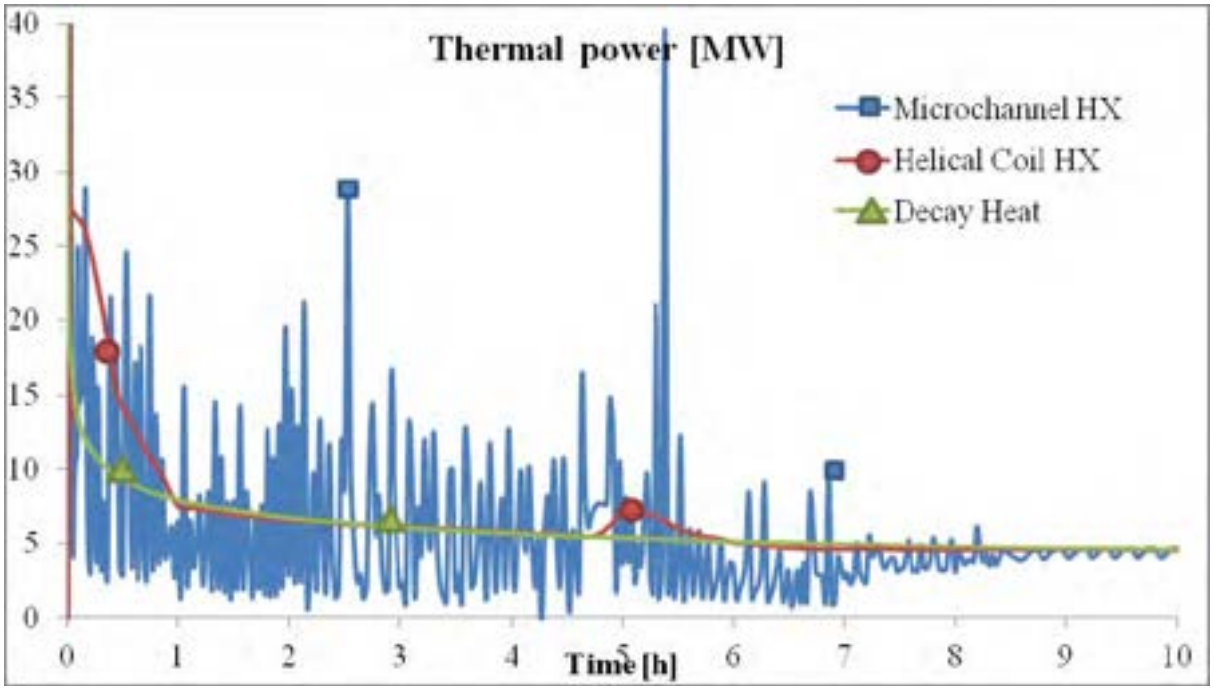

Figure 86. Thermal power in the first 10 hours (Case 3+4)

8.2 Case 1+2: Air Cooled Heat Exchanger as final heat sink

In this second paragraph, the results obtained with the two configurations analysed (microchannel configuration and helical coil configuration) in which the final heat sink is constituted by an air heat exchanger will be presented and discussed. The detailed description of the accidental sequence is reported in chapter 5.3.

Primary pressure

Figures 87, 88 and 89 shows the pressure in the primary system. At the beginning of the transient (figure 89) there is a rapid pressure decrease helped by the combination of the scram which reduces the power production and of the secondary system which continues to remove heat from the system during the first 100 seconds giving time to the DHR to rise in temperature and pressure. The microchannel configuration permits a more rapid depressurization of the system at the beginning of the transient. During the first 10 hours the primary pressure in the microchannel configuration reaches the value of 40 bar which is kept nearly constant during the whole time of the transient. The final pressure reached by the primary system after 72 hours is of 36 bar. In the case of the helical coil configuration the primary pressure continues to decrease further and the final value reached is 2 bar.

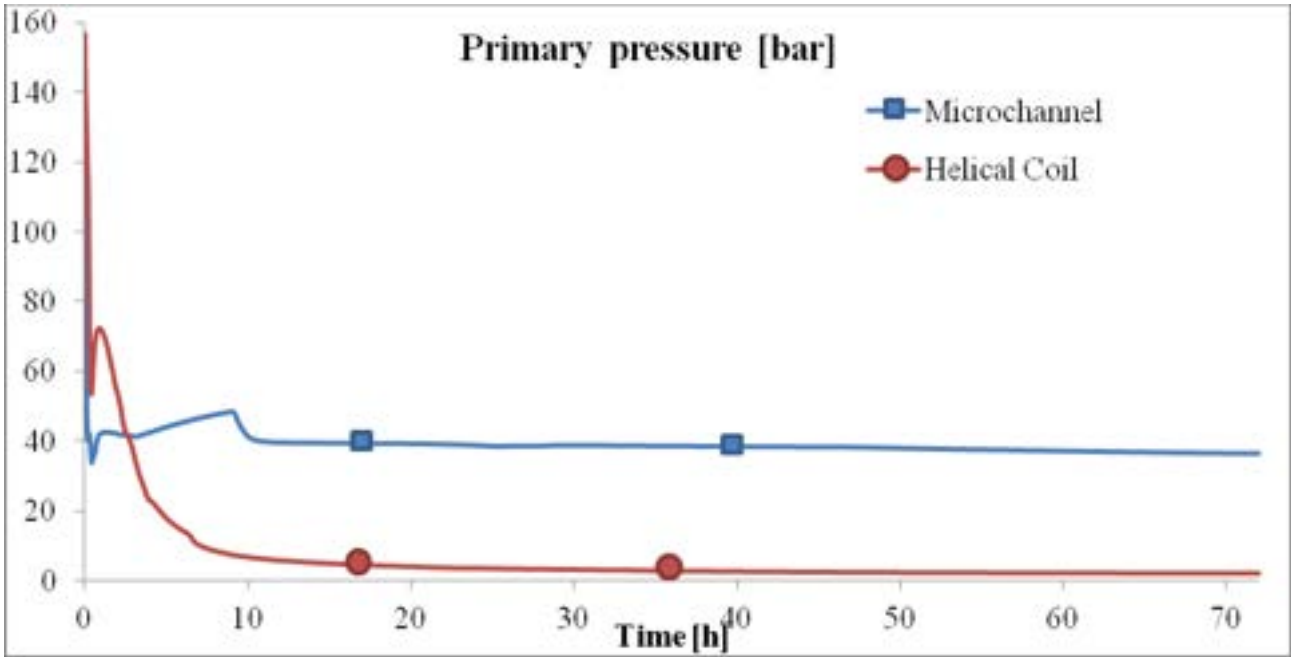

Figure 87. Primary system's pressure (Case 1+2)

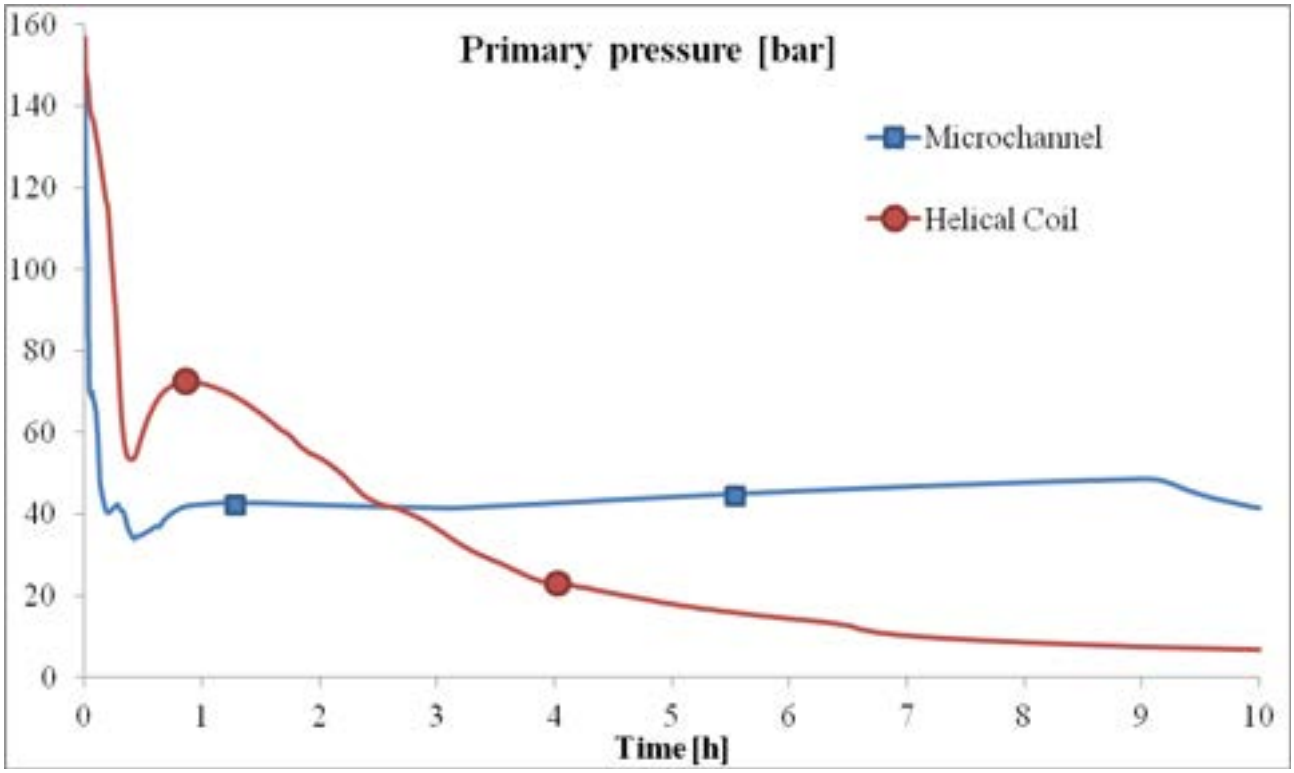

Figure 88. Primary system's pressure in the first 10 hours (Case 1+2)

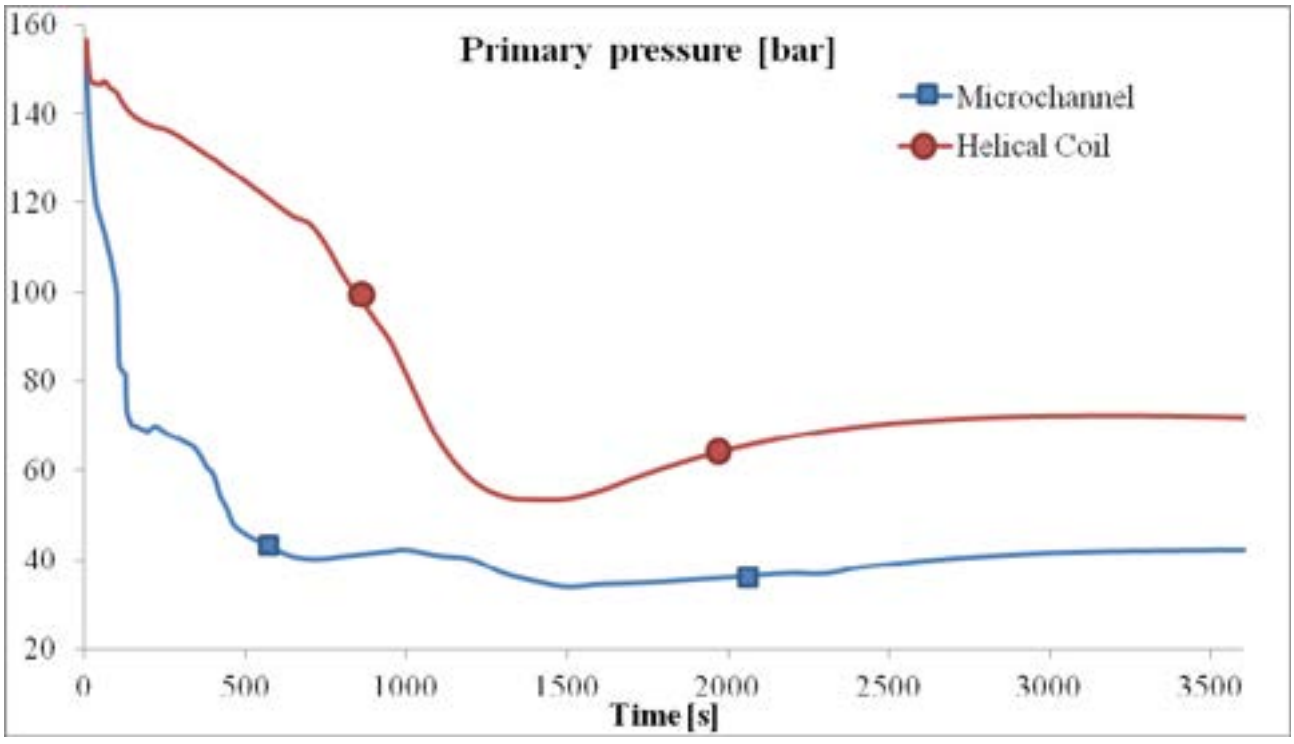

Figure 89. Primary system's pressure in the first hour (Case 1+2)

Primary temperatures

Figures from 90 to 92 show the behaviour of the primary system's temperatures. In the first seconds of the transient (figure 92) a strong temperature reduction is experienced in both system caused by the cold water injection from the DHR system. This effect is more evident in the helical coil configuration. As seen in the previous case in chapter 8.1, the temperature difference between inlet and outlet of the core is higher in the case of the microchannel configuration.

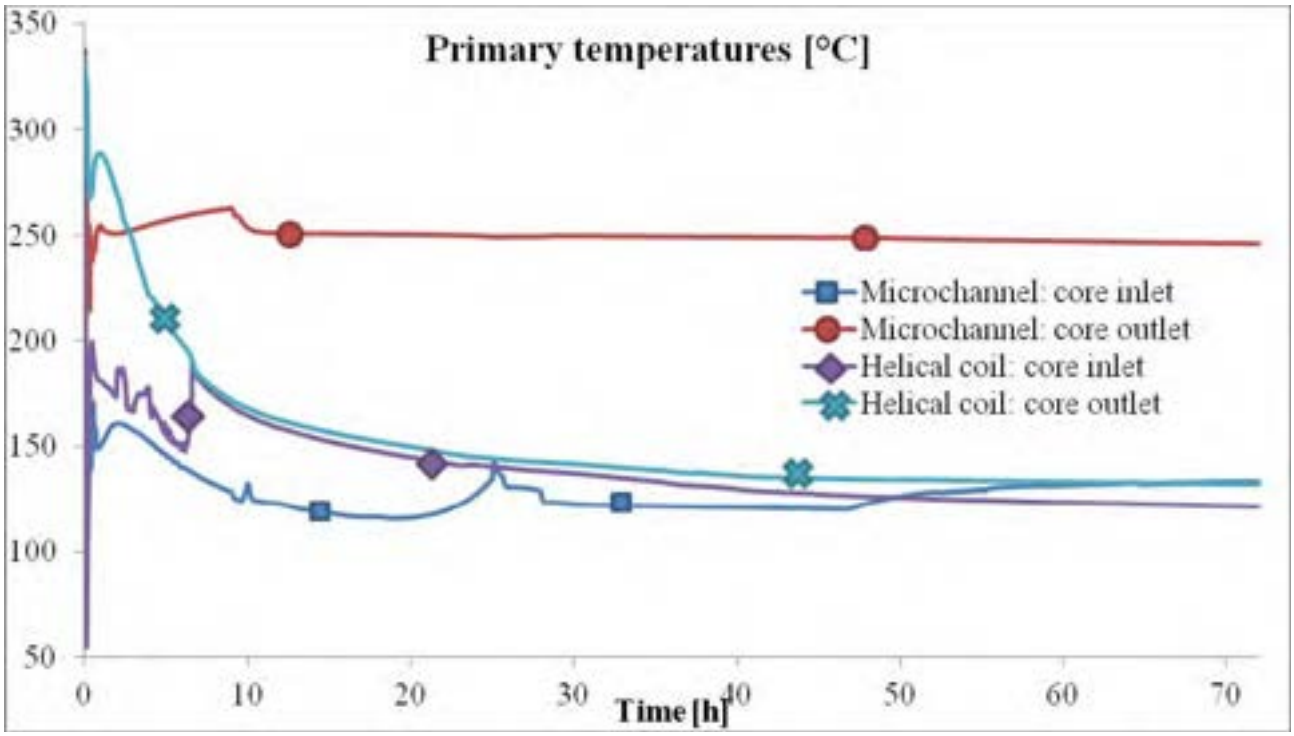

Figure 90. Primary temperatures (Case 1+2)

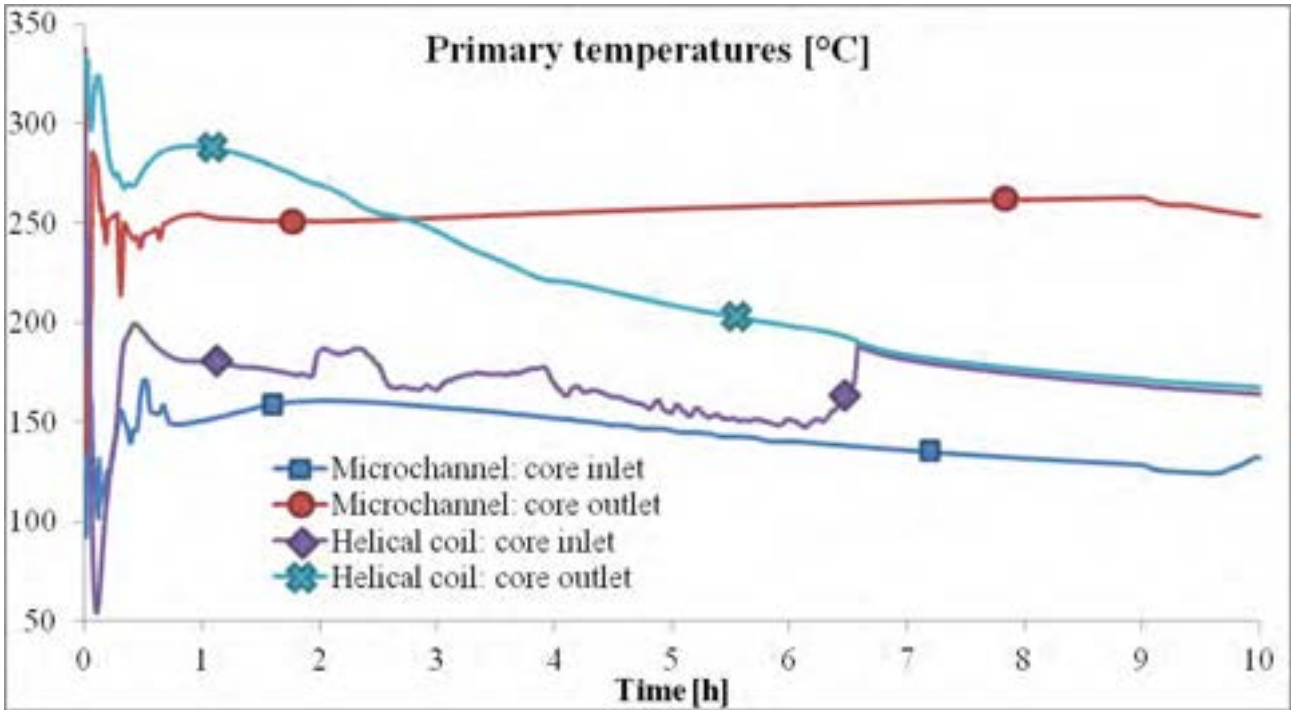

Figure 91. Primary temperatures in the first 10 hours (Case 1+2)

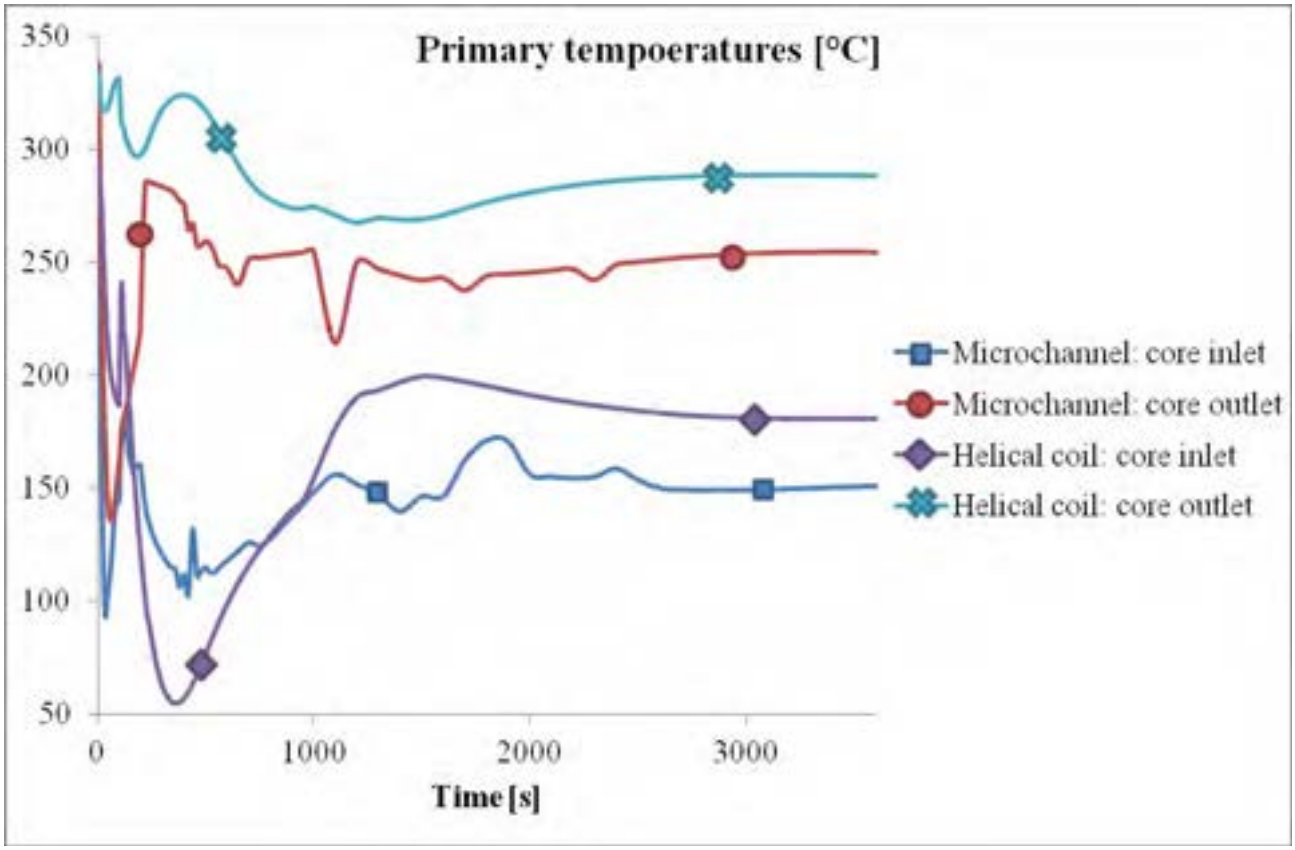

Figure 92. Primary temperatures at the beginning of the transient (Case 1+2)

Primary flow rate

Figures 93 and 94 show the behaviour of the core flow rate. In the first seconds of the transient the flow rate is driven by the pump inertia. As the pump is stopped (t = 100 s) a negative flow rate is experienced in the microchannel configuration. In the long term of the transient the flow rate circulating in the system is different, with the helical coil being the configuration with an higher flow rate. The abrupt flow rate change in the helical coil configuration in figure 93 is due to a density difference increase inside the primary system due to a steam production increase inside the core.

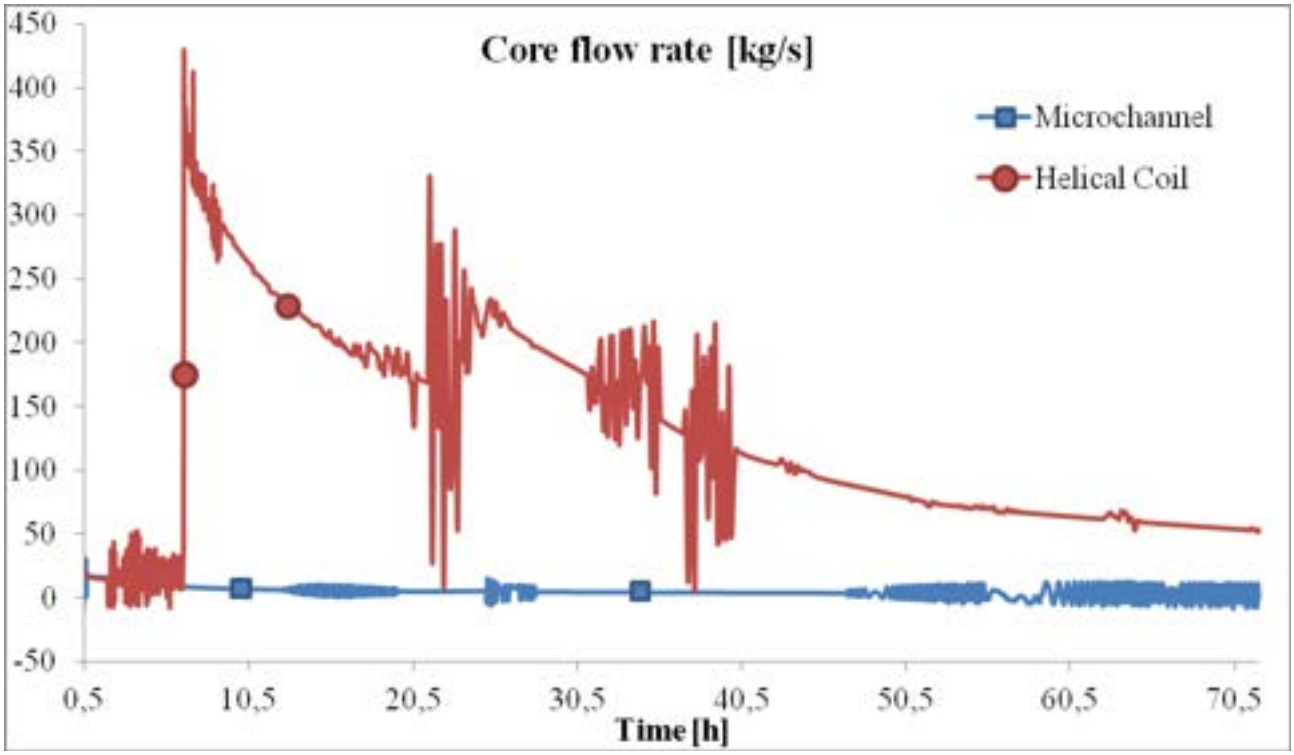

Figure 93. Core flow rate (Case 1+2)

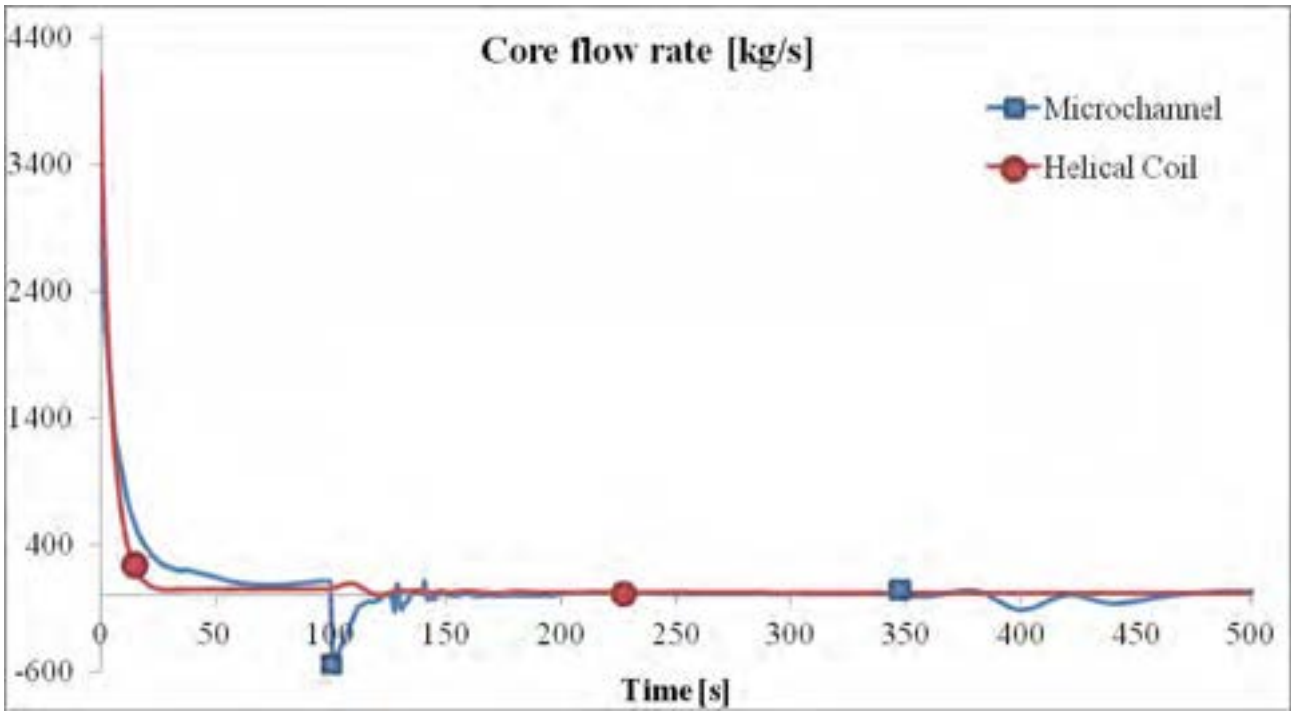

Figure 94. Core flow rate at the beginning of the transient (Case 1+2)

Intermediate loop pressure

Figures 95 and 96 show the behaviour of the intermediate loop pressure. At the beginning of the transient the thermal contact between the primary system and the intermediate loop causes pressure wave oscillations in the system. These oscillations reduces over time as natural circulation is established. The pressure maximum value reached by the system in the helical coil configuration (20 bar) is higher than the one obtained in the microchannel configuration (14 bar). As the system reaches its maximum point the pressure starts decreasing sharply. The higher pressure variation in the long term cooling is recorded in the microchannel configuration which experiences a series of depressurizations after 24 hours and after 55 hours.

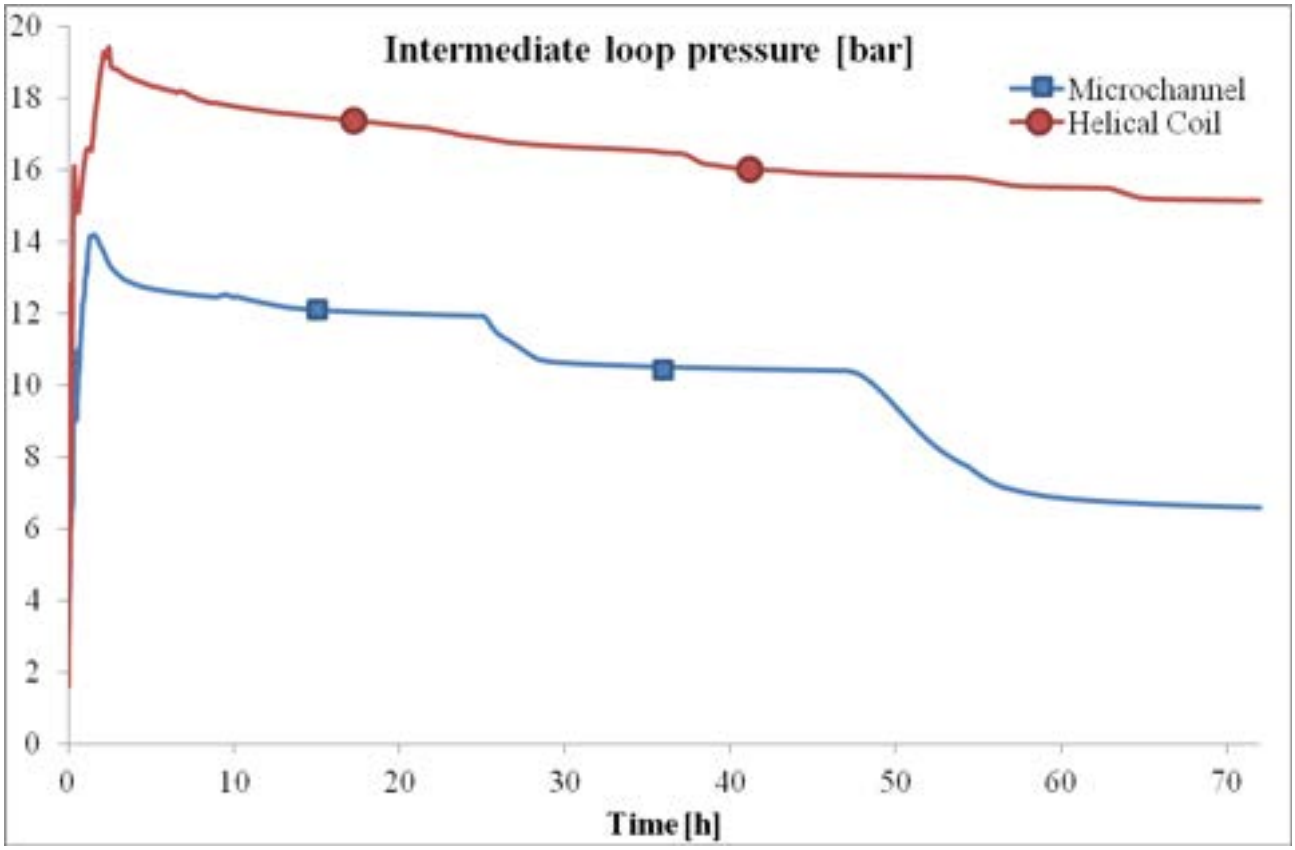

Figure 95. Intermediate loop pressure (Case 1+2)

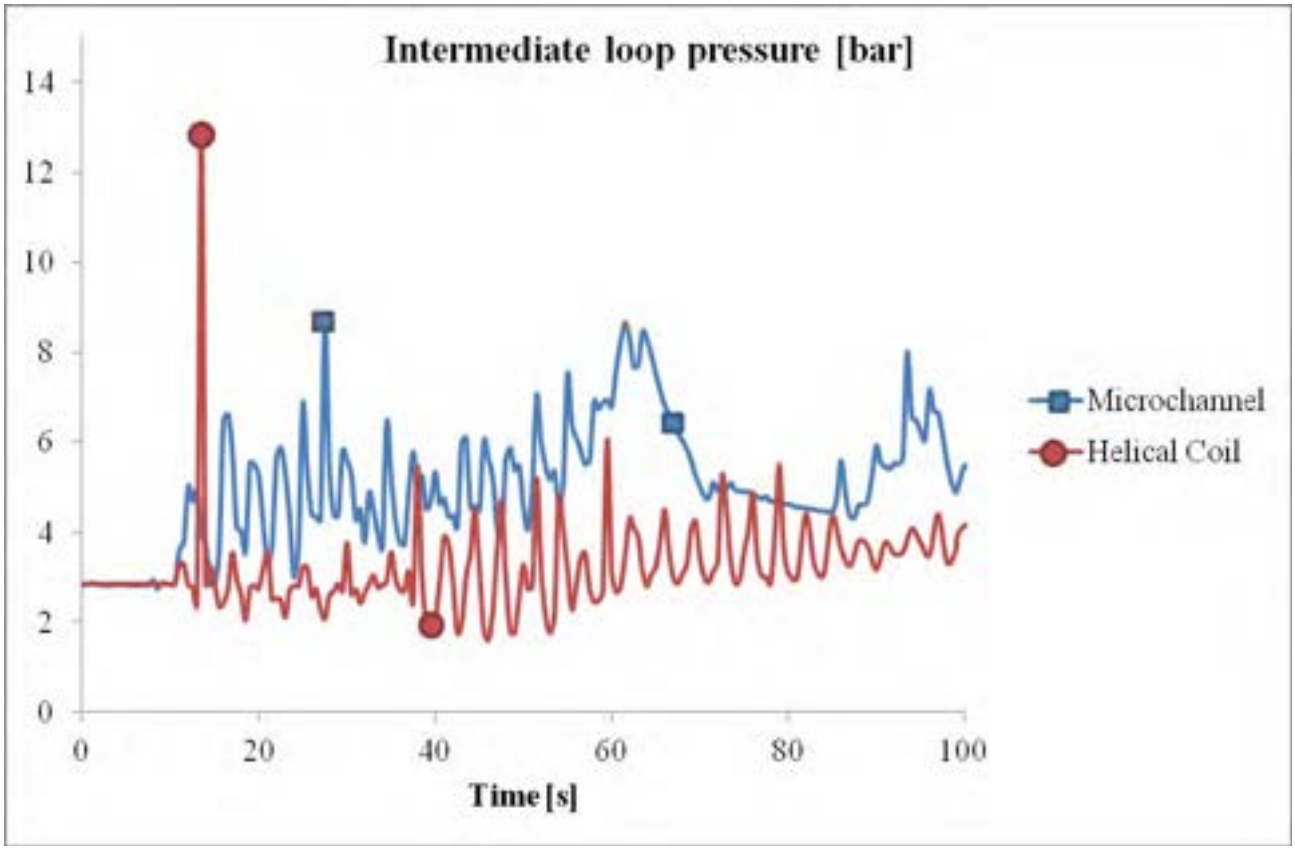

Figure 96. Intermediate loop pressure at the beginning of the transient (Case 1+2)

Intermediate loop temperature

Figures 97 and 98 show the behaviour of the intermediate loop temperatures. In this case the helical coil configuration and the microchannel configuration show a comparable behaviour during the long term cooling of the transient with a constant temperature difference between inlet and outlet of the heat exchanger which is in the order of 20°C. At the beginning of the transient the thermal contact causes flow rate oscillations, which in turn affect the temperature evolution. From figure 98 it is possible to observe that this phenomena have a little effect on the inlet temperature in the helical coil configuration.

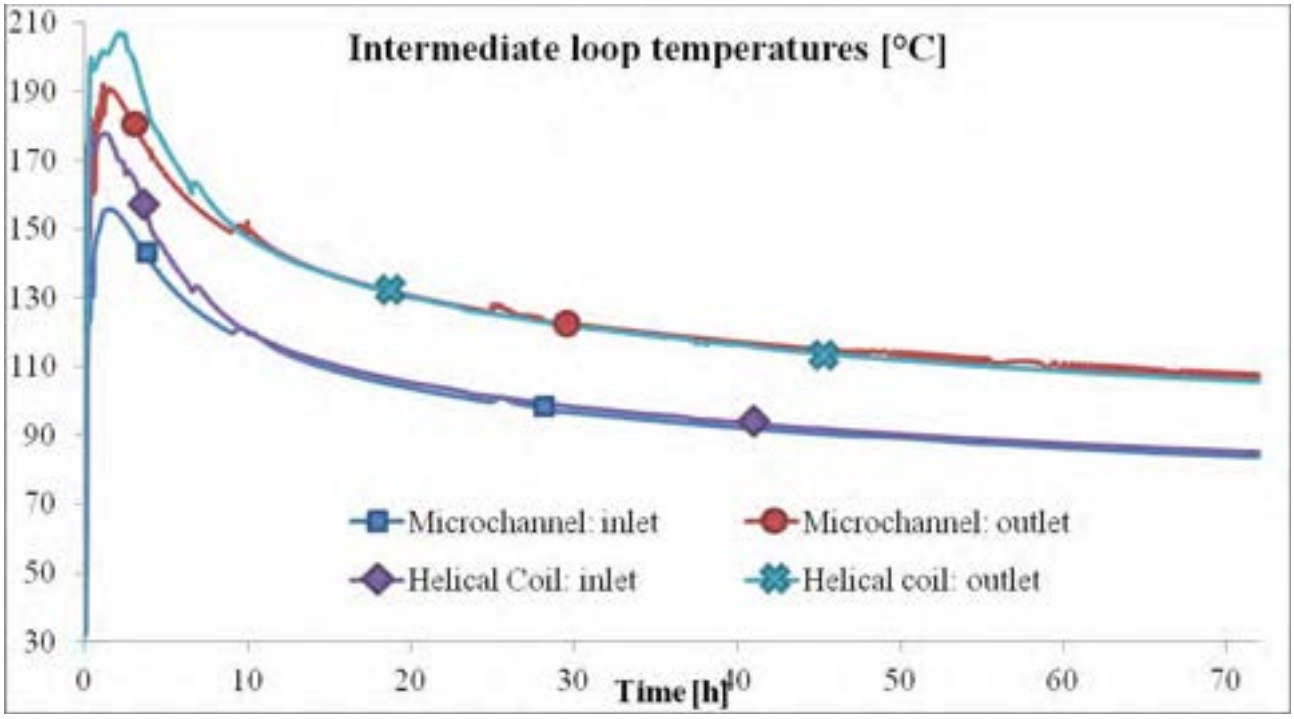

Figure 97. Intermediate loop temperatures (Case 1+2)

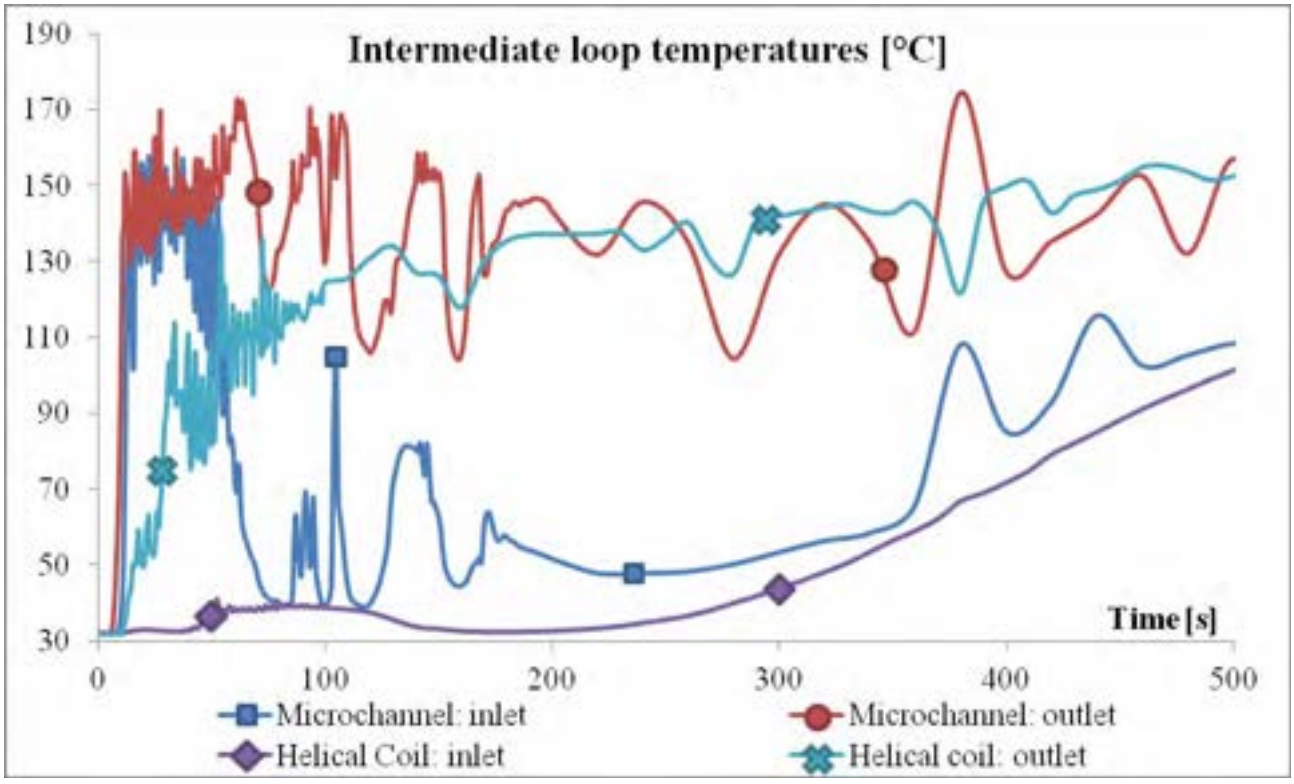

Figure 98. Intermediate loop temperatures at the beginning of the transient (Case 1+2)

Intermediate loop flow rate

Figures 99 and 100 show the behaviour of the intermediate loop flow rate. In the long term cooling the flow rates in the two cases are comparable, with the helical coil configuration having a fairly higher flow rate in the order of the 10%. At the beginning of the transient (figure 100) the flow rate is intermittent in the two cases and the oscillations decrease during time. Both natural circulation phenomena and numerical errors affect the thermal contact phase, and other studies will be required to describe in detail this effects.

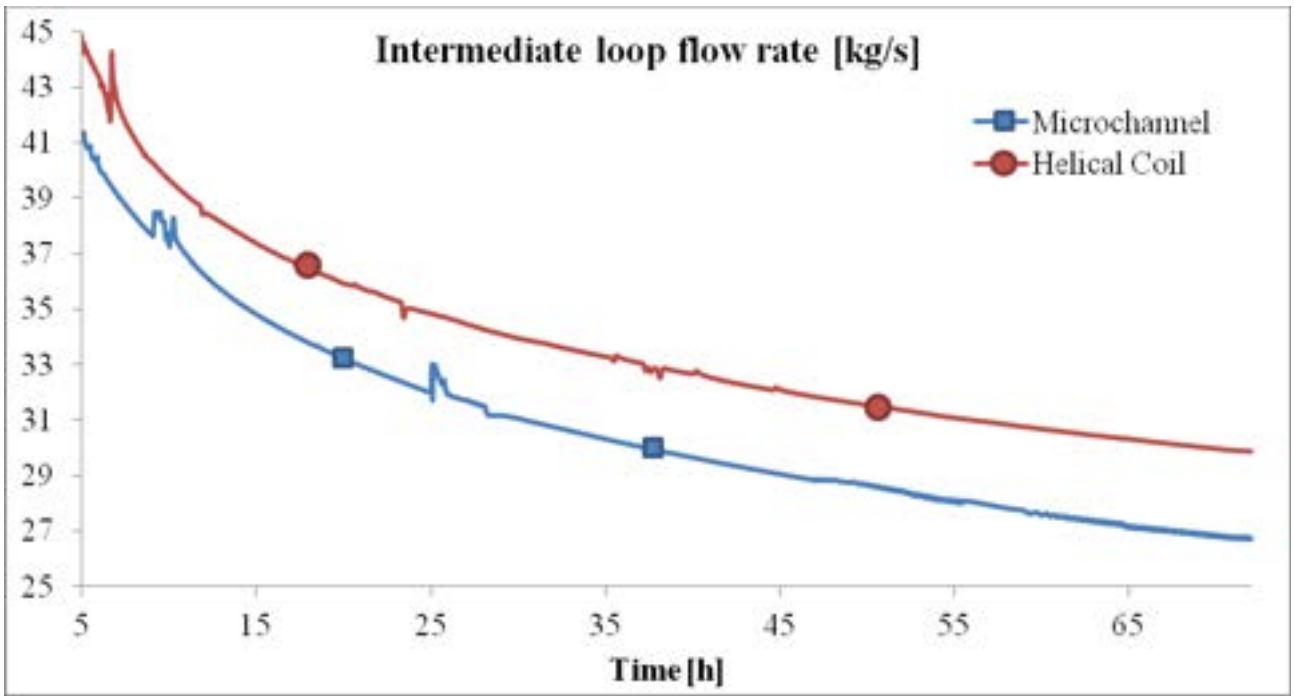

Figure 99. Intermediate loop flow rate (Case 1+2)

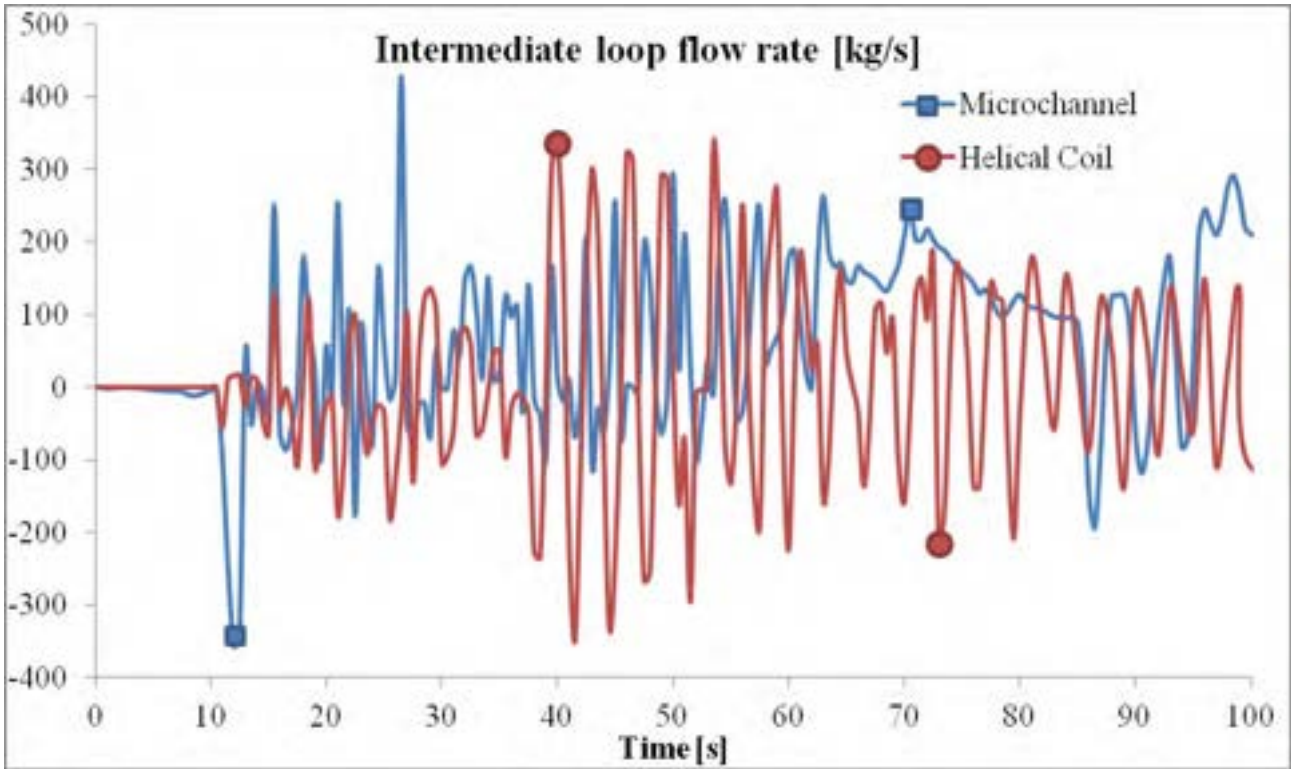

Figure 100. Intermediate loop flow rate at the beginning of the transient (Case 1+2)

Final heat sink temperatures

Figures 101 and 102 show the air temperature in the final heat sink during the transient. As for the temperatures in the intermediate loop, Even in this case the long term cooling is characterized with a comparable behaviour for the two system. The maximum temperature reached by the air is higher in the case of the helical coil configuration (195 °C) while the case with microchannel configuration is characterized with a maximum temperature of 180 °C. At the beginning of the transient (figure 102) it seems that the air heat exchanger is able to start natural circulation sooner in the case of microchannel configuration being different the delay time of the systems.

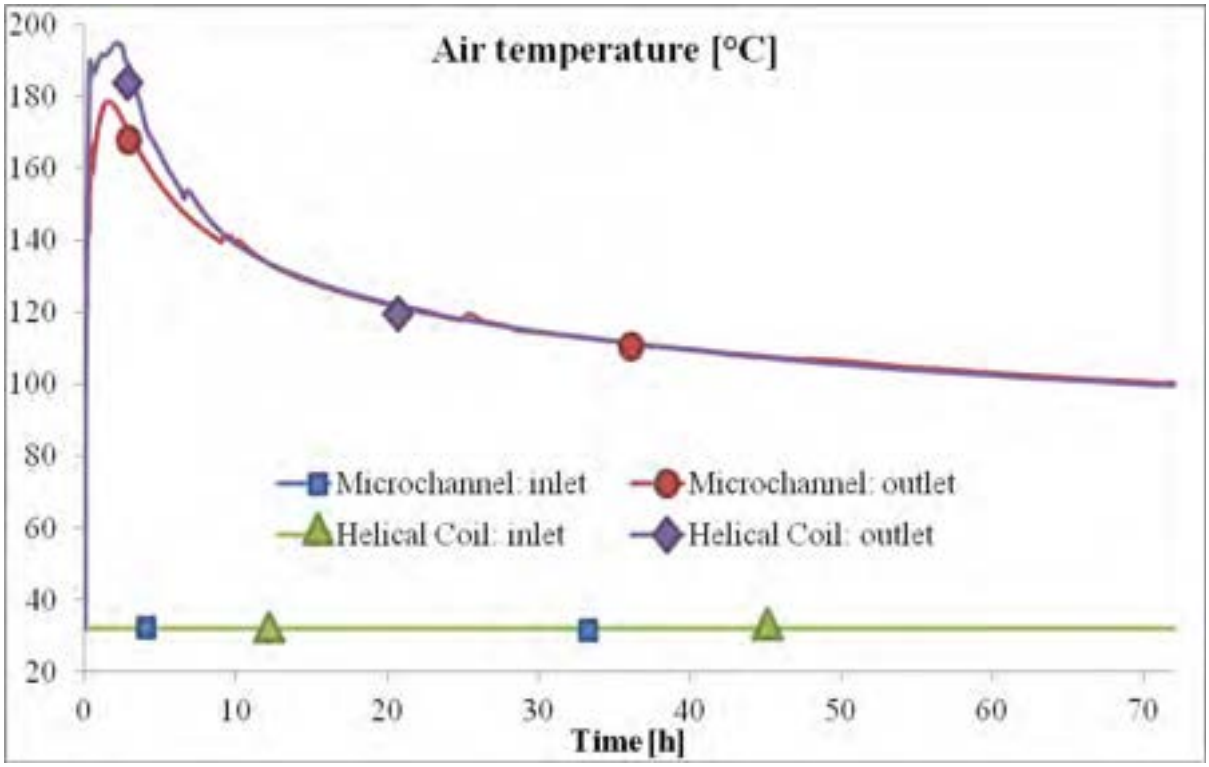

Figure 101. Air temperature (Case 1+2)

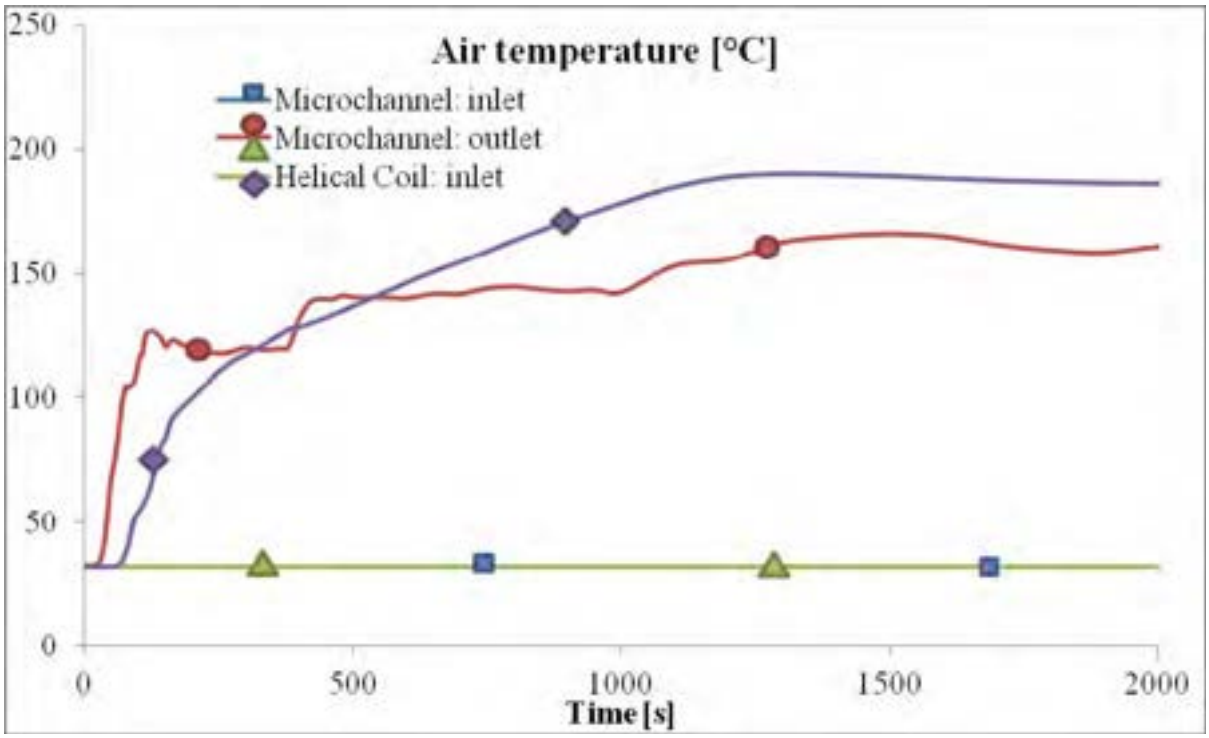

Figure 102. Air temperature at the beginning of the transient (Case 1+2)

Final heat sink flow rate

As for the temperature behaviour, the air flow rate in the two cases is comparable. The microchannel configuration seems able to start air natural circulation sooner with respect to the helical coil configuration. No flow rate oscillations have been recorded in the final heat sink.

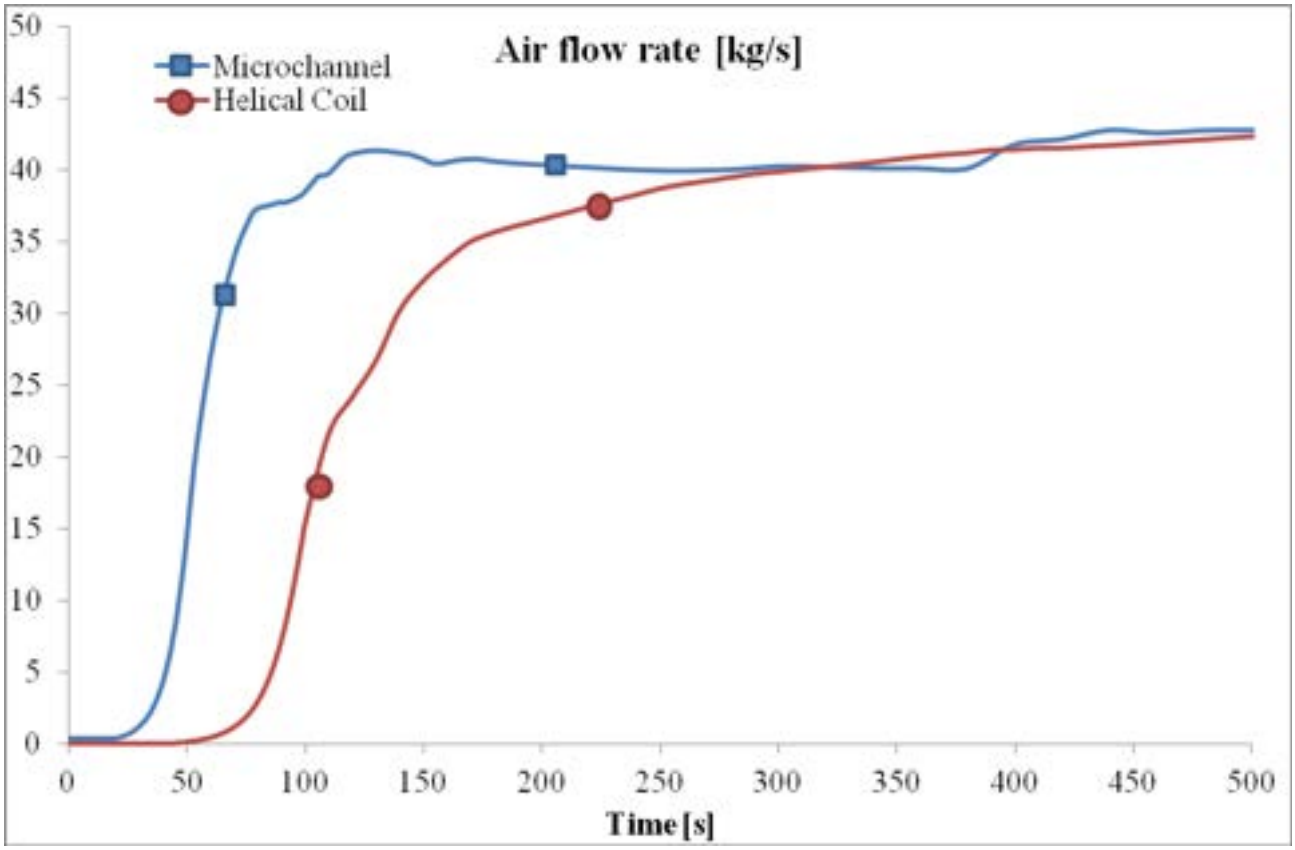

Figure 103. Air flow rate at the beginning of the transient (Case 1+2)

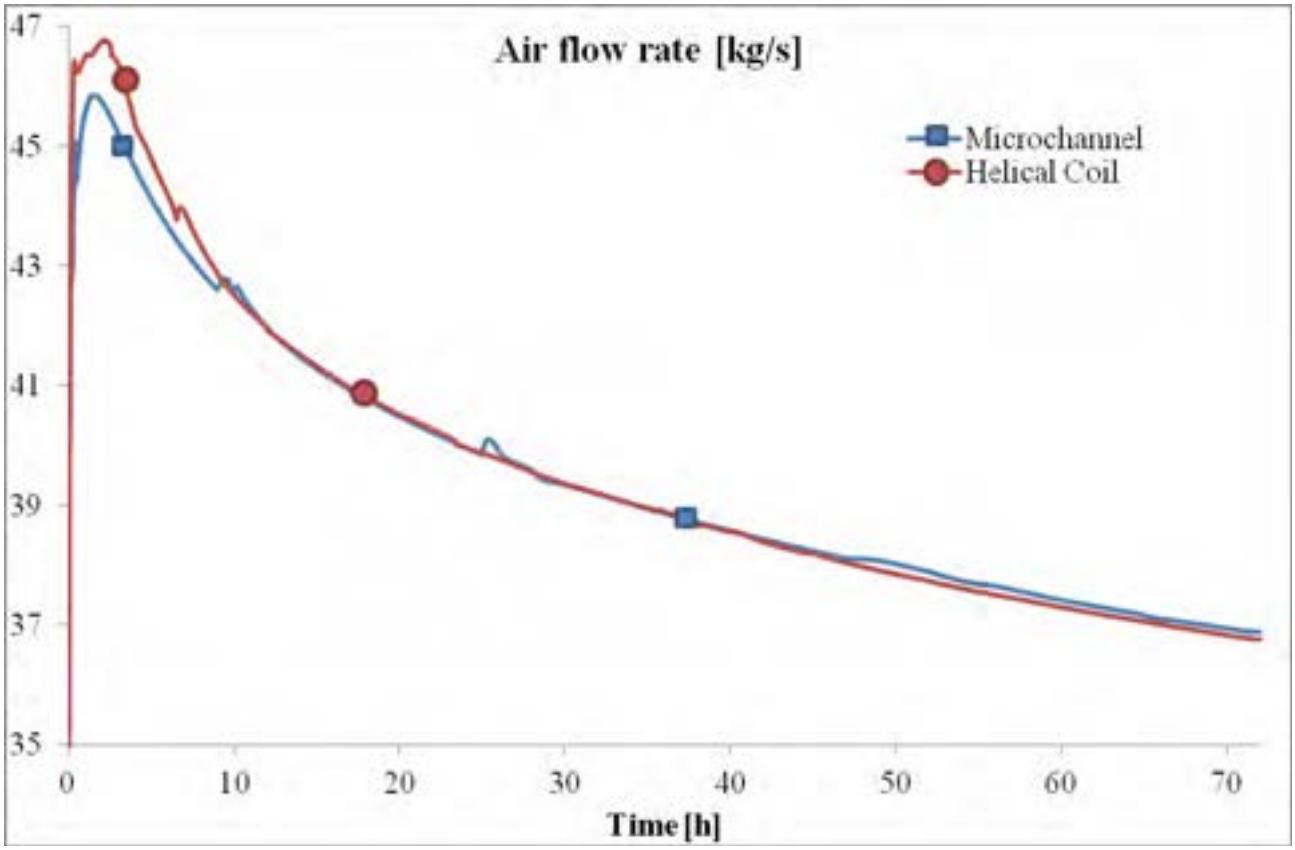

Figure 104. Air flow rate (Case 1+2)

9 Conclusions

The current study gave the possibility to deepen the knowledge about innovative heat exchangers such as microchannel heat exchanger and helical coil heat exchanger both in steady state conditions and natural circulation conditions. This study also permitted to analyse innovative passive systems based on natural circulation.

From the steady state analysis of the heat exchangers it is possible to conclude that microchannel heat exchangers offer the potential to remove high values of thermal power with a high degree of compactness. The compactness of microchannel heat exchangers is higher than the one obtainable with a helical coil configuration. The heat transfer enhancement is paid at the price of an higher friction pressure drop: the price is mitigated on the secondary side thanks to their small length, but the friction pressure drops on the primary side are considerably higher than the ones obtainable with a shell and coil heat exchanger.

The power load variation in steady state conditions permitted to observe that microchannel heat exchangers performances rely almost entirely on the conditions of the fluids, while the helical coil heat exchanger showed a more robust behaviour near the operating condition point. Other studies will be however required to assess geometrical effects and extend the comparison to other configurations.

From the analysis of the accidental sequence it is possible to conclude that helical coil heat exchangers are able to provide higher flow rates in the primary system and thus enhance a better natural circulation than microchannel heat exchangers. Other than that, the horizontal configuration of microchannel heat exchangers aggravates the performance during natural circulation. The results obtained with Relap code showed a large scattering in temperature and power behaviour of the microchannel configuration, and this opens the possibility for further studies to validate the code prediction capability of these components.

10 References

[1] **IAEA-TECDOC-626**, *Safety related terms for advanced nuclear plants*, September 1991.

[2] **IAEA-TECDOC-1624**, *Passive Safety Systems and Natural Circulation in Water Cooled Nuclear Power Plants*, November 2009.

[3] **IAEA-TECDOC-1474**, *Natural circulation in water cooled nuclear power plants*, November 2005.

[4] **INL**, *RELAP5/MOD3.3 2001 Code manual Vol. 1* (Information Systems Laboratories Inc.).

[5] **Mazzi, Brendstrup**, *CAREM project development activities*, 18th International Conference on Structural Mechanics in Reactor Technology (SMiRT 18), Beijing, China, August 7-12, 2005.

[6] **Jordi Freixa, Tae-Wan Kim, Annalisa Manera**, T*hermal-hydraulic analysis of an intermediate LOCA test at the ROSA facility including uncertainty evaluation*, Nuclear Engineering and Design 249 (2012) 97–103.

[7] **Taisuke Yonomoto, Iwao Ohtsu, Yoshinari Anoda**, *Thermal–hydraulic characteristics of a next-generation reactor relying on steam generator secondary side cooling for primary depressurization and long-term passive core cooling*, Nuclear Engineering and Design 185 (1998) 83–96.

[8] **Martina Scheuerer , Johannes Weis**, *Transient computational fluid dynamics analysis of emergency core cooling injection at natural circulation conditions*, Nuclear Engineering and Design 253 (2012) 343–350.

[9] **Takeshi Takeda, Hideaki Asaka, Hideo Nakamura**, *Analysis of the OECD/NEA ROSA Project experiment simulating a PWR small break LOCA with high-power natural circulation*, Annals of Nuclear Energy 36 (2009) 386–392.

[10] **Jun Yang, Sung-Won Choi, Jaehyok Lim, Doo-Yong Lee, Somboon Rassame, Takashi Hibiki, Mamoru Ishii**, *Counterpart experimental study of ISP-42 PANDA tests on PUMA facility*, Nuclear Engineering and Design 258 (2013) 249–257.

[11] **IAEA-TECDOC-1281**, *Natural circulation data and methods for advanced water cooled nuclear power plant designs*, Proceedings of a Technical Committee meeting held in Vienna, 18–21 July 2000.

[12] **Lindsey K. Fiddes, Neta Raz, Suthan Srigunapalan, Ethan Tumarkan, Craig A. Simmons,Aaron R. Wheeler, Eugenia Kumacheva**, *A circular cross-section PDMS microfluidics system for replication of cardiovascular flow conditions*, Biomaterials 31 (2010) 3459–3464.

[13] **Natanel Korin, Avishay Bransky, Uri Dinnar**, *Theoretical model and experimental study of red blood cell (RBC) deformation in microchannels*, Journal of Biomechanics 40 (2007) 2088–2095.

[14] **Tuckerman D. B., Pease R. F. W**., *High-Performance Heat Sinking for VLSI*, IEEE ELECTRON DEVICE LETTERS, VOL. EDL-2, NO. 5, MAY 1981.

[15] **Satish G. Kandlikar, Srinivas Garimella, Dongqing Li, Stéphane Colin, Michael R. King**, *HEAT TRANSFER AND FLUID FLOW IN MINICHANNELS AND MICROCHANNELS*, Elsevier, 2006.

[16] **Hornbeck, R.W**., *Laminar flow in the entrance region of a pipe*, Appl. Sci. Res., 13, 224–232, 1964.

[17] **Chen, R.Y**., *Flow in the entrance region at low Reynolds numbers*, J. Fluid. Eng., 95, 153–158, 1972.

[18] **Shah, R. K. and London, A. L.,** *Laminar Flow Forced Convection in Ducts*, Supplement 1 to Advances in Heat Transfer, New York: Academic Press, 1978.

[19] **Phillips, R. J.**, *Forced convection, liquid cooled, microchannel heat sinks*, MS Thesis, Department of Mechanical Engineering, Massachusetts Institute of Technology, Cambridge, MA, 1987.

[20] **Jones Jr., O. C.,** *An improvement in the calculation of turbulent friction in rectangular ducts*, J. Fluid. Eng., 98, 173–181, 1976.

[21] **Bucci, A., Celata, G. P., Cumo, M., Serra, E., and Zummo, G.,** *Water single-phase fluid flow and heat transfer in capillary tubes*, Paper No. ICMM2004-2406, Second International Conference on Microchannels and Minichannels, Rochester, NY USA, June 17–19, 221–228, 2004. International Conference on Microchannels and Minichannels. Paper 1037, ASME, 319–326.

[22] **Kakac, S., Shah, R. K., and Aung, W.**, *Handbook of Single-Phase Convective Heat Transfer*, New York: JohnWiley and Sons, Inc., 1987.

[23] **Phillips, R. J.**, *Microchannel heat sinks*, Advances in Thermal Modeling of Electronic Components and Systems, NewYork, NY: Hemisphere Publishing Corporation, 1990, Chapter 3.

[24] **Adams, T. M., Abdel-Khalik, S. I., Jeter, M., and Qureshi, Z. H.,** *An experimental investigation of single-phase forced convection in microchannels*, Int. J. Heat. Mass Trans., 41(6–7), 851–857, 1997.

[25] **Gnielinski, V**., *New equations for heat and mass transfer in turbulent pipe and channel flow*, Int. Chem. Eng., 16, 359–368, 1976.

[26] Nuclear Engineering International, *The Integral Inherently Safe Light Water Reactor*, 28 April 2014, http://www.neimagazine.com/features/featurethe-integral-inherently-safe-light-water-reactor-4253617/

[27] **Satish G. Kandlikar & William J. Grande**, E*volution of Microchannel Flow Passages - Thermohydraulic Performance and Fabrication Technology*, Heat Transfer Engineering, 24:1, 3-17.

[28] **Madou, M**, *Fundamentals of Microfabrication*, CRC Press, Inc., Boca Raton, FL, 1997.

[29] **Trimmer, W. S.,** ed., *Micromechanics and MEMS: Classic and Seminal Papers to 1990*, IEEE Press, New York, NY, 1997.

[30] **Ciofalo, M., Di Liberto, M., & Di Piazza, I,** *Steady, periodic, quasi-periodic and chaotic flow regimes in toroidal pipes*. In Esculapio Editrice (Ed.) Proceedings of the 30th UIT Heat Transfer Conference, Bologna, 2012, pp. 5-16.

[31] **Andrea Cioncolini, Lorenzo Santini**, *On the laminar to turbulent flow transition in diabatic helically coiled pipe flow*, Experimental Thermal and Fluid Science 30 (2006) 653–661.

[32] **P. Naphon, S. Wongwises**, *A review of flow and heat transfer characteristics in curved tubes*, Renewable and Sustainable energy Reviews 10 (2006) 463-490.

[33] **S. Vashisth, V. Kumar, K. D. P. Nigam**, *A review on the potential applications of curved geometries in process industry*, Ind. Eng. Chem. Res. 47 (2008) 3291-3337.

[34] **Berger S. A., Talbot L., Yao L. S**., *Flow in curved pipes*, Annu. Rev. Fluid Mech., 1983, 15, 461.

[35] **K Nandakumar, J. H. Masliyah**, *Swirling flow and heat transfer in coiled and twisted pipes*, Adv. Transport. Process 4, 49-112.

[36] **Shah R. K., Joshi S. D.,** *Convective heat transfer in curved ducts*, Handbook of single-phase Convective heat transfer; Kacac S., Shah R. K., Aung W., Eds.; Wiley: New York, 1987; Chapter 5, pp 5.3-5.47 and 3.1-3.147.

[37] **Saxena A. K., Nigam K. D. P.,** *Residence time distribution in straight and curved tubes.* Encyclopaedia of fluid mechanics 1; Cheremishinoff N. P., Ed., Gulf Publishing Co.: Houston, TX, 1986; p. 675.

[38] **Young, M. A.; Bell, K. J**. *Review of two phase flow and heat transfer phenomena in helically coiled tubes*. Am. Inst. Phys. 1991, 1214.

[39] **Mori, Y.; Nakayama, W**. *Study on forced convective heat transfer in curved pipes*. Int. J. Heat Mass Transfer, Part I 1965, 8, 67; Int. J. Heat Mass Transfer, Part II 1967, 10, 37; Int. J. Heat Mass Transfer, Part III 1967, 11, 681.

[40] **Chen, J. C**, 1966, *A Correlation for Boiling Heat Transfer to Saturated Fluids in Convective Flow*, Industrial and Engineering Chemistry, Process Design and Development, Vol. 5, No. 3, pp. 322-329.

[41] **Owhadi, A., Bell, K.J., Crain Jr., B.**, 1968. *Forced convection boiling inside helically-coiled tubes*. Int. J. Heat Mass Trans. 11, 1779–1793.

[42] **H. Ito**, *Friction factors for turbulent flow in curved pipes*, J. Basic Eng. (1959) 123–134.

[43] **Lorenzo Santini, Andrea Cioncolini, Carlo Lombardi, Marco Ricotti**, *Two-phase pressure drops in a helically coiled steam generator*, International Journal of Heat and Mass Transfer 51 (2008) 4926–4939.

[44] **G. Caruso, M. Fatone, A. Naviglio**, "*An Experimental Study on Natural Draft-dry Cooling Tower as a Part of the Passive System for the Residual Decay Heat Removal*", Proceedings of ICAPP 2007, Nice, France, May 13 – 18, 2007.

[45] Boiling Water Reactor **GE BWR/4**,Technology *Advanced Manual Chapter 6.0 BWR Differences*, USNRC Technical Training Centre.

[46] **General electric Itachi**, *ESBWR Plant general description*, 6/1/2011.

[47] **J. Hart, W.J.M. Slegers, S.L. de Boer, M. Huggenberger, J. Lopez Jimenez, J.L. Munoz-Cobo Gonzalez, F. Reventos Puigjaner**, *TEPSS—Technology enhancement for passive safety systems*, Nuclear Engineering and Design 209 (2001) 243–252.

[48] **Domenico Paladino, Joerg Dreier**, *Passive containment cooling system (PCCS) response with Drywell Gas Recirculation System (DGRS) activated during a postulated Loss of Coolant Accident (LOCA),* Nuclear Engineering and Design 241 (2011) 3925– 3934.

[49] **T.L. Schulz,** *Westinghouse AP1000 advanced passive plant*, Nuclear Engineering and Design 236 (2006) 1547–1557.

[50] **Wang Weiwei, Tian Wenxi, Su Guanghui, Qiu Suizheng**, *Development of a thermalhydraulic safety analysis code RETAC for AP1000*, Progress in Nuclear Energy 55 (2012) 49-60.

[51] **B. Petrovic,** *Integral Inherently Safe Light Water Reactor (I2S-LWR) – Concept Overview,* Trans. Am. Nucl. Soc., 109, (2013).

[52] **Koroush Shirvan, Pavel Hejzlar, Mujid S. Kazimi**, *The design of a compact integral medium size PWR*, Nuclear Engineering and Design 243 (2012) 393–403.

[53] **Carelli, M.D., Conway, L.E., Oriani, L., Petrovic, B., Lombardi, C.V., Ricotti, M.E., Barroso, A.C.O., Collado, J.M., Cinotti, L., Todreas, N.E., Grgic, D., Moraes, M.M., Boroughs, R.D., Ninokata, H., Ingersoll, D.T., Oriolo, F.,** 2004. *The design and safety features of the IRIS reactor.* Nuclear Engineering and Design 230, 151–167.

[54] **Mario D. Carelli**, *The exciting journey of designing an advanced reactor,* Nuclear Engineering and Design 239 (2009) 880–887.

[55] **Bojan Petrovic**, *Integral Inherently Safe Light Water Reactor (I2S-LWR) Concept*.

[56] **ANL**, 2012. *http: //web.anl.gov/eesa/pdfs/success_stories/ 48_Nanofluids_Heat_Transfer_v2.pdf.*

[57] **Wang X.Q., Mujumdar, A.S**., 2007. *Heat transfer characteristics of nanofluids: a review*. Int. J. Therm. Sci., 46(1), p. 1-19.

[58] **Nathan V. Hoffer, Piyush Sabharwall, Nolan A. Anderson**, *Modeling a Helical-coil Steam Generator in RELAP5-3D for the Next Generation Nuclear Plant,* 2001 INL/EXT-10-19621.

[59] **Memmott, M.J., Manera, A.**, 2014. *The use of a flashing drum to generate steam in the Integral, Inherently Safe (I2S) Light Water Reactor*, Proc. of ICAPP2014, Charlotte, USA, Apr. 6 – 9 (selected for publication in special issue of Nuclear Technology).

[60] **Manera, A., Memmott, M.J.**, 2014. *Design and trade-off of the Passive Decay Heat Removal System (DHRS) of the Integral, Inherently Safe Light Water Reactor (I2S-LWR)*, Proc. of 10th International Conf. on the Nuclear Option in Countries with Small and Medium Electricity Grids, Zadar, Croatia, June 1 - 4.

11 Appendix: components of the system

11.1 Primary system

Component	Lower plenum						
type	Single volume						
Card number	110						
Volumes	1						
Volumes	Area [m^2]	Length [m]	Volume [m^3]	inclination [deg]	Δz	Rugosity	Hydraulic diameter
1	0.992783791	1.8015	1.7885	90	1.8015	0.000003	0

Initial conditions	Pressure [bar]	Temperature [K]
	155	566

Component	core bottom					
type	Single junction					
Card number	501					
From	110					
To	101					
Initial conditions	Liquid flow rate [kg/s]	Gas flow rate [kg/s]	Area [m^2]	Af	Ar	jefvcahs
	4105.3	0	0	1.3	1.3	0

Component	Active core						
type	Pipe						
Card number	101						
Volumes	10						
Volumes	Area [m^2]	Length [m]	Volume [m^3]	inclination [deg]	Δz	Rugosity	Hydraulic diameter
10	0.8817	0.365676	0.322416529	90	0.365676	0.000001	0.011243

Initial conditions	Pressure [bar]	Temperature [K]	Liquid flow rate [kg/s]	Gas flow rate [kg/s]
	155	575	4135	0

Component	Core top					
type	Single junction					
Card number	502					
From	101					
To	102					
Initial conditions	Liquid flow rate [kg/s]	Gas flow rate [kg/s]	Area [m^2]	Af	Ar	jefvcahs
	4135	0	0	1	1	0

Component	Inactive core						
type	Pipe						
Card number	102						
Volumes	5						
Volumes	Area [m^2]	Length [m]	Volume [m^3]	inclination [deg]	Δz	Rugosity	Hydraulic diameter
5	1.787	2.11898	3.78661726	90	2.11898	0.000001	0

Initial conditions	Pressure [bar]	Temperature [K]	Liquid flow rate [kg/s]	Gas flow rate [kg/s]
	155	597	4135	0

Component	Upper plenum					
type	Single junction					
Card number	503					
From	102					
To	103					
Initial conditions	Liquid flow rate [kg/s]	Gas flow rate [kg/s]	Area [m^2]	Af	Ar	jefvcahs
	4135	0	0	1.3	1.3	0

Component	Upper plenum						
type	Single volume						
Card number	103						
Volumes	1						
Volumes	Area [m^2]	Length [m]	Volume [m^3]	inclination [deg]	Δz	Rugosity	Hydraulic diameter
1	0.32125	0.7875	0.252984375	90	0.7875	0.000001	0

Initial conditions	Pressure [bar]	Temperature [K]
	155	597

Component	Top upper plenum						
type	Single junction						
Card number	519						
From	103						
To	104						
Initial conditions	Liquid flow rate [kg/s]	Gas flow rate [kg/s]	Area [m^2]	Af	Ar	jefvcahs	
	0	0	0	1	0.5	0	

Component	Pressurizer						
type	Time dependent volume						
Card number	104						
Volumes	1						
Volumes	Area [m^2]	Length [m]	Volume [m^3]	inclination [deg]	Δz	Rugosity	Hydraulic diameter
1	1	5	5	0	0	0	0

Initial conditions	Pressure [bar]	Temperature [K]
	155	596

Component	Downcomer			
type	Time dependent junction			
Card number	504			
From	103			
To	105			
Initial conditions	Liquid flow rate [kg/s]	Gas flow rate [kg/s]	Area [m^2]	jefvcahs
	4105.3	0	0	0

Component	Downcomer						
type	Pipe						
Card number	105						
Volumes	1						
Volumes	Area [m^2]	Length [m]	Volume [m^3]	inclination [deg]	Δz	Rugosity	Hydraulic diameter
1	1.76	3.069666	5.40261216	-90	3.069666	0.000001	0.7

Initial conditions	Pressure [bar]	Temperature [K]	Liquid flow rate [kg/s]	Gas flow rate [kg/s]
	155	597	0	0

Component	HX inlet					
type	Single junction					
Card number	522					
From	105					
To	106					
Initial conditions	Liquid flow rate [kg/s]	Gas flow rate [kg/s]	Area [m^2]	Af	Ar	jefvcahs
	4135	0	0	0.5	0.5	0

Component	HX inlet						
type	Pipe						
Card number	106						
Volumes	1						
Volumes	Area [m^2]	Length [m]	Volume [m^3]	inclination [deg]	Δz	Rugosity	Hydraulic diameter
1	0.416	6	2.496	-90	6	0.000001	0.698

Initial conditions	Pressure [bar]	Temperature [K]	Liquid flow rate [kg/s]	Gas flow rate [kg/s]
	155	597	0	0

Component	HX inlet					
type	Single junction					
Card number	520					
From	106					
To	107					
Initial conditions	Liquid flow rate [kg/s]	Gas flow rate [kg/s]	Area [m^2]	Af	Ar	jefvcahs
	4135	0	0	1	1	0

Component	HX						
type	Pipe						
Card number	107						
Volumes	10						
Volumes	Area [m^2]	Length [m]	Volume [m^3]	inclination [deg]	Δz	Rugosity	Hydraulic diameter
10	0.9	0.01924	0.017316	0	0	0	0.001

Initial conditions	Pressure [bar]	Temperature [K]	Liquid flow rate [kg/s]	Gas flow rate [kg/s]
	155	580	4135	0

Component	HX outlet					
type	Single junction					
Card number	521					
From	107					
To	108					
Initial conditions	Liquid flow rate [kg/s]	Gas flow rate [kg/s]	Area [m^2]	Af	Ar	jefvcahs
	4135	0	0	0.5	0.5	0

Component	HX outlet						
type	Pipe						
Card number	108						
Volumes	1						
Volumes	Area [m^2]	Length [m]	Volume [m^3]	inclination [deg]	Δz	Rugosity	Hydraulic diameter
1	0.416	6	2.496	-90	6	0.000003	0.698

Initial conditions	Pressure [bar]	Temperature [K]	Liquid flow rate [kg/s]	Gas flow rate [kg/s]
	155	580	0	0

Component	Bottom downcomer					
type	Single junction					
Card number	523					
From	108					
To	109					
Initial conditions	Liquid flow rate [kg/s]	Gas flow rate [kg/s]	Area [m^2]	Af	Ar	jefvcahs
	4135	0	0	1	1	0

Component	Bottom downcomer						
type	Pipe						
Card number	109						
Volumes	5						
Volumes	Area [m^2]	Length [m]	Volume [m^3]	inclination [deg]	Δz	Rugosity	Hydraulic diameter
5	1.76	1.031168	1.81485568	-90	1.031168	0.000003	1.321

Initial conditions	Pressure [bar]	Temperature [K]	Liquid flow rate [kg/s]	Gas flow rate [kg/s]
	155	580	4135	0

Component	up lower plenum					
type	Single junction					
Card number	505					
From	109					
To	110					
Initial conditions	Liquid flow rate [kg/s]	Gas flow rate [kg/s]	Area [m^2]	Af	Ar	jefvcahs
	4135	0	0	0.5	0.5	0

Component	DHR inlet			
type	Time dependent junction			
Card number	506			
From	103			
To	112			
Initial conditions	Liquid flow rate [kg/s]	Gas flow rate [kg/s]	Area [m^2]	jefvcahs
	0	0	0	0

Component	Helical coil DHR						
type	Pipe						
Card number	112						
Volumes	50						
Volumes	Area [m^2]	Length [m]	Volume [m^3]	inclination [deg]	Δz	Rugosity	Hydraulic diameter
50	0.027335751	0.766411	0.02095042	-12.05	-0.16	0.000003	0.0107

Initial conditions	Pressure [bar]	Temperature [K]	Liquid flow rate [kg/s]	Gas flow rate [kg/s]
	155	305	0	0

Component	DHR outlet					
type	Single junction					
Card number	508					
From	112					
To	113					
Initial conditions	Liquid flow rate [kg/s]	Gas flow rate [kg/s]	Area [m^2]	Af	Ar	jefvcahs
	0	0	0	1	1	0

Component	DHR outlet						
type	Pipe						
Card number	113						
Volumes	5						
Volumes	Area [m^2]	Length [m]	Volume [m^3]	inclination [deg]	Δz	Rugosity	Hydraulic diameter
5	0.025447	1.2505	0.031821474	-90	1.2505	0.000003	0

Initial conditions	Pressure [bar]	Temperature [K]	Liquid flow rate [kg/s]	Gas flow rate [kg/s]
	155	305	0	0

Component	DHR outlet					
type	Single junction					
Card number	509					
From	113					
To	110					
Initial conditions	Liquid flow rate [kg/s]	Gas flow rate [kg/s]	Area [m^2]	Af	Ar	jefvcahs
	0	0	0	1.2	1.2	0

Component	Core				
type	Heat structure				
Card number	101				
Axial mesh	10				
Radial mesh	5				
Left radius [m]	0				
Interval	Material	right radius [m]	T(t=0) [K]		
2	Fuel	0.0041625	1000		
1	Gap	0.0041656	1000		
1	S-steel	0.004572	1000		
Left BC	From	Step	Type	Safac	Volume
	0	0	Adiabatic	0	10
Right BC	From	Step	Type	Safac	Volume
	101-01	10000	Convection	3717.584	10
Source	Type	mult	Volume		
	Nominal power	0.0245	1		
	Nominal power	0.071	2		

	Nominal power	0.1106	3
	Nominal power	0.1394	4
	Nominal power	0.1545	5
	Nominal power	0.1545	6
	Nominal power	0.1394	7
	Nominal power	0.1106	8
	Nominal power	0.071	9
	Nominal power	0.0245	10

Component	Primary HX				
type	Heat structure				
Card number	107				
Axial mesh	10				
Radial mesh	2				
Left radius [m]	0				
Interval	Material	right radius [m]	T(t=0) [K]		
1	S-steel	0.00041	558		
Left BC	From	Step	Type	Safac	Volume

	107-01	10000	Convection	94	10
Right BC	From	Step	Type	Safac	Volume
	402-10	-10000	Convection	94	10

Component	Helical coil DHR				
type	Heat structure				
Card number	112				
Axial mesh	50				
Radial mesh	10				
Left radius [m]	0.00537				
Interval	Material	right radius [m]	T(t=0) [K]		
1	S-steel	0.0065	305		
Left BC	From	Step	Type	Safac	Volume
	112-50	-10000	Convection	233	50
Right BC	From	Step	Type	Safac	Volume
	201-01	10000	Convection	233	50

11.2 Intermediate loop

Component	II inlet						
type	Time dependent volume						
Card number	401						
Volumes	1						
Volumes	Area [m^2]	Length [m]	Volume [m^3]	inclination [deg]	Δz	Rugosity	Hydraulic diameter
1	1	5	5	0	0	0	0

Initial conditions	Pressure [bar]	Temperature [K]
	69.2	496.15

Component	II HX inlet
type	Time dependent junction
Card number	550

From	401			
To	402			
Initial conditions	Liquid flow rate [kg/s]	Gas flow rate [kg/s]	Area [m^2]	jefvcahs
	2213	0	0	0

Component	DHR outlet						
type	Pipe						
Card number	402						
Volumes	10						
Volumes	Area [m^2]	Length [m]	Volume [m^3]	inclination [deg]	Δz	Rugosity	Hydraulic diameter
10	0.9	0.01924	0.017316	0	0.01924	0	0.001

Initial conditions	Pressure [bar]	Temperature [K]	Liquid flow rate [kg/s]	Gas flow rate [kg/s]
	69.2	500	0	0

Component	II outlet
type	Single junction
Card number	551

From	402					
To	403					
Initial conditions	Liquid flow rate [kg/s]	Gas flow rate [kg/s]	Area [m^2]	Af	Ar	jefvcahs
	2213	0	0	0	0	0

Component	II outlet						
type	Time dependent volume						
Card number	403						
Volumes	1						
Volumes	Area [m^2]	Length [m]	Volume [m^3]	inclination [deg]	Δz	Rugosity	Hydraulic diameter
1	1	5	5	0	0	0	0

Initial conditions	Pressure [bar]	Temperature [K]
	69.2	558

Component	DHR intermediate						
type	Pipe						
Card number	201						
Volumes	50						
Volumes	Area [m^2]	Length [m]	Volume [m^3]	inclination [deg]	Δz	Rugosity	Hydraulic diameter
50	0.1315	0.16	0.02104	90	0.16	0.000003	0.0052
Initial conditions	Pressure [bar]	Temperature [K]	Liquid flow rate [kg/s]	Gas flow rate [kg/s]			
	1	305	0	0			

Component	DHR top
type	Single junction
Card number	510

From	201						
To	202						
Initial conditions	Liquid flow rate [kg/s]	Gas flow rate [kg/s]	Area [m^2]	Af	Ar	jefvcahs	
	0	0	0	0	0	0	

Component	Intermediate loop						
type	Pipe						
Card number	202						
Volumes	5						
Volumes	Area [m^2]	Length [m]	Volume [m^3]	inclination [deg]	Δz	Rugosity	Hydraulic diameter
5	0.2	3	0.6	90	3	0.000003	0

Initial conditions	Pressure [bar]	Temperature [K]	Liquid flow rate [kg/s]	Gas flow rate [kg/s]
	1	305	0	0

Component	DHR - IC
type	Single junction

Card number	511					
From	202					
To	203					
Initial conditions	Liquid flow rate [kg/s]	Gas flow rate [kg/s]	Area [m^2]	Af	Ar	jefvcahs
	0	0	0	2.6	2.6	0

Component	Isolation condenser						
type	Pipe						
Card number	203						
Volumes	10						
Volumes	Area [m^2]	Length [m]	Volume [m^3]	inclination [deg]	Δz	Rugosity	Hydraulic diameter
10	2.62665	0.5111	1.342480815	-90	0.5111	0.000003	0.0746

Initial conditions	Pressure [bar]	Temperature [K]	Liquid flow rate [kg/s]	Gas flow rate [kg/s]
	1	305	0	0

Component	II top

type	Single junction						
Card number	512						
From	202						
To	204						
Initial conditions	Liquid flow rate [kg/s]	Gas flow rate [kg/s]	Area [m^2]	Af	Ar	jefvcahs	
	0	0	0	1	0.5	0	

Component	II pressurizer						
type	Time dependent volume						
Card number	204						
Volumes	1						
Volumes	Area [m^2]	Length [m]	Volume [m^3]	inclination [deg]	Δz	Rugosity	Hydraulic diameter
1	1.5	5	7.5	9	0	0	0

Initial conditions	Pressure [bar]	Temperature [K]	Air quality
	1	558	0.1

Component	IC out					
type	Single junction					
Card number	513					
From	203					
To	205					
Initial conditions	Liquid flow rate [kg/s]	Gas flow rate [kg/s]	Area [m^2]	Af	Ar	jefvcahs
	0	0	0	0.5	0.5	0

Component	II DHR inlet						
type	Pipe						
Card number	205						
Volumes	5						
Volumes	Area [m^2]	Length [m]	Volume [m^3]	inclination [deg]	Δz	Rugosity	Hydraulic diameter
5	0.2	3.58	0.716	-90	3.58	0.000003	0

Initial conditions	Pressure [bar]	Temperature [K]	Liquid flow rate [kg/s]	Gas flow rate [kg/s]
	1	305	0	0

Component	II DHR inlet					
type	Single junction					
Card number	514					
From	205					
To	201					
Initial conditions	Liquid flow rate [kg/s]	Gas flow rate [kg/s]	Area [m^2]	Af	Ar	jefvcahs
	0	0	0	2.1	2.1	0

Component	Isolation Condenser				
type	Heat structure				
Card number	203				
Axial mesh	10				
Radial mesh	5				
Left radius [m]	0.00397				
Interval	Material	right radius [m]	T(t=0) [K]		
1	S-steel	0.0048	305		
Left BC	From	Step	Type	Safac	Volume

	203-10	-10000	Convection	10648.7	10
Right BC	From	Step	Type	Safac	Volume
	303-01	10000	Convection	10648.7	10

11.3 Primary system: microchannel heat exchanger

Component	Microchannel DHR						
type	Pipe						
Card number	112						
Volumes	10						
Volumes	Area [m^2]	Length [m]	Volume [m^3]	inclination [deg]	Δz	Rugosity	Hydraulic diameter
10	0.51	0.1924	0.098124	0	0	0	0

Initial conditions	Pressure [bar]	Temperature [K]	Liquid flow rate [kg/s]	Gas flow rate [kg/s]
	155	305	0	0

11.4 Final heat sink: Pool loop

Component	I water pool						
type	Pipe						
Card number	303						
Volumes	15						
Volumes	Area [m^2]	Length [m]	Volume [m^3]	inclination [deg]	Δz	Rugosity	Hydraulic diameter
10	39.3	0.2	7.86	90	0.2	0	0
15	39.3	0.6	23.58	90	0.6	0	0

Initial conditions	Pressure [bar]	Temperature [K]	Liquid flow rate [kg/s]	Gas flow rate [kg/s]
	1	305	0	0

Component	II water pool						
type	Pipe						
Card number	307						
Volumes	15						
Volumes	Area [m^2]	Length [m]	Volume [m^3]	inclination [deg]	Δz	Rugosity	Hydraulic diameter
10	39.3	0.2	7.86	90	0.2	0	0
15	39.3	0.6	23.58	90	0.6	0	0
Initial conditions	Pressure [bar]	Temperature [K]	Liquid flow rate [kg/s]	Gas flow rate [kg/s]			

	1	305	0	0

Component	I pool junction					
type	Single junction					
Card number	518					
From	303					
To	305					
Initial conditions	Liquid flow rate [kg/s]	Gas flow rate [kg/s]	Area [m^2]	Af	Ar	jefvcahs
	0	0	0	1	1	0

Component	II pool junction					
type	Single junction					
Card number	308					
From	307					
To	309					
Initial conditions	Liquid flow rate [kg/s]	Gas flow rate [kg/s]	Area [m^2]	Af	Ar	jefvcahs
	0	0	0	1	1	0

Component	Pools connection					
type	Single junction					
Card number	306					
From	303					
To	307					
Initial conditions	Liquid flow rate [kg/s]	Gas flow rate [kg/s]	Area [m^2]	Af	Ar	jefvcahs
	0	0	0	1	1	0

Component	I Pool pressure						
type	Time dependent volume						
Card number	305						
Volumes	1						
Volumes	Area [m^2]	Length [m]	Volume [m^3]	inclination [deg]	Δz	Rugosity	Hydraulic diameter
1	200	5000	1000000	0	0	0	0

Initial conditions	Pressure [bar]	Temperature [K]	Air quality
	1	305	1

Component	II Pool pressure						
type	Time dependent volume						
Card number	309						
Volumes	1						
Volumes	Area [m^2]	Length [m]	Volume [m^3]	inclination [deg]	Δz	Rugosity	Hydraulic diameter
1	200	5000	1000000	0	0	0	0

Initial conditions	Pressure [bar]	Temperature [K]	Air quality
	1	305	1

11.5 Final heat sink: Air heat exchanger

Component	Air sink
type	Time dependent volume
Card number	301
Volumes	1

Volumes	Area [m^2]	Length [m]	Volume [m^3]	inclination [deg]	Δz	Rugosity	Hydraulic diameter
1	10	1	10	90	1	0	8

Initial conditions	Pressure [bar]	Temperature [K]	Air quality
	1	305	1

Component	Air inlet					
type	Single junction					
Card number	515					
From	301					
To	302					
Initial conditions	Liquid flow rate [kg/s]	Gas flow rate [kg/s]	Area [m^2]	Af	Ar	jefvcahs
	0	43.636	0	0.5	0.5	0

Component	Air downcomer
type	Pipe
Card number	302
Volumes	5

Volumes	Area [m^2]	Length [m]	Volume [m^3]	inclination [deg]	Δz	Rugosity	Hydraulic diameter
5	20	7.62	152.4	-90	7.62	0	0
Initial conditions	Pressure [bar]	Temperature [K]	Liquid flow rate [kg/s]	Gas flow rate [kg/s]			
	155	305	0	43.636			

Component	Air inlet					
type	Single junction					
Card number	517					
From	302					
To	303					
Initial conditions	Liquid flow rate [kg/s]	Gas flow rate [kg/s]	Area [m^2]	Af	Ar	jefvcahs
	0	43.636	0	0.9	0.9	0

Component	Air riser
type	Pipe
Card number	303

Volumes	10						
Volumes	Area [m^2]	Length [m]	Volume [m^3]	inclination [deg]	Δz	Rugosity	Hydraulic diameter
10	10.67634	0.51	5.4449334	90	0.51	0	0.02657

Initial conditions	Pressure [bar]	Temperature [K]	Liquid flow rate [kg/s]	Gas flow rate [kg/s]
	1	305	0	43.636

Component	Air outlet					
type	Single junction					
Card number	516					
From	303					
To	304					
Initial conditions	Liquid flow rate [kg/s]	Gas flow rate [kg/s]	Area [m^2]	Af	Ar	jefvcahs
	0	43.636	0	0.5	0.5	1

Component	Air outlet
type	Pipe
Card number	304

Volumes	5						
Volumes	Area [m^2]	Length [m]	Volume [m^3]	inclination [deg]	Δz	Rugosity	Hydraulic diameter
5	8	6.6	52.8	90	6.6	0	0.02657

Initial conditions	Pressure [bar]	Temperature [K]	Liquid flow rate [kg/s]	Gas flow rate [kg/s]
	1	305	0	43.636

Component	Air outlet					
type	Single junction					
Card number	518					
From	304					
To	305					
Initial conditions	Liquid flow rate [kg/s]	Gas flow rate [kg/s]	Area [m^2]	Af	Ar	jefvcahs
	0	43.636	0	1.0	1.0	1

Component	Air sink
type	Time dependent volume

Card number	305						
Volumes	1						
Volumes	Area [m^2]	Length [m]	Volume [m^3]	inclination [deg]	Δz	Rugosity	Hydraulic diameter
1	10	1	10	90	1	0	8

Initial conditions	Pressure [bar]	Temperature [K]	Air quality
	1	305	1

Working group scientific curricula

POLITO

The working group from Politecnico di Torino is constituted by three members of the Energy Department.

Bruno Panella is Senior professor since 2013 at Politecnico di Torino, where he has been full professor of Nuclear Engineering since 1980, former President of the Nuclear Engineering Course, former Director of the Energy Engineering PhD Course, former Head of the Energy Department, Former Director of the "Quality Center". He is member of American Nuclear Society, of the Italian Nuclear Society and of Italian Thermal Fluid-dynamic Society, Vice-President of CIRTEN (Interuniversity Consortium for Technological Nuclear Research); he has been the CIRTEN (and Italian) delegate for ten years in the ENEN (European Nuclear Education Network) Board. On behalf of CIRTEN he has been involved in several European projects, coordinated by ENEN, concerning the Nuclear Engineering Education and Training. He has been the Chairman of the XV and XXIX National Heat Transfer Conference. His scientific researches have concerned mainly the Nuclear Reactors Thermal hydraulics from the reactors safety point of view, like High heat flux Thermal Crisis modelling, Small break LOCA, Safety Passive systems, Thermal properties of alloys to be used in plasma facing components, Fluid dynamics of two phase flow in gas driven loops with no pumps, Fluid dynamics of proton windowless target with reference to the Accelerator Driven Systems, Helical steam generators experiments related to the Small Modular Reactors, Two-phase flow parameters measurements. He has also performed researches on heat pipes for space applications (capillary pumped lines), on thermal aspects of the polymer membrane fuel cells (dehumidification of humid air at the exit of the cells) and on the Hydrogen liquefaction and transport, coupled to the electricity transport in superconducting cables. He has published one hundred and eighty scientific papers (some of them in international journals like "Experimental Heat and Mass Transfer", "Nuclear Engineering and Design", "Nuclear Technology", "Journal of Nuclear Materials", "Sciences and Technology of Nuclear Installations"), two books for students and the chapter "Design Basis Accidents" of the Module "Nuclear Power Plant" of the UNESCO Distant Learning

Postgraduate Course on Energy Engineering. He is in the scientific Board of the International Journal of Nuclear Science and Technology and is a reviewer of several International Journals and International Conferences.

Mario De Salve is full professor of nuclear plants At Politecnico di Torino. He is full professor of the courses "nuclear and conventional power plants" and "nuclear technologies" in the master of science of energy and nuclear engineering. It's research activities concern the theoretical and experimental study of single-phase and two-phase thermal fluid-dynamic in the field of conventional and nuclear power plants, on instrumentation, decommissioning and radioactive waste management, environmental impact, material behaviour under irradiation. He collaborates in the research activities supported by CIRTEN, ENEA, ANSALDO and REGIONE PIEMONTE.

Marco Caramello is a PhD student at the first year followed by the tutors Mario De Salve, Bruno Panella and Cristina Bertani. It's research field is concentrated in the analysis of the thermal hydraulics of steam generators and safety systems for advanced nuclear reactors.

POLIMI

The working group of Politecnico di Milano is constituted by a full professor of the Department of Energy and a PhD student.

Prof. Marco E. Ricotti is involved since more than 20 years in R&D activities in the field of Nuclear Engineering, in particular on thermalhydraulics, safety, economic aspects of nuclear energy. He has carried out and has coordinated experimental and numerical investigations performed by the Nuclear Reactors Group of Politecnico di Milano-Dept. of Energy, publishing the research results on international scientific journals and conferences. He already coordinated several PAR actions in the last years and co-authored the corresponding Reports. More details on the R&D activities and the most recent publications are available on the web site of his POLIMI research group (http://www.nuclearenergy.polimi.it).

Ing. Giuseppe Maronati graduated in Nuclear Engineering (MSc) at Politecnico di Milano in the 2012-2013 Academic Year, with a thesis work on "Optimization of Passive Decay Heat Removal Systems for the Integral Inherently Safe Light Water Reactor (I2S-LWR)". The work has been carried out almost entirely in collaboration with prof. Bojan Petrovich at Georgia Tech

(USA). Later he begun a period of research at Politecnico di Milano and finally he entered the PhD programme at Georgia Tech, where he is currently performing his R&D activity. His competences refer today mainly to thermal hydraulics and safety of innovative nuclear reactors.